Journal
of
The Franklin Institute
Devoted to Science and the Mechanic Arts

Vol. 243 MAY, 1947 No. 5

THE ELECTRON MECHANICS OF INDUCTION ACCELERATION.

BY

JAN A. RAJCHMAN and WILLIAM H. CHERRY,

RCA Laboratories Division, Princeton, New Jersey.

PART II.

BETATRON WITH AN ADDITIONAL ELECTRIC FIELD.

The injection of electrons from a cylindrical cathode coaxial with the magnetic field with the help of an additional radial electric field has tempted many investigators. A priori, it seems that large space charge could be captured by this means since electrons are injected in initially intense fields, a condition which is known to yield large rotating charges in magnetrons. In addition, the problems of an assymetrically located gun are eliminated. The following analysis shows the requirements in the variations of the fields necessary to obtain equilibrium and stability. These turn out to be more complex and to have narrower tolerances than in the case of a purely magnetic betatron. It is shown also that no substantial gain in space charge can actually be realized.

The analysis is restricted to a toroidal region whose radial and axial limits are small compared to the average radius and also, to non-relativistic speeds. It is convenient to use a power expansion of the total potential of forces $V_t = V_{M0} - V_E$ around a position $z = 0$ and $r = r_e$, or $x = 0$ when $r - r_e$ is abbreviated by x, where r_e is the asymptotic equilibrium orbit of the purely magnetic instrument with synchronous field variation defined by equation (23).

The expansion, limited to cubic terms:

$$V_t = V_t(0, 0) + x\frac{\partial V_t}{\partial x} + \tfrac{1}{2}x^2\frac{\partial^2 V_t}{\partial x^2} + \tfrac{1}{2}z^2\frac{\partial^2 V_t}{\partial z^2} + \tfrac{1}{6}x^3\frac{\partial^3 V_t}{\partial x^3} + \tfrac{1}{2}xz^2\frac{\partial^3 V_t}{\partial x \partial z^2}, \quad (52)$$

(Note—The Franklin Institute is not responsible for the statements and opinions advanced by contributors in the JOURNAL.)

where the derivatives are understood to be for $x = z = 0$, has no terms with odd powers of z because of the assumed symmetry about the $z = 0$ plane. It is convenient also to break up this expansion into separate ones for V_{M0} and V_E and to introduce for the former two new symbols, B_e and B_q, defined as follows:

$$B_e = B_z(r_e, 0, t), \tag{53}$$

$$B_q = \frac{1}{r_e^2}\left[\int_0^{r_e} B_{\substack{z \\ z=0}} r dr - \int_0^{r_0} B_{\substack{z \\ \substack{z=z_0 \\ t=t_0}}} r dr + \frac{m_0}{e} r_0^2 \theta_0\right]$$

$$= \frac{1}{r_e^2}\int_0^{r_e} B_{\substack{z \\ z=0}} r dr + \frac{C}{r_e^2}. \tag{54}$$

It is seen that B_e is the magnetic field at the main equilibrium orbit and B_q is proportional to the angular momentum of the electrons at the position $r = r_e$ and $z = 0$ and is also equal to $\frac{1}{2}\pi r_e^2$ times the flux linking the circle $r = r_e$, $z = 0$, at any time, plus a constant which depends on the initial configuration of the magnetic field within the initial circle $r = r_0$, $z = z_0$ as well as the initial position and angular momentum of the electron.

The expansion of V_{M0}, expressed in terms of B_e and B_q with the relation between the spacial derivatives of B taken into account, takes the form:

$$\begin{aligned} V_{M0} = {} & \tfrac{1}{2}\frac{e}{m_0} r_e^2 B_q^2 + x\frac{e}{m_0} r_e B_q[B_e - B_q] \\ & + \tfrac{1}{2}x^2\frac{e}{m_0}[B_e^2 + 3B_q^2 - (3+n)B_e B_q] + \tfrac{1}{2}z^2\frac{e}{m_0} n B_e B_q \\ & + \tfrac{1}{6}x^3\frac{e}{m_0}\frac{1}{r_e}[-(3+3n)B_e^2 - 12B_q^2 + (12+4n+n_2)B_e B_q] \\ & + \tfrac{1}{2}xz^2\frac{e}{m_0}\frac{1}{r_e}[nB_e^2 - (n+n_2)B_e B_q], \end{aligned} \tag{55}$$

where the numerical coefficients n and n_2 are defined as:

$$n = -\frac{r}{B_z}\frac{\partial B_z}{\partial r}\bigg|_{\substack{r=r_e \\ z=0}}, \quad n_2 = \frac{r^2}{B_z}\frac{\partial^2 B_z}{\partial r^2}\bigg|_{\substack{r=r_e \\ z=0}}. \tag{56}$$

If the magnetic field varies synchronously in the region of validity of the expansion, n and n_2 are constants and the coefficients of the expansion are second order polynomials of the two variables B_e and B_q. These variables must be particular functions of time for particular modes of operation. To analyze all possible modes, it is convenient to assume at first that B_e and B_q vary independently and later to consider the effect of their actual functional dependence. The assumption

that B_e and B_q are arbitrary functions of time requires that the flux linking the circle $r = r_e$ and $z = 0$ and the field at that circle be controlled independently, and implies that the flux exterior to and linking the toroid is independent of the field within the toroid since some of the flux linking r_e is controlled by B_e. A large degree of independent control was actually obtained in an experimental double yoke magnetic circuit.

The analysis of the variation of the potential functions V_t is greatly facilitated by a diagram having B_e as abscissa, B_q as ordinate and showing curves for which the values of the coefficients of the expansions V_t, V_{M0} or V_E remain constant. Fig. 3 is such a diagram for a particular choice of geometrical parameters. The lines of constant coefficients of V_{M0} are conic sections and each coefficient is represented by a family of concentric and homothetic conics. For example, the lines of constant $\partial V_{M0}/\partial x$ are hyperbolas whose asymptotes are the B_e axis and the 45° line $B_q = B_e$. The asymptotes themselves are lines of $\partial V_{M0}/\partial x = 0$ and they divide the B_q–B_e plane into positive and negative regions of $\partial V_{M0}/\partial x$.

In the expansion of the electrostatic potential V_E, the coefficients are related by Laplace's equation, assuming the space charge to be negligible. Assuming also the spatial distribution of the electrostatic potential to remain similar to itself as the potential varies in time, that is, a synchronous variation of the electrostatic field, the ratios of $\partial^2 V_E/\partial x^2$ and $\partial^2 V_E/\partial z^2$ to $\partial V_E/\partial x$ remain constant, and it is possible to express them in terms of a numerical factor k:

$$\frac{\partial^2 V_E}{\partial z^2} = \frac{k}{r_e}\frac{\partial V_E}{\partial x} \quad \text{and} \quad \frac{\partial^2 V_E}{\partial x^2} = -\frac{k+1}{r_e}\frac{\partial V_E}{\partial x}. \tag{57}$$

The expansion of V_E limited to cubic terms is therefore:

$$V_E = V_E(0,0) + x\frac{\partial V_E}{\partial x} - \tfrac{1}{2}x^2\frac{k+1}{r_e}\frac{\partial V_E}{\partial x} + \tfrac{1}{2}z^2\frac{k}{r_e}\frac{\partial V_E}{\partial x} + \tfrac{1}{6}x^3\frac{\partial^3 V_E}{\partial x^3} + \tfrac{1}{2}xz^2\frac{\partial^3 V_E}{\partial x \partial z^2}. \tag{58}$$

The conditions (17) for stable equilibrium, or the existence of a minimum of the function $V_t = [V_M - V_E]$, can now be conveniently analyzed. In general, the capture of charge can occur as long as the minimum is within the toroidal region but we will consider at first only the case of electrons whose equilibrium orbit is always in the center of the toroidal region $x = 0$, $z = 0$, and later compare other captured electrons to these "normal" electrons. The first order condition (17a) requires that at all times:

$$\frac{\partial V_{M0}}{\partial x} = \frac{\partial V_E}{\partial x} = \frac{e}{m_0} r_e B_q [B_e - B_q]. \tag{59}$$

The lines of constant $\partial V_{M0}/\partial x$, identical with $\partial V_E/\partial x$, on the focusing diagram show what value of electric field must be applied for a given magnetic field B_e, and a given equivalent change of flux B_q in order to balance the electric, Lorentz and centrifugal forces at every instant.

Consider the location of the representative point on the B_q–B_e diagram for the instant of emission. ($\dot{\theta}_0$ is zero, neglecting the thermal velocities of emission.) The value of B_q can be expressed approximately in terms of B_e by expanding the integrals of equation (54):

$$B_q = sB_e = \left[-\frac{x_0}{r_e} + \frac{1-n}{2}\left(\frac{x_0}{r_e}\right)^2 - \frac{n}{3}\left(\frac{x_0}{r_e}\right)^3 - \frac{n}{2}\left(\frac{z_0}{r_e}\right)^2 \frac{r_0}{r_e} \right] B_e. \quad (60)$$

The constant s is hence approximately equal to $-(x_0/r_e)$, x_0 being the initial value of x. The representative point at the emission time is therefore on the $B_q = sB_e$ line shown on the figure for two values of $s = \pm 1/16$. Subsequent to emission, the value of B_q will increase in an actual induction accelerator since the kinetic energy is an increasing monotonic function of B_q. No matter how B_e is related to the increase of B_q, eventually the operating point (B_q, B_e) must end on or near the asymptote $B_q = B_e$ for otherwise the values of $\partial V_E/\partial x$ would have to become unpractically large to balance the magnetic and inertial forces which increase rapidly with speed. Therefore, the focusing problem consists essentially in analyzing the conditions at points between the lines $B_q = sB_e$ and $B_q = B_e$ and on the line $B_q = B_e$ itself. It is interesting to observe that these limiting lines are representative of the field conditions in a static magnetron and a purely magnetic betatron respectively. The electric field at the emission time

$$\left.\frac{\partial V_E}{\partial x}\right|_{t=t_0} = \frac{e}{m_0} r_e s(1-s) B_{e0}^2, \quad (61)$$

where B_{e0} is the value of B_e at $t = t_0$, is approximately the value of the cut-off electric field of the magnetron, while on the line $B_q = B_e$, the electric field is zero, the characteristic of a conventional purely magnetic betatron. The betatron with radial injection by an auxiliary electric field operates toward the end of the acceleration cycle, as a purely magnetic instrument. Thus, it may be considered as the superposition on a magnetic betatron with its main sinusoidal power source and synchronously varying magnetic field of auxiliary means to alter the field and flux by the incremental values B_{ec} and B_{qc} necessary to obtain equilibrium in combination with the electric field.

Consider now the conditions imposed on the variations of the magnetic and electric fields by the second order conditions (17b and c) for the existence of a potential minimum at $x = z = 0$. Since the values of

$\partial^2 V_E/\partial x^2$ and $\partial^2 V_E/\partial z^2$ are proportional to $\partial V_E/\partial x$, equations (57), they can be expressed in terms of B_e and B_q if it is assumed that the electric field $\partial V_E/\partial x$ is actually adjusted at every instant in accordance with the first order minimum condition (59). The second derivatives of V_t are thus:

$$\frac{\partial^2 V_t}{\partial x^2} = \frac{\partial^2 V_{M0}}{\partial x^2} - \frac{\partial^2 V_E}{\partial x^2}$$

$$= \frac{e}{m_0}\left[B_e^2 + 3B_q^2 - (3+n)B_eB_q + (k+1)B_q(B_e - B_q)\right], \quad (62)$$

$$\frac{\partial^2 V_t}{\partial z^2} = \frac{\partial^2 V_{M0}}{\partial z^2} - \frac{\partial^2 V_E}{\partial z^2} = \frac{e}{m_0}\left[nB_eB_q - kB_q(B_e - B_q)\right]. \quad (63)$$

The lines of constant curvatures $\partial^2 V_t/\partial x^2$ and $\partial^2 V_t/\partial z^2$ are conic sections depending on the parameters n and k characteristic of the geometrical configurations of the magnetic and electric fields. In order for these curvatures to be positive as the operating point moves from the line $B_q = sB_e$ to and on the line $B_q = B_e$, these parameters must have appropriate values. The value of n must satisfy the relation, $0 < n < 1$, as in condition (22), of the limiting magnetic betatron. This can be seen by making $B_q = B_e$ in equations 62 and 63.

The permissible limits of k can be found by considering at first the lines of constant $\partial^2 V_t/\partial z^2$ which form a family of concentric and homothetic hyperbolas whose asymptotes, or lines of zero value, are the lines $B_q = 0$ and $B_q = B_e(1 - n/k)$. Obviously, the operating line must not cross the asymptotes, so that for the starting point (B_{q0}, B_{e0}) on the line $B_q = sB_e$, B_{q0} must be positive or $sB_{e0} > 0$. This means that the initial magnetic field must be positive with an internal cathode ($s > 0$) and negative for an external cathode ($s < 0$) as illustrated on the focusing diagram. In order for the asymptote $B_q = B_e(1 - n/k)$ to be outside of the operating angle, it is easy to show that $k < (n/1 - s)$ for $s > 0$ and $k > (n/1 - s)$ for $s < 0$.

The lines of constant $\partial^2 V_t/\partial x^2$ are ellipses if the discriminant of the polynomial in B_e and B_q is negative, a condition occurring when:

$$n - 2\sqrt{1-n} < k < n + 2\sqrt{1-n}. \quad (64)$$

If k lies outside of the limits of this inequality the equivalue lines $\partial^2 V_t/\partial x^2$ are hyperbolas and there are points in the B_q, B_e plane for which $\partial^2 V_t/\partial x^2 < 0$. It can be shown that, if $0 < n < 1$ and the inequalities required by $\partial^2 V_t/\partial z^2 > 0$ are satisfied, some of these negative points are necessarily in the operating angle, so that inequalities (64) must be satisfied.

The focusing conditions in the radial and axial directions within

the operating ranges are therefore:

$$0 < n < 1,$$

$$n - 2\sqrt{1-n} < k < \frac{n}{1-s} \quad \text{for internal cathode } s > 0,$$

$$\frac{n}{1-s} < k < n + 2\sqrt{1-n} \quad \text{for external cathode } s < 0. \tag{65}$$

The parameters used in drawing the diagram of Fig. 3 are those of an experiment performed by the authors. The magnetic field was so adjusted that the measured values were $r_e = 1.6''$, $n = .565$ and $n_2 \cong 0$. The two cylindrical electrodes both carried electron emissive areas so that either could be made the cathode. ($x_0 = \pm .1''$, making $s = \mp \frac{1}{16}$.) See Fig. 6. A definite curvature of electric field was obtained by adjusting the potential of the end shields or "hats." Measurements in an electrolytic tank of a scale model showed that when the hats were connected to the cathode $k = -.6$ for an internal cathode and $k = 1.15$ for an external cathode. These values of s, k and n satisfy the inequalities (65).

With the help of the focusing diagram, feasible modes of operation can be predicted by considering what variations of magnetic field increment B_{ec}, flux increment B_{qc} and electric field $\partial V_E/\partial x$ produce focusing and among them, which are most easily obtained in practice. Linear variations of the flux B_q and field B_e are particularly simple if the corresponding lines in the diagram are parallel to the asymptotes of the equivalues of $\partial V_{M0}/\partial x$ because the required variation of $\partial V_E/\partial x$ is then also linearly related to the field or flux. For short enough phase angles of a sinusoidal drive, these variations are also linear with respect to time. Two such operating lines have been shown on the focusing diagram, one for an internal and the other for an external cathode, and the corresponding time variations in Fig. 4. It can be observed in the case of an internal cathode, that B_q takes two different values for some values of B_e so that B_e must necessarily be non-monotonic and consequently both field and flux must be controlled by the increments B_{ec} and B_{qc}. On the other hand, control of the flux alone is sufficient with an external cathode. In this case, at the emission time, the magnetic field is negative and therefore defocusing in the axial direction. The electric field overcompensates that effect and is also responsible for giving stability to the electron orbits at the instant when there is no magnetic field at all. This shows, incidentally, that the B_q axis illustrates the conditions of a purely electrostatic system.

The focusing diagram showing the conditions for a minimum at $x = z = 0$ is convenient for finding further conditions for capturing the charge. It is evident that a finite range of electron emission times must be considered, for infinite current densities would be necessary if

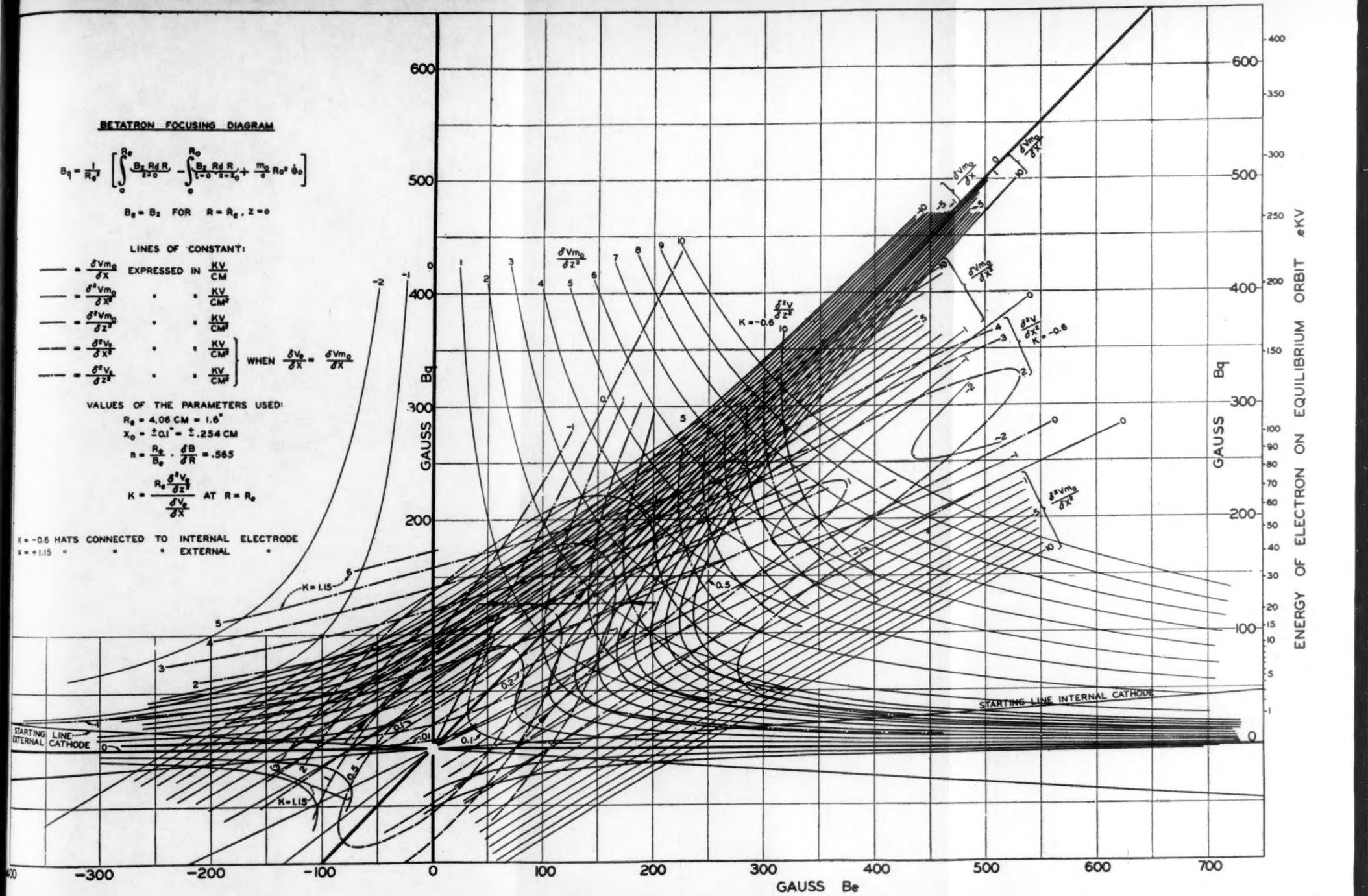
BETATRON FOCUSING DIAGRAM
$B_q = \frac{1}{R_0^2}\left[\int_0^{R_0} \frac{B_z R d R}{z=0} - \int_0^{R_0} \frac{B_z R d R}{t=0\ z=z_0} + \frac{m_0}{e} R_0^2 \dot{\theta}_0\right]$
$B_e = B_z$ FOR $R = R_0$, $z = 0$
LINES OF CONSTANT:
$= \frac{\delta V m_0}{\delta x}$ EXPRESSED IN $\frac{KV}{CM}$
$= \frac{\delta^2 V m_0}{\delta x^2}$ " " $\frac{KV}{CM^2}$
$= \frac{\delta^2 V m_0}{\delta z^2}$ " " $\frac{KV}{CM^2}$
$= \frac{\delta^2 V_0}{\delta x^2}$ " " $\frac{KV}{CM^2}$
$= \frac{\delta^2 V_0}{\delta z^2}$ " " $\frac{KV}{CM^2}$
WHEN $\frac{\delta V_0}{\delta x} = \frac{\delta V m_0}{\delta x}$
VALUES OF THE PARAMETERS USED:
$R_0 = 4.06\ CM = 1.6"$
$X_0 = \pm .01" = \pm .254\ CM$
$n = \frac{R_0}{B_0} \cdot \frac{\delta B}{\delta R} = .565$
$K = \frac{R_0 \frac{\delta^2 V_0}{\delta z^2}}{\frac{\delta V_0}{\delta x}}$ AT $R = R_0$
K = -0.6 HATS CONNECTED TO INTERNAL ELECTRODE
K = +1.15 " " " EXTERNAL "
GAUSS Bq
GAUSS Be
ENERGY OF ELECTRON ON EQUILIBRIUM ORBIT eKV
STARTING LINE INTERNAL CATHODE
STARTING EXTERNAL LINE-CATHODE
K=1.15
K=-0.6

FIG. 3. Betatron focusing diagram.

the o

T
an ex
adjus
The t
that
$s = z$
tained
urem
hats
and
satisf
W
can b
creme
ing a
Linea
the c
of the
is the
angle
to tir
diagr
the c
case
value
quent
and I
an ex
field
electr
giving
magn
trates
T
$x = z$
the cl
must

all the emission were to occur at one particular instant. For every emission time there is a different potential function V_{M0} because the constant C involving the initial flux is different. Since the electrostatic potential V_E is necessarily the same for all electrons, the minima of $V_t = V_{M0} - V_E$, if existing, will be, in general, at different instantaneous positions x_i and have different curvatures $\partial^2 V_t/\partial x^2$ and $\partial^2 V_t/\partial z^2$ for each electron. The electrons will be captured for such shifts of instantaneous orbits x_i and such changes in the depth of the potential trough which will effectively prevent them from hitting the bounding electrodes. It is obvious that the initial position x_{i0} of the instan-

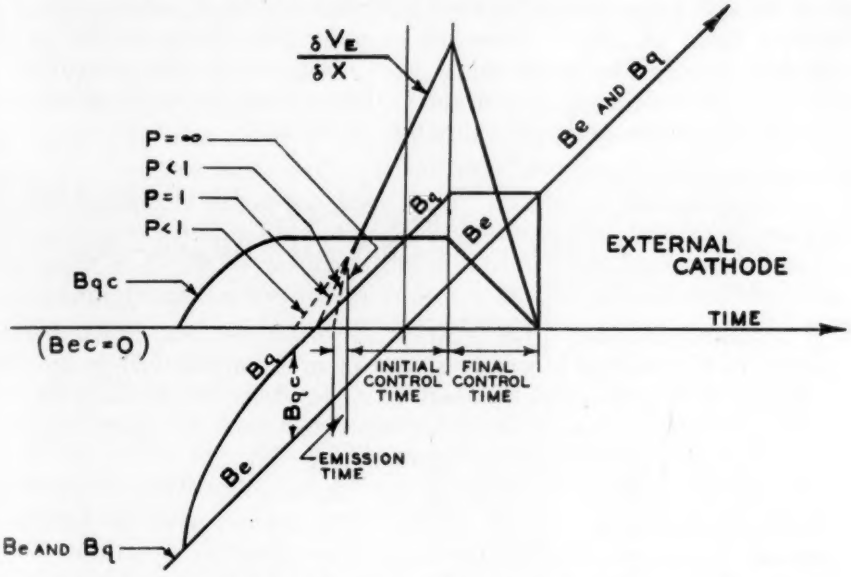

FIG. 4. Time variation of the magnetic field, magnetic flux and electric field.

taneous equilibrium orbit x_i, must be closer to the cathode than the anode;

$$0 < \frac{x_{i0}}{x_0} < 1. \tag{66}$$

Furthermore, if at no time the orbit is closer to the cathode or anode than it was originally to the cathode, or

$$|x_i| < |x_{i0}|, \tag{67}$$

capture will be insured as long as $\partial^2 V_t/\partial x^2$ and $\partial^2 V_t/\partial z^2$ remain no smaller than their initial values.

We shall restrict the analysis to the case, described above, of linear field variations providing an equilibrium at $x = 0$ for so-called normal electrons for which the variables $B_q = B_{qn}$, B_e and $\partial V_E/\partial x$ satisfy

equation (59) and B_{qn} is given on the successive segments of the operating line by:

$$B_{qn} = B_e - (1 - s)B_{e0n},\ B_{qn} = \text{constant},\ B_{qn} = B_e, \tag{68}$$

while $\partial V_e/\partial x$ can be expressed on the first of these by:

$$\frac{\partial V_E}{\partial x} = \frac{e}{m_0} r_e(1 - s)B_{e0N}(B_e - (1 - s)B_{e0N}), \tag{69}$$

where B_{e0N} is the initial value, B_{e0}, of B_e at the emission time of the normal electron. The potential V_{M0} of other electrons finding themselves in the same magnetic field will depend on B_e and a value B_q differing from B_{qn} by a constant amount ΔB_q characteristic of the emission time. The position of the minimum of the potential $V_t = V_{M0} - V_E$ will be at a position x_i determined for times subsequent to normal emission and approximately equal to:

$$x_i = \frac{-\dfrac{\partial V_t}{\partial x}}{\dfrac{\partial^2 V_t}{\partial x^2}} = -r_e \frac{\Delta B_q(B_e - 2B_{qN})}{B_e^2 + 3B_q^2 - (3+n)B_eB_q + (k+1)B_{qN}(B_e - B_{qN})}. \tag{70}$$

The initial equilibrium orbit position x_{i0} of an electron emitted subsequently to the normal electron is seen from equation (70) to have the same sign as B_{e0}, therefore opposite to x_0, in violation of condition (66), an understandable result since for late electrons the electric field is stronger than cut-off of an analogous magnetron.

Therefore, only early electrons are capturable. Whether this will actually occur depends on the electric field, which, prior to the normal emission, is not specified by the normal equilibrium equations 59 and 69. It will be assumed to vary linearly with B_e at a rate p times faster than immediately subsequent to normal emission. With this assumption, both V_{M0} and V_E are determined for early electrons and it is possible to compute the instantaneous position x_i of the potential minimum of $V_t = V_{M0} - V_E$ for each instant t and each emission time t_e in the emission period extending from the instant t_0 at which the electric field is zero to the instant t_n of the emission of the normal electron. It is convenient to introduce the numerical factors $q = t_e/(t_n - t_0)$ characteristic of the emission time and $\lambda = t/(t_n - t_e)$ characteristic of any instant in the period between the emission of any electron and the normal electron. With these abbreviations, the result of the computation is:

$$x_i = x_0(1 - q)\left(1 - \lambda + \frac{\lambda}{p}\right), \tag{71}$$

when terms in $(x_0/r_e)^2$ are neglected with respect to terms in (x_0/r_e).

Therefore the initial position x_{i0} of the position minimum ($\lambda = 0$) and the position x_{in} at the time of the normal emission ($\lambda = 1$) are:

$$x_{i0} = x_0(1 - q), \tag{72}$$

$$x_{in} = x_0 \frac{(1 - q)}{p}. \tag{73}$$

Equation (72) shows that the initial equilibrium orbit is at the cathode for the earliest emission time ($q = 0$) and in the center of the tube at the latest ($q = 1$). The amplitude of oscillation at the emission time of any electron is $(x_0 - x_{i0}) = |qx_0|$ and becomes slightly smaller at the normal emission time in virtue of the increase of $\partial^2 V_t/\partial x^2$ in the interim.

At the instant of emission of the normal electron, there are already in the tube a series of electrons all oscillating around different equilibrium orbits with different amplitudes. In order for (x_{in}) to be less than (x_{i0}) in accordance with relation (67), p must be greater than one. At the limiting value when the rate of change of the electric field at the emission period is equal to the rate subsequent to normal emission time, or $p = 1$, the instantaneous equilibrium orbit of any electron does not change from the instant of emission to the normal emission time, $x_i = x_{i0} = x_{in}$, and the electrons all oscillate so as to come back to the cathode at each swing.

After the emission of the normal electrons, the position x_i of the equilibrium orbits is given by equation (70). The constants ΔB_q can be eliminated by comparing the instantaneous equilibrium positions x_i, to those, x_{in}, the electrons had at the time t_n of the emission of the normal electron:

$$\frac{x_i}{x_{i_n}} \cong \frac{B_e - 2B_{qN}}{B_{e0N} - 2B_{q0N}} \frac{\left.\dfrac{\partial^2 V_t}{\partial x^2}\right|_{t_n}}{\left.\dfrac{\partial^2 V_t}{\partial x^2}\right|_{t}} = f_n. \tag{74}$$

The function f_n is determined for every point of the operating line on the B_q–B_e diagram. For the lines shown in Fig. 3, for an external cathode f_n varies from 1, passes through a maximum of 2 and eventually tends asymptotically to zero, while for an internal cathode f_n varies from one, passes through zero to a minimum value of -2.5 and eventually also tends to zero.

The position x_i of the orbit at any time subsequent to the emission period can be compared now to its initial position by combining equations (72), (73) and (74).

$$\frac{x_i}{x_{i0}} = \frac{f_n}{p}, \tag{75}$$

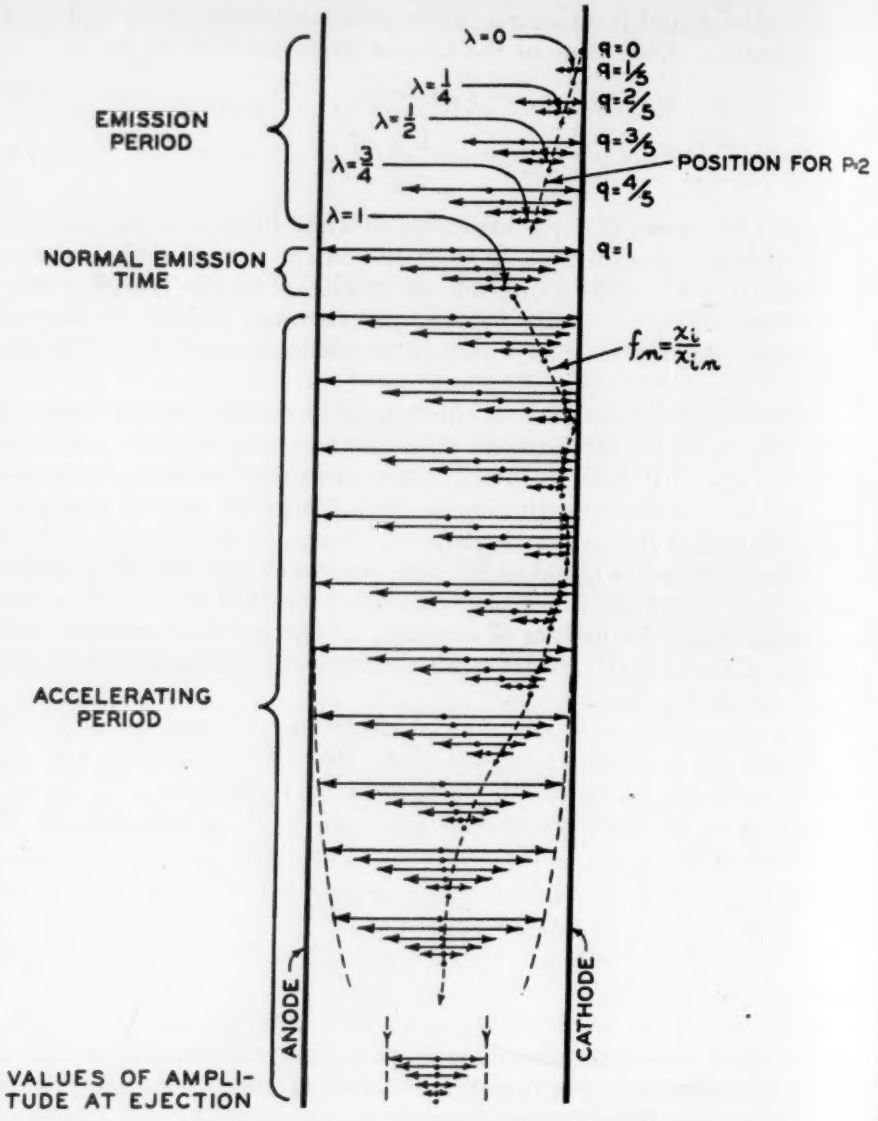

FIG. 5. Schematic history of oscillations.

showing that x_i/x_{i0} is independent of the emission time q. In order to satisfy condition (67):

$$p \geq |f_n|_{\max}. \tag{76}$$

This shows that the rate of increase of the electric field during emission time must be greater than subsequently by a factor p which depends on the particular subsequent mode of operation. In our example $p > 2$ for external cathode and $p > 2.5$ for internal cathode. Higher rates

than necessary insure more positively that the electrons will miss striking the bounding electrodes but the emission period is shortened so that high cathode emission is necessary to inject a given charge. However, for most practical parameters, as in the examples illustrated, the emissivity of the cathode is no limiting factor.

The schematic history of the instantaneous equilibrium position and amplitude of oscillation of Fig. 5 summarizes graphically the above considerations. When the electric field becomes zero, the conditions are those of a purely magnetic betatron and the instantaneous orbits tend towards the center while the amplitude of oscillation diminishes, as explained before.

The analysis of the emission period made above on the basis of the motion of the electrons in the radial direction only, were based on the two first terms of the expansion of the potential of forces. Actually, the two dimensional motion in the r-z plane should be considered by taking into account the effects of the actual boundaries, such as the cathode, for which the second order terms approximation breaks down. Such a detailed analysis was made for a specific example by using the cubic terms for V_{M0} and an actual electrolytic plot for V_E and confirmed essentially the conclusions of the simpler analysis.

The magnetic field B_e, the flux linking the circle $r = r_e$, $z = 0$, as characterized by B_q, and the electrostatic field $\partial V_E/\partial x$ must be related through equation (59) at all times. It is significant to consider the tolerances on the variations of these variables by computing the differential changes in the time variables which cause a shift Δx in the equilibrium orbit:

$$\Delta\left(\frac{\partial V_E}{\partial x}\right) = -\Delta x \frac{\partial^2 V_t}{\partial x^2}, \tag{77}$$

$$\Delta B_q = -\Delta x \frac{\dfrac{\partial^2 V_t}{\partial x^2}}{\dfrac{e}{m_0} r_e(B_e - 2B_q)}, \tag{78}$$

$$\Delta B_e = -\Delta x \frac{\dfrac{\partial^2 V_t}{\partial x^2}}{\dfrac{e}{m_0} r_e B_q}. \tag{79}$$

The maximum permissible value of Δx is the space between the point of maximum oscillating displacement and the cathode or anode, which for times subsequent to the emission period is:

$$\Delta x = (1 - q)\left(\pm 1 - \frac{f_n}{p}\right) x_0. \tag{80}$$

It is apparent that there is no tolerance for the normal electron ($q = 1$), and the maximum tolerance for the earliest emitted electron ($q = 0$). If half of the initial emission is sacrificed a reasonable value for Δx is $\pm x_0/4$ for practical values of f_n and p.

The tolerances for the operating lines shown on the focusing diagram are as follows: Since $\partial^2 V_t/\partial x^2$ remains approximately constant when $\partial V_E/\partial x \neq 0$, the absolute tolerance of $\partial V_E/\partial x$ remains constant and tends to a minimum relative error of .6 per cent at maximum voltage. The tolerance ΔB_q is expressible as

$$\Delta B_q = \frac{\Delta x}{x_0} \cdot \frac{s(1-s)}{f_n} B_{e0N},$$

so that the least relative tolerance in the control flux B_{qc}, $\Delta B_q/B_{qc} = \Delta B_q/B_{e0N}$ is about .5 per cent. for the maximum value of f_n. Similarly, the relative tolerance in B_e is of the order of .7 per cent., well within the approximate linearity of a sine function at the phase angles of the injection period. These tolerances of a few tenths of a per cent. on the variation of the electric field and magnetic flux constitute very close requirements for electronic circuits controlling appreciable power at reasonably high frequencies.

The ejection of the accelerated charge in a betatron with a system of injection using a radial electric field can of course be obtained by a non-synchronous change of flux or field as is done in the purely magnetic betatron. It could be achieved also, in principle, by applying an ejecting electric field on the existing injecting electrode structure. However, the required gradients would be impractically high.

It was shown that space charge determines the ultimate limit to the charge which can be captured and accelerated. In the purely magnetic betatron this limit increases with the energy of the electrons so that far more charge is potentially supportable near ejection time than can possibly be introduced at injection time. As mentioned before, the addition of an electrostatic field might be expected to provide a means for taking some advantage of this potentiality since the electrons could be injected into a much stronger initial magnetic field, as is the case in static magnetrons which are known to have high current densities. Actually the gain of supportable charge can be only very small, for the following reasons.

The Laplacian of the magnetic potential was shown to represent the limiting space charge density of stationary electrons at any point. This limit ρ at the minimum of V_M can be found by introducing the equilibrium condition $\frac{\partial V_E}{\partial r} = \frac{\partial V_M}{\partial r}$ into equation (27).

$$\rho = \epsilon_0 \left\{ \frac{\left(\frac{\partial V_E}{\partial r}\right)^2}{2V_M} + \frac{2V_M}{r^2} \right\}. \tag{81}$$

For a given electric field $\partial V_E/\partial r$, ρ is a minimum when $V_M = \frac{r}{2}\left|\frac{\partial V_E}{\partial r}\right|$, a value which V_M must assume necessarily at some time since it passes continuously from nearly zero at emission time to values much larger than $\frac{r}{2}\left|\frac{\partial V_E}{\partial r}\right|$. Therefore, the upper limit of capturable space charge density at the minimum of the potential for a given largest value of the electric field is:

$$\rho = \epsilon_0 \frac{2}{r}\frac{\partial V_E}{\partial r}, \tag{82}$$

whatever the particular variation of the magnetic flux and fields and electric field chosen to satisfy the equilibrium conditions. The similar limit for a purely magnetic instrument was found to be equation (27), $\rho = \epsilon_0 \frac{2V_M \text{ injection}}{r^2}$, and therefore the relative gain in space charge density obtained from the electric field can be at most $\frac{\partial V_E}{\partial r}\frac{r}{V_M}$. If the maximum voltage V_E applied across the tube is equal to the injection voltage, this ratio becomes approximately $r/\Delta r$, assuming the gradient at r to be equal to the average gradient. The ratio of capturable charges themselves will be also $r/\Delta r$ if the volumes occupied by the charges are the same in both cases. In practice, however, the region of acceleration is smaller for radial injection, while the limit imposed by breakdown on the applicable voltage is likely to be higher. Therefore, the gain in space charge limit, if any, is not very important.

In the example used in the preceding analysis, the actual limit of capturable charge can be estimated by applying Gauss' theorem over the bounding electrodes.

$$Q = \epsilon_0 \int\int_S \text{grad}_n\, V_t ds \cong \epsilon_0 4\pi r_e \left[z_0 \left.\frac{\partial V_t}{\partial x}\right|_{\substack{x=x_0\\z=0}} + x_0 \left.\frac{\partial V_t}{\partial z}\right|_{\substack{x=0\\z=z_0}} \right]. \tag{83}$$

The value of $\left.\frac{\partial V_t}{\partial x}\right|_{\substack{x=x_0\\z=0}}$ can be approximated by assuming a parabolic variation of V_t in the radial direction, while the value of $\left.\frac{\partial V_t}{\partial z}\right|_{\substack{x=0\\z=z_0}}$, which is very sensitive to the sharp boundary conditions due to the hats, can be conveniently assumed equal to $\frac{x_0}{z_0}\cdot\left.\frac{\partial V_t}{\partial x}\right|_{\substack{x=0\\z=0}}$. Hence Q is approximately:

$$Q = \epsilon_0 4\pi r_e \frac{\partial^2 V_t}{\partial x^2} x_0^2 \left[\frac{z_0}{x_0} + \frac{x_0}{z_0}\right]. \tag{84}$$

Since Q is proportional to $\partial^2 V_t/\partial x^2$, it will be most for a given $\partial V_E/\partial x$ at a time when $\dfrac{\partial V_E}{\partial x} \Big/ \dfrac{\partial^2 V_t}{\partial x^2}$ is extremum or, on the focusing diagram, when an elliptical equivalue of $\partial^2 V_t/\partial x^2$ is tangent to a hyperbolic equivalue of $\partial V_E/\partial x$. For this point the discriminant of the quadratic equation for B_q^2, which can be obtained by substituting B_e from equation (63) in equation (62), is zero, a condition occurring when:

$$\frac{\partial V_E}{\partial r} = \frac{\partial^2 V_t}{\partial x^2} r_e \frac{(k-n) \pm 2\sqrt{1-n}}{(k-n) - 4(1-n)}, \tag{85}$$

in which the plus sign refers to an external and the minus to an internal cathode. Therefore Q:

$$Q = 4\pi\epsilon_0 x_0^2 \frac{(k-n) - 4(1-n)}{(k-n) \pm 2\sqrt{1-n}} \left[\frac{z_0}{x_0} + \frac{x_0}{z_0}\right] \frac{\partial V_E}{\partial x}$$

$$= 4\pi\epsilon_0 x_0^2 h \frac{\partial V_E}{\partial x} \simeq 2\pi\epsilon_0 x_0 h V_{E\,\max}, \tag{86}$$

is seen to be proportional to the maximum applied voltage, the linear dimensions, and a factor h which depends on the geometry of the boundaries of the fields. Actually, this optimum ratio of $\partial V_E/\partial x$ to $\partial^2 V_E/\partial x^2$ is not realized if the three equilibrium variables, magnetic flux and field and electric field vary linearly with respect to each other. Taking this factor into account, for the parameters indicated on the diagram and a maximum applied voltage of 4,000 volts, this maximum charge turns out to be 5×10^{-11} coulomb.

EXPERIMENTAL.

In order to investigate the injection mechanisms and current limitations the present authors built a small but special betatron with which some relevant experimental results were obtained.

The primary feature of the magnetic circuit was the independent control of the field at—and the flux linking—the main equilibrium orbit. The pole pieces were composed of two coaxial sets, an outer set with a return link in the form of a C carrying the field exciting coils, and an inner set relying on leakage for a return path and having its flux coils inside of the hollow outer pieces. This shape of the outer poles minimized the leakage between the inner and outer circuits so that only one-fifth of the variation on one was perceptible in the other. A coil on the outer circuit in series with a coil on the inner, tuned by a bank of condensers to the driving frequency of 420 cycles, was coupled through a transformer to a 5 KW generator. This main circuit was adjusted to produce the conventional magnetic betatron field with its 1:2 condition for the equilibrium orbit. Another system of coils comprising one on

the outer field link in antiseries with another on the inner, flux pole piece was adjusted to have no coupling with the main circuit. The excitation of this auxiliary, isolated circuit produced a differential in the flux and field and could be used for both ejection and injection in experiments either with conventional injection or with an additional electric field. Fig. 6 shows a cross section of the pole pieces.

The ends of the outer pieces were made of laminations stacked radially in a bakelite holder and forming a 78° cone of about $4\frac{3}{8}''$ diameter which produced the radial variation of field shown in Fig. 1. The remainder of the pole pieces consisted of a sheet of steel wound with proper insulation in a spiral to form an approximate cylinder $3\frac{3}{8}''$ high, $3\frac{1}{2}''$ I.D., $4\frac{3}{8}''$ O.D. This wound section equalized the flux angularly to better than 1 per cent. in spite of dissymmetries in the air gaps between the pole pieces and the yoke. The inner pole pieces were laminated cylinders, 1″ in diameter.

Measurements of the field distribution showed that when the angular dissymmetry exceeded 4 per cent. no tubes were operative, but improvement down to 1 per cent. had no further beneficial effect in conventional, purely magnetic betatrons. Instead of computing the main potential function from the radial distribution of the magnetic field obtained with a search coil, it was found less tedious to use a special system of 23 concentric coils whose numbers of turns were made inversely proportional to their respective radii. The position of the equilibrium orbit could be determined easily by switching to the coil with minimum signal on a peak voltmeter. The position of the equilibrium orbit at injection was obtained from a direct measurement while that at ejection was obtained by first passing the signal through an integrating circuit.

The glass envelope of the purely magnetic betatron had the shape of a doughnut $4\frac{1}{2}''$ O.D., $1\frac{3}{8}''$ I.D., and was blown by conventional techniques with the help of special carbon molds. The internal glass surface was platinized to insure that all the region of electron acceleration is an electrostatic equipotential. To prevent excessive heating by eddy currents, this metallization was very thin and was interrupted along a radius. The electron injector sealed in a side tube was of conventional type including an oxide coated cathode (or tungsten filament), a focusing negative element and an accelerating anode, and was made to inject electrons in both directions so that some charge was captured at each half cycle. The target was a tungsten rod mounted on the side diametrically opposed to the gun and on the inside of the equilibrium orbit.

An attempt was made at first to make the gun as small as possible (distance d from electron emission point to edge of gun .016″) in order to minimize its obstruction effects. It was soon observed, however, that the output increased with the voltage far beyond the limit given

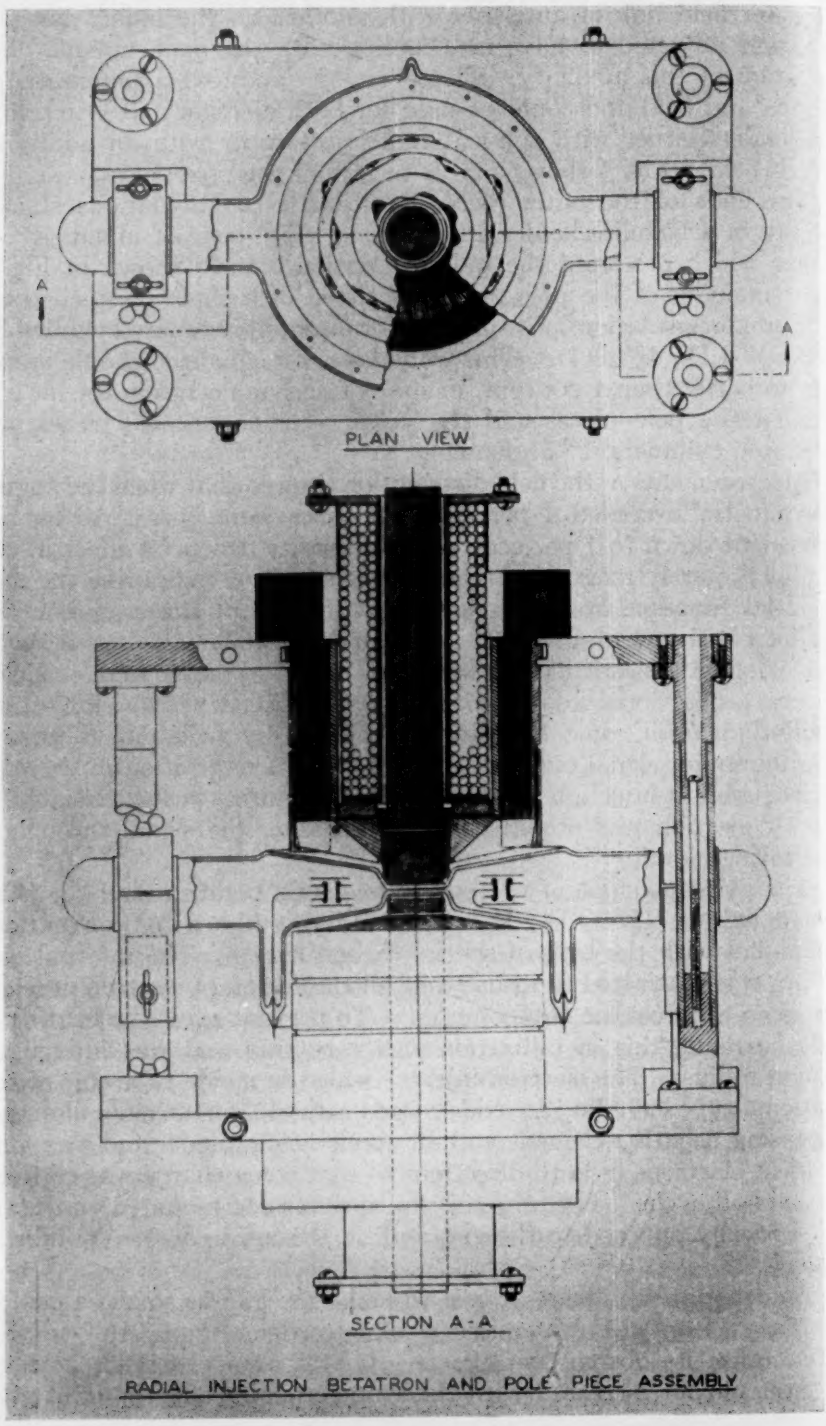

FIG. 6. Cross-section of pole pieces and tube for radial injection test.

by the elementary notion by which missing of the gun occurs and the practical limit was the voltage breakdown of the gun. Larger guns ($d = .055''$) supported more voltage and provided more output. An auxiliary experiment was made in this connection. As an obstructing vane protruded into the orbital region for a distance varying up to about d beyond one of these large guns, the output at constant voltage diminished gradually to zero. The exact measurement of the dependence of the output on the voltage of injection was complicated by the fact that the output is a critical function of the heater current and the grid bias. In spite of these, it was observed: that there is a threshold injection voltage of a few hundred volts below which no output could be detected, there is a general trend of increase of the output with the voltage, and finally that there are large fluctuations superimposed on that trend. Although no definite explanation of these observations is offered, it is probable that the threshold voltage is related to the scattering of slow electrons in their long, low velocity paths and that the general increase of output is due to the deeper potential troughs at higher voltages. An increase of the beam current at a given voltage of injection, resulting from the control of the grid bias or heater current, resulted in an initial increase of the output up to a flattening point, and for low injection voltages, to a maximum beyond which the output seemed actually to decrease. These effects are due probably to the role the space charge is playing in the mechanisms of missing the gun.

The output of the betatron was measured by the radiated X-rays rather than by the difficult direct measure of the small, high speed electron target current. The most sensitive detector was a Geiger-Mueller counter used either with an electronic counter or an oscilloscope. A slightly less sensitive but far more convenient instrument was obtained in irradiating a fluorescent screen with the X-rays and measuring the visible light thus produced with a multiplier phototube. The electrostatic focusing of the multiplier (RCA 931A or 1P22) being spoiled by the strong stray magnetic field near the betatron tube itself, it was necessary to remove the phototube to a distance of about 40 cm. and use an optical system to gather as much light as possible from the screen. A zinc sulfide screen (RCA Code 33-z-20A) with a time constant of about 100 microseconds was found particularly sensitive. Phase measurements of the X-ray bursts were made possible by displaying the multiplier output on an oscilloscope, while an accurate quantitative measurement of the intensity was obtained by a direct measure of the D.C. output current of the multiplier. The multiplier X-ray meter was calibrated with respect to a standard Victoreen Roentgen meter. The Victoreen meter itself was also used for the measurement of the stronger radiations of the betatron at the higher output level.

Absorption measurements of the hardness of the betatron radiation were consistent with the electron energies computed from flux measure-

ments. Energies of 800 KV with an equilibrium orbit at 1.3″ to 1.6″ in a field of about 1,000 gauss were typical of our small instrument. The highest observed average output current was estimated at .02 microampere on the basis of extrapolation from the results of Van Atta and Northrup giving the yields of X-rays for high speed electrons. This was obtained with an injection at every half cycle (840 times a second) with a pulsed injection voltage of 3,000 volts from a gun located at $r = 1.9''$ and an equilibrium orbit $r_e = 1.3''$. The limit of capturable space charge in the "normal" potential trough corresponding to those parameters is of the order of 4×10^{-9} coulomb and therefore about 160 times more than the observed amount. This large discrepancy may be due to the fact that most electrons which succeed in missing the gun are actually captured in a much shallower potential trough, as was explained in the theory.

An interesting phenomenon (40) observed with the multiplier phototube detector is the occurrence of multiple—most frequently double—peaks of X-rays in each quarter cycle when ejection was by means of the slow shift of the equilibrium orbit resulting from the saturation of a central core. The relative strength and phase of those peaks depended on the intensity of excitation of the magnet and all parameters of the gun injection. This effect is consistent with the view that the electrons are grouped in definite families according to their emission time and that they oscillate all at different amplitudes which do not diminish by a large proportion in a device with a relatively small final energy so that they can be "skimmed off" by the target at definite phases in the slow shift of their orbits.

An experimental test of a betatron with an additional electric field yielded a negative result. It required, unfortunately, rather elaborate techniques. The glass envelope had to have a re-entrant shape to permit the introduction of the ring shaped cathode-anode structure, shown in Fig. 7 which also illustrates the detail of the pole piece construction. The necessary variations of the magnetic flux and field and of the electric field required special electronic circuits. The linearity of the variations of the electric field was obtained by charging and discharging a condenser with a constant current from current regulating tubes while the linear variations of the flux were obtained by applying suddenly, constant voltages derived from a thyratron tube to the almost entirely inductive coils of the control circuit. The variations of the parameters were within tolerances of the best checking instruments which themselves were just about at the limit of the theoretically computed tolerances. It is probable that by varying the parameters near their nominal values, the tube was actually tested under operative conditions. The lack of output resulted most likely from the defects in angular symmetry, which in spite of every effort—machining of the electrodes, careful tube centering and improvements

in pole piece construction—remained sufficient for the electrons to experience some obstruction in their multiple initial swings to and from the cathode.

ACKNOWLEDGMENT.

The authors wish to express their appreciation to Dr. V. K. Zworykin for his guiding interest and continued encouragement in their work.

REFERENCES.

Articles

1. BREIT, G., TUVE, M. A., AND DAHL, O., Carnegie Institution Year Book (1927–28), No. 27, p. 209.
2. WIDEROE, R., "Über ein neues Prinzip zur Herstellung hoher Spannungen," *Archiv f. Elektrotechnik*, **21**, 387–406 (1928).
3. WALTON, E. T. S., "The Production of High-speed Electrons by Indirect Means," *Proc. Camb. Phil. Soc.*, **25**, Part IV, 469–481 (October 1929).
4. JASSINSKY, W. W., *Journal of Experimental and Theoretical Physics, U.S.S.R.*, **5**, 983 (1935).
5. JASSINSKY, W. W., *Electricity, U.S.S.R.*, **3**, 37 (1936).
6. JASSINSKY, W. W., "Beschleunigung der Elektronen im Elektromagnetischen Weschselstromfeld," *Archiv f. Elektrotechnik*, **30**, 590–603 (1936).
7. VAN ATTA, L. C., AND NORTHRUP, "Measurement of X-ray Production," *Am. J. Roentgen. Rad. Ther.*, **41**, 633 (1939).
8. KERST, D. W., Letter to the Editor: "Acceleration of Electrons by Magnetic Induction," *Phys. Rev.*, **58**, 841 (1940).
9. KERST, D. W., "The Acceleration of Electrons by Magnetic Induction," *Phys. Rev.*, **60**, 47–53 (July 1941).
10. KERST, D. W., AND SERBER, R., "Electronic Orbits in the Induction Accelerator," *Phys. Rev.*, **60**, 53–58 (July 1941).
11. KERST, D. W., Abstract: "Induction Electron Accelerator," *Phys. Rev.*, **59**, 110 (1941).
12. TERLETZKY, J. P., *Journal of Experimental and Theoretical Physics, U.S.S.R.*, **11**, 96 (1941).
13. KERST, D. W., "A 20-Million Electron-Volt Betatron or Induction Accelerator," *Rev. Sci. Inst.*, **13**, 387–394 (1942).
14. KERST, D. W., "The Betatron," *American Journal of Physics*, **10**, No. 5, 219–224 (October 1942).
15. KERST, D. W., "The Betatron," *Radiology*, **40**, 115–119 (1943).
16. KOCH, H. W., KERST, D. W., AND MORRISON, P., "Experimental Depth Dose for 5, 10, 15 and 20 Million Volt X-rays," *Radiology*, **40**, 120–127 (1943).
17. STEENBECK, M., "Beschleunigung von Elektronen durch elektrische Wirbelfelder," *Naturwiss.*, **31**, 234–235 (May 7, 1943).
18. IWANENKO, D., AND POMERANCHUK, I, *C. R. Acad. Sci. U.S.S.R.*, **44**, 315 (1944).
19. IWANENKO, D., AND POMERANCHUK, I., *Phys. Rev.*, **65**, 343 (1944).
20. WANG, T. J., "The Betatron," *Electronics* (June 1945).
21. VEKSLER, V., "A New Method of Acceleration of Relativistic Particles," *Journal of Physics, U.S.S.R.*, IX, No. 3, 153 (1945).
22. TERLETZKY, J., "On the Stability of the Electron Motion in the Induction Accelerator of the Betatron Type," *Journal of Physics, U.S.S.R.*, IX, No. 3, 159 (1945).
23. WESTENDORP, W. F., AND CHARLTON, E. E., "A 100-Million Volt Induction Accelerator," *J. Appl. Physics*, **16**, 591 (1945).
24. WESTENDORP, W. F., *J. App. Physics*, **16**, 657 (1945).
25. MCMILLAN, EDWIN M., "The Synchrotron, a Proposed High Energy Particle Accelerator," *Phys. Rev.*, **68**, 143 (Sept. 1945).
26. MCMILLAN, EDWIN M., "Radiation from a Group of Electrons Moving in a Circular Orbit," *Phys. Rev.*, **68**, 144 (Sept. 1945).

27. BLEWETT, JOHN P., "Radiation Losses in the Electron Induction Accelerator," *Phys. Rev.*, 69, 87 (1946).
28. ARZIMOVICH, L., AND POMERANCHUK, I., "The Radiation of Fast Electrons in the Magnetic Field," *Jour. of Phys. of the U.S.S.R.*, IX, 267 (1945).
29. KERST, D. W., "Historical Development of the Betatron," *Nature*, **157**, 90 (1946).
30. SCHIFF, L. I., "Production of Particle Energies Beyond 200 Mev," *Rev. of Sci. Inst.*, 17, 6 (1946).

U. S. Patents

31. SLEPIAN, J., 1, 645,304 (Oct. 11, 1927), X-ray Tube.
32. STEENBECK, M., 2,103,303 (Dec. 28, 1937), Device for Producing Electron Rays of High Energy.
33. SMITH, C. G., 2,143,459 (Jan. 10, 1939), Electron Discharge Device.
34. PENNY, G. W., 2,193,602 (March 12, 1940), Device for Accelerating Electrons to very High Speeds.
35. KERST, D. W., 2,297,305 (Sept. 29, 1942), Magnetic Induction Accelerator.
36. BALDWIN, G. C., 2,331,768 (Oct. 12, 1943), Magnetic Induction Accelerator.
37. KERST, D. W., 2,335,014 (Nov. 23, 1943), Magnetic Induction Accelerator.

Notes added in proof reading

38. The successful ejection of a well defined electron beam has recently been announced. See: Skaggs, L. S., Almy, S. M., Kerst, D. W., and Lanze, L. H., Letter to the Editor, "Removal of the Electron Beam from the Betatron," *Phys. Rev.* **70**, 95 (July 1946).
39. SCHWINGER, J., Abstract, "Electron Radiation in High Energy Accelerators," *Phys. Rev.* **70**, 798 (Nov. 1946).
40. Similar observations made on the G.E. 70 Mev Synchrotron were announced by H. C. Pollock, R. V. Langmuir and F. R. Elder, at the American Physical Society Meeting on Feb. 1, 1947, in New York City.

STRESSES IN TURBINE DISKS AT HIGH TEMPERATURES.[1]

BY

E. P. POPOV,[2]

Berkeley, Calif.

With the ever increasing use of high pressure steam systems and the advent of the gas turbine, the service conditions imposed on the rotating disks are very severe. The rotational speeds are high and the operating temperatures are in the range where creep of the material occurs. The stress distribution in a rotating disk under these conditions cannot be properly estimated on the basis of the elastic theory. In addition to this, usually the fit of the disk on the shaft and the clearance between the turbine buckets and the housing must not vary more than certain prescribed amounts.[3] Thus the small plastic dimensional changes of a rotating disk with time must also be determined.

This paper covers a study of stress distribution and creep deformation in rotating disks. The study is however primarily confined to stress distribution and deformations that occur during the steady state, i.e., for service periods beyond the interval in which rather rapid transient creep takes place. In the steady state, the stresses become stabilized and depend only on the final or steady creep rates. The solution presented, although lacking completeness in not considering the transient period, seems of some practical value, and may suffice in many actual design problems. A modified solution of a current method which depends only on the data derivable from tension creep tests is presented. This results in the simplification of the solution and greatly expands the use of the normally available test data. Metallographical transformations at high temperatures are not discussed. The stress analyses presented apply only to materials found stable for high temperature service.

The problem of rotating disks involves combined stresses and we will first consider the formulation of creep laws under such stresses.

CREEP UNDER COMBINED STRESS.

Creep of material under combined stress is a complex phenomenon and its mathematical formulation is not completely settled. However,

[1] This paper is an abridged portion from a dissertation submitted in partial fulfillment of the requirements for the Ph.D. at Stanford University, May, 1946. Other portions of the dissertation, on relaxation and bending, will appear later.

[2] Assist. Prof. Civ. Eng., University of California, Berkeley, Calif.

[3] Some design requirements limit the creep rate to 10^{-9} inches per inch per hour for turbine disks pressed on shafts. K. Baumann, "Some Considerations Affecting Future Developments of the Steam Cycle," *Engineering* (London), Vol. CXXX, Nov. 7, 1930, p. 597.

there are several theories of material's behavior under such conditions. These theories may be divided into two groups. One group of such theories considers creep as a function of distortion strain energy, and the other bases it on certain idealized concepts of viscosity of the material.[4,5] The first group appears to have a better experimental justification, and we will limit our further discussion to it. Several investigators, among them Odquist,[6] Bailey,[7] and Soderberg,[8,9] proposed formulations for creep under combined stresses. These formulations are fundamentally alike and are essentially extensions of the theory of plastic flow in crystalline materials.[10] The assumptions directly utilized are:

1. The directions of the principal strains coincide with those of the principal stresses.
2. The density of the material remains constant.
3. The principal shear strains are proportional to the principal shear stresses.[11]

In addition to these for creep, another assumption [12] is introduced that

4. The yielding follows the Mises-Hencky criterion in which the distortion strain energy is the determining factor affecting the creep of the material.

These strain energy considerations [8] utilize the invariants

$$s = \frac{1}{\sqrt{2}}\sqrt{(\sigma_1 - \sigma_2)^2 + (\sigma_2 - \sigma_3)^2 + (\sigma_3 - \sigma_1)^2} \qquad (1)$$

[4] J. J. Kanter, "The Interpretation and Use of Creep Results," *J.A.S.M.*, Vol. 24, 1936, p. 870.

[5] A. Nadai, "On the Creep of Solids at Elevated Temperatures," *J. Applied Physics*, Vol. 8, No. 6, 1937, pp. 418–432.

[6] Odquist, F., "Plasticitetsteori Med Tillämpuingar, a monograph published through Ingeniörsvetenskampsakademien (IVA)," Stockholm, 1934. See also *Proc. 4th Intern. Cong. Applied Mechanics*, 228, 1934.

[7] R. W. Bailey, "The Utilization of Creep Test Data in Engineering Design," *Proc. Inst. of Mech. Engrs.* (London), Vol. 131, November 1935, pp. 131–349.

[8] C. R. Soderberg, "The Interpretation of Creep Tests for Machine Design," *Trans. A.S.M.E.*, Vol. 58, 1936, pp. 733–743.

[9] Discussion by C. R. Soderberg of "Design Aspects of Creep," by R. W. Bailey, *J. App. Mech.*, Vol. 3, No. 1, 1935.

[10] A. Nadai, Plasticity, Engineering Societies Monographs, McGraw-Hill, New York, 1931.

[11] It is of interest to note that such assumptions were used much earlier by B. de St. Venant for his work in plasticity based on the tests by Tresca. See his "Sur l'établissement des equations des mouvements interieurs opérés dans les corps solides ductiles au délà des limites ou l'élasticité pourrait les rameher á leur premier état," *Compt. Rend.*, **70**, 473, 1870.

[12] For a complete derivation see ref. 8, or for a modified method of derivation based on corrected St. Venant's equations for creep, see J. Marin, "Design of Members Subjected to Creep at High Temperature," *J. App. Mech.*, Vol. 4, No. 1, March, 1937, p. A-21. Odquist's theory giving essentially the same results in a tensor form will not be discussed here.

and

$$e = \frac{\sqrt{2}}{3}\sqrt{(\epsilon_1 - \epsilon_2)^2 + (\epsilon_2 - \epsilon_3)^2 + (\epsilon_3 - \epsilon_1)^2} \tag{2}$$

where σ_1, σ_2 and σ_3 are the three principal stresses; ϵ_1, ϵ_2 and ϵ_3 are the three principal strains, and s and e represent the stress and strain, respectively, in the octahedral plane. The octahedral stress and strain merge into the ordinary stress and strain for the unidirectional stress.

Using the above notions of stress and strain, together with the three assumptions stated formerly, the laws of plastic flow for creep transform [8] for constant stresses into the following simple relations:

$$\begin{aligned} \epsilon_1 &= \frac{\partial s}{\partial \sigma_1} e, \\ \epsilon_2 &= \frac{\partial s}{\partial \sigma_2} e, \\ \epsilon_3 &= \frac{\partial s}{\partial \sigma_3} e. \end{aligned} \tag{3}$$

These relations express the law of plastic deformation in a suitable form for use in studying creep. They are general and may be used for calculating creep strains during the initial as well as steady state.

Let us limit their generality for the present to the steady state conditions, and let us further assume that

5. For the steady state of creep, the exponential creep law is satisfactory and is applicable to the octahedral strains and stresses.

Then we may write an equation

$$u^* = Bs^n \tag{4}$$

where B and n are constants from the exponential law, s is the octahedral stress, and u^* is the steady or minimum creep rate of the octahedral strain.

But for the steady state, the strains are equal to minimum creep rates multiplied by time, or

$$\begin{aligned} e &= u^* t, \\ \epsilon_1 &= u_1^* t, \\ \epsilon_2 &= u_2^* t, \\ \epsilon_3 &= u_3^* t, \end{aligned} \tag{5}$$

where subscripts to the plastic strain ϵ and minimum creep rates u^* represent their respective directions, and t is time. Substituting these

equations into eq. (3), and eliminating time, we obtain

$$u_1^* = B\frac{\partial s}{\partial \sigma_1}s^n,$$

$$u_2^* = B\frac{\partial s}{\partial \sigma_2}s^n, \tag{6}$$

$$u_3^* = B\frac{\partial s}{\partial \sigma_3}s^n.$$

Then performing the partial differentiations of function s (eq. 1), and substituting for s its value in terms of the principal stresses, we obtain the general equations for the steady creep.

$$u_1^* = \frac{B}{2^{(n+1)/2}}\left[(\sigma_1-\sigma_2)^2+(\sigma_2-\sigma_3)^2+(\sigma_3-\sigma_1)^2\right]^{(n-1)/2} \times\left[(\sigma_1-\sigma_2)-(\sigma_3-\sigma_1)\right],$$

$$u_2^* = \frac{B}{2^{(n+1)/2}}\left[(\sigma_1-\sigma_2)^2+(\sigma_2-\sigma_3)^2+(\sigma_3-\sigma_1)^2\right]^{(n-1)/2} \times\left[(\sigma_2-\sigma_3)-(\sigma_1-\sigma_2)\right], \tag{7}$$

$$u_3^* = \frac{B}{2^{(n+1)/2}}\left[(\sigma_1-\sigma_2)^2+(\sigma_2-\sigma_3)^2+(\sigma_3-\sigma_1)^2\right]^{(n-1)/2} \times\left[(\sigma_3-\sigma_1)-(\sigma_2-\sigma_3)\right].$$

These equations give the steady creep rates in the direction of the principal stresses using only two experimental constants B and n. These constants are the same as in the usual exponential creep law relation:

$$u^* = B\sigma^n. \tag{8}$$

Equations (7) reduce to eq. (8) for a uni-directional stress. The above formulae represent one theory; now we will examine another which had considerable experimental support.

BAILEY'S THEORY OF CREEP UNDER COMPOUND STRESS.

Bailey,[7] having observed that thin-walled tubes under torsion or internal fluid pressure show no axial creep, deduced the following expression:

$$u_1^* = \frac{B}{2^{m+1}}\left\{(\sigma_1-\sigma_2)^2+(\sigma_2-\sigma_3)^2+(\sigma_3-\sigma_1)^2\right\}^m \times\left\{(\sigma_1-\sigma_2)^{n-2m}-(\sigma_3-\sigma_1)^{n-2m}\right\} \tag{9}$$

and similar expressions for u_2^* and u_3^*, which are obtained by cyclic permutation of subscripts. In these equations, constants B and n are established from tension creep tests. Constant m may be obtained by fitting it so that expressions would agree with results of some compound

stress tests, or more conveniently, from torsion test performed at the shearing stress one-half the tensile test stress, or tube pressure vessel with the hoop stress at the value of tensile test stress, then the value of m is calculated from the measured creep rates ratio by equation

$$\frac{u^* \text{ in tension}}{u^* \text{ of shear or tube's circumference}} = \frac{2}{(\frac{3}{4})^m[1 + (\frac{1}{2})^{n-2m}]}. \quad (10)$$

The right-hand side of this equation is obtained from eq. (9), and in a ratio, stress cancels out.

The above theory at present has perhaps the best experimental support, although it may be considered nearly empirical because of some liberties taken with handling signs in its derivation, but, compared with the one first presented, it has the disadvantage of requiring the knowledge of an additional material constant m. Much of the available data [13] is obtained from the tension tests alone, which is sufficient information for the first theory. Moreover, it has been shown [14] that reasonable agreement exists between the two theories in several special cases of compound stress. Thus it seems significant to compare the two theories for the case of rotating disks. Reasonable agreement between the two theories would serve as a verification of the adequacy of the simpler first, and would be more useful for the turbine design purposes.

MODIFIED THEORY FOR THE STEADY STATE OF STRESS IN A ROTATING DISK.

After an interval of time, the stresses in a rotating disk become stabilized and may be calculated provided certain conditions of equilibrium, compatibility and creep are fulfilled. In the usual design, the rotor's thickness is variable as shown in Fig. 1, and even for simpler cases, direct mathematical solution leads to involved expressions. However, a method of solution by successive approximations has been developed by Bailey [7] for disks that is more convenient for the purpose. The method presented here follows closely his scheme, but is modified, as the first of the creep theories under the combined stress is used.

In the following solution, it is assumed that the disk thickness is small enough at any radius r so that there is no axial stress, Fig. 1, that the disk is symmetrical and the disk faces are not greatly inclined to the radial direction. The disk thickness is taken as $z = f(r)$, radial and circumferential stresses σ_1 and σ_2 are as shown in the figure, γ is the density of the material, ω the angular velocity in radians per second, g the gravitational acceleration, unit stress σ_{1d} is known or assumed stress at the bore radius d (such as pressure due to shrink fit which

[13] Compilation of Available High-Temperature Creep Characteristics of Metals and Alloys, A.S.M.E.-A.S.T.M. Joint Research Committee on Effect of Temperature on the Properties of Metals, 1938.

[14] J. Marin, "Mechanical Properties of Materials and Design," McGraw-Hill, 1942.

would be negative to the direction shown), and unit stress σ_{1b} is a radial load at radius b (such as caused by buckets and shrouds in a rotating disk).

For a rotating disk of variable thickness, it can be shown [15] that the equation of equilibrium for an element is

$$\frac{d}{dr}(\sigma_1 rz) - z\sigma_2 + \frac{\gamma}{g} z\omega^2 r^2 = 0 \tag{11}$$

which must hold whether stresses are elastic or plastic. Now if we let w^* be the rate of steady change with time of the radial displacement, then the radial displacement during the steady state is w^*t, where t is

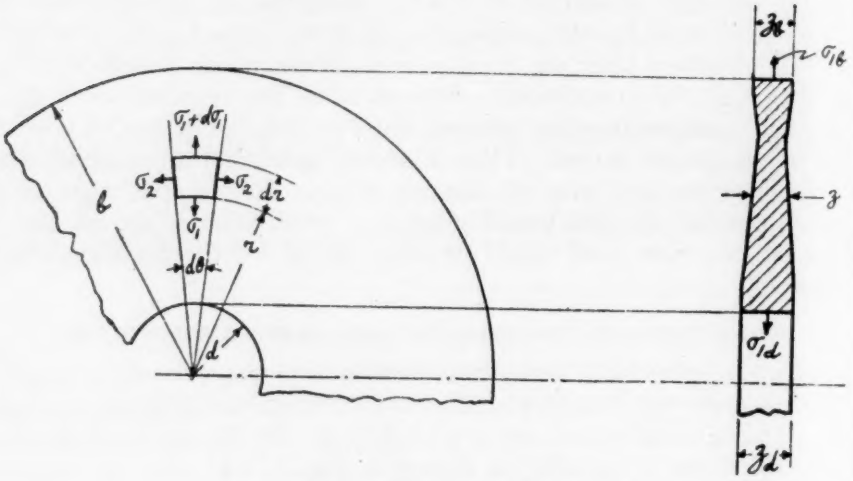

FIG. 1. Elements of a disk.

time. From this it follows that the radial plastic strain is $\epsilon_1 = (dw^*/dr)t$, and the circumferential creep strain is $\epsilon_2 = (w^*/r)t$. But from eq. (5), since $u_1^* = \epsilon_1/t$ and $u_2^* = \epsilon_2/t$, we may express the steady creep rates as

$$u_1^* = \frac{dw^*}{dr} \quad \text{and} \quad u_2^* = \frac{w^*}{r} \tag{11a}$$

for the radial and the circumferential directions, respectively.

In our case of the thin rotating disk, the axial stress vanishes, i.e., $\sigma_3 = 0$. So by writing eq. (7) with only the two principal stresses, we obtain for the steady radial creep rate

$$u_1^* = \frac{dw^*}{dr} = \frac{B}{2^{(n+1)/2}}\left[(\sigma_1 - \sigma_2)^2 + \sigma_1^2 + \sigma_2^2\right]^{(n-1)/2}(2\sigma_1 - \sigma_2) \tag{12}$$

[15] S. Timoshenko, "Theory of Elasticity," McGraw-Hill, 1934, p. 69.

and for the circumferential creep rate

$$u_2^* = \frac{w^*}{r} = \frac{B}{2^{(n+1)/2}}[(\sigma_1 - \sigma_2)^2 + \sigma_1^2 + \sigma_2^2]^{(n-1)/2}(2\sigma_2 - \sigma_1) \quad (13)$$

where all the terms have the meaning explained before.

Equation (11) previously stated may be integrated between the limits d and r

$$\sigma_1 zr - \sigma_{1d} z_d d - \int^r \sigma_2 z dr + \frac{\gamma}{g}\omega^2 \int_d^r zr^2 dr = 0 \quad (14)$$

but here $\int_d^r zr^2 dr$ is the moment of inertia of the cross section of the disk up to a radius r, about the axis of the disk. Let this integral be called I_r, and at radius b be I. Then rewriting we have

$$\sigma_1 zr - \sigma_{1d} z_d d - \int_d^r \sigma_2 z dr + \frac{\gamma}{g}\omega^2 I_r = 0. \quad (15)$$

Now to use the method of successive approximations, the stresses are first found by assuming σ_2 in the above equation as constant over the entire cross-sectional area of the disk, although it, as well as z, is a function of radius r, giving

$$\sigma_2 = \frac{\sigma_{1b} z_b b - \sigma_{1d} z_d d + \frac{\gamma}{g}\omega^2 I}{A} \quad (16)$$

where A is the radial cross-sectional area of the disk equal to $\int_d^b z dr$. The first approximation for σ_1, now that σ_2 is known, is obtained from eq. (15) by substituting into it eq. (16) and is given by

$$\sigma_1 = \frac{1}{zr}\left[\sigma_{1d} z_d d + \frac{a}{A}\left(\sigma_{1d} z_d b - \sigma_{1d} z_d d + \frac{\gamma\omega^2}{g}\right) - \frac{\gamma\omega^2}{g} I_r\right] \quad (17)$$

or

$$\sigma_1 = \frac{1}{zr}\left[\left(1 - \frac{a}{A}\right)\sigma_{1d} z_d d + \frac{a}{A}\sigma_{1b} z_b b + \frac{\gamma}{g}\omega^2\left(\frac{a}{A} I - I_r\right)\right]. \quad (18)$$

In these equations a is the radial cross-sectional area of the disk from the radius d to r, i.e., $\int_d^r z dr$.

In a particular case, solution of eq. (16) gives a constant average stress in the tangential direction. Equation (18) gives corresponding stresses in the radial direction. Such a solution is the first approximation for the stresses σ_1 and σ_2. With this set of approximate values for σ_1 and σ_2 we may form a function $\phi(r)$ which is expressed in terms of the stress ratio $R = \sigma_1/\sigma_2$ from eqs. (12) and (13)

$$\phi(r) = \frac{u_1^*}{u_2^*} = \frac{dw^*}{dr}\frac{r}{w^*} = \frac{2R - 1}{2 - R} \quad (19)$$

where R at a particular point is approximately known from the stresses already determined. This equation may be rearranged, thus

$$\frac{dw^*}{w^*} = r^{-1}\phi(r)dr \tag{20}$$

which, after integration between the limits d and r, gives

$$\frac{w^*}{r} = \frac{w_d^*}{r} e^{\int_d^r r^{-1}\phi(r)dr} \tag{21}$$

where w_d^* is the radial creep at radius d.

Equation (13), which is an expression for w^*/r, may also be written in terms of the stress ratio R as

$$\frac{w^*}{r} = \tfrac{1}{2}B\sigma_2^n(R^2 - R + 1)^{(n-1)/2}(2 - R) \tag{22}$$

or

$$\frac{w^*}{r} = B\sigma_2^n\psi(r) \tag{23}$$

where

$$\psi(r) = \tfrac{1}{2}(R^2 - R + 1)^{(n-1)/2}(2 - R). \tag{24}$$

Setting the right-hand terms of eqs. (21) and (23) equal to each other, and solving for the circumferential stress σ_2, we obtain

$$\sigma_2 = \left(\frac{w_d^*}{B}\right)^{1/n}\left[\frac{e^{\int_d^r r^{-1}\phi(r)dr}}{r\psi(r)}\right]^{1/n} \tag{25}$$

or

$$\sigma_2 = \left(\frac{w_d^*}{B}\right)^{1/n}\Phi(r) \tag{25a}$$

where

$$\Phi(r) = \left[\frac{e^{\int_d^r r^{-1}\phi(r)dr}}{r\psi(r)}\right]^{1/n}. \tag{26}$$

The value of $(w_d^*/B)^{1/n}$ is obtained from eq. (15), when integration is carried from d to b, and is

$$\left(\frac{w_d^*}{B}\right)^{1/n} = \frac{\sigma_{1b}z_b b - \sigma_{1d}z_d d + \dfrac{\gamma}{g}\omega^2 I}{\displaystyle\int_d^b z\Phi(r)dr}. \tag{27}$$

Equations (25) and (27) give new values of σ_2 at various distances r, which are closer approximations than σ_2 obtained by eq. (16). Corresponding closer approximations of σ_1 are determined from eq. (15) as

$$\sigma_1 = \frac{1}{zr}\left[\sigma_{1d}z_d d + \left(\frac{w_d^*}{B}\right)^{1/n}\int_d^r z\Phi(r)dr - \frac{\gamma}{g}\omega^2 I_r\right]. \tag{28}$$

The convergence of this solution to the true stresses of σ_1 and σ_2 is very rapid. An additional cycle with the new set of values obtained from eqs. (25) and (28) repeated in eqs. (19), (24), (25) and (28) usually gives stresses sufficiently close for all practical purposes. Once the stresses are calculated, say by three approximations, corresponding to the different radial distances, steady creep strain rates at any point are given by eqs. (12) and (13) for u_1^* and u_2^*. The creep strain rate in the axial direction, i.e., the disk thickness creep rate, is obtained from the constancy of volume condition, and is

$$u_3^* = -(u_1^* + u_2^*). \tag{29}$$

In a practical problem the solution indicated above, including integrations, may be carried out graphically and arithmetically in tables by sub-dividing the disk's outer radius into several parts. To illustrate the procedure a numerical example follows:

NUMERICAL EXAMPLE—ROTATING DISK WITH A BORE.

Let us consider a rotating steel disk at 3,000 R.P.M. (314 radians per second) that is 20 inches in diameter with a 2-inch bore and of unit thickness at 850° F. The value of the stress exponent n is taken equal to 6. The boundary stresses σ_{1d} and σ_{1b} are assumed to be negligible. We will determine the stress distribution and relative creep rates in this disk under steady creep conditions. This particular problem has been solved by Bailey [7] by his method, using the values of 6 for n and one for m, so that our results will be directly comparable.

Let $\gamma = 0.283$ lbs./cu.in. and $g = 386$ in./sec.^{2}

For a disk of unit thickness:

$$I_r = \tfrac{1}{3}(r^3 - 1) \quad \text{and} \quad I = 333 \text{ in.}^4,$$
$$a = r - 1 \text{ sq. in.} \quad \text{and} \quad A = 9 \text{ sq. in.}$$

Then from eq. (16) the first approximation for the circumferential stress is determined:

$$\sigma_2 = \frac{0.283 \times 314^2 \times 333}{386 \times 9} = 2{,}680 \text{ psi}$$

and expression for the first approximation of the radial stress is made from eq. (18),

$$\sigma_1 = \frac{\gamma\omega^2}{gr}\left[\frac{333}{9}(r-1) - \frac{1}{3}(r^3 - 1)\right]$$

or

$$\sigma_1 = 24.1\,\frac{1}{r}\,[111(r-1) - (r^3 - 1)].$$

Calculations for this stress are carried out in Table I, where several

TABLE I.

First Approximation of σ_1.

r	$r-1$	$111(r-1)$	r^3-1	$111(r-1)-(r^3-1)$	σ_1
1	0	0	0	0	0
1.5	0.5	55.5	2.375	53.1	853
2	1	111	7	104	1252
3	2	222	26	196	1572
4	3	333	63	270	1626
5	4	444	124	320	1542
6	5	555	215	340	1366
7	6	666	342	324	1116
8	7	777	511	266	801
9	8	888	728	160	428
10	9	999	999	0	0

TABLE II.

Solution for First Approximation of $\int_1^r r^{-1}\phi(r)dr$.

r	R	$2R-1$	$2-R$	$r^{-1}\phi(r)$	$\int_1^r r^{-1}\phi(r)dr$
1	0	−1	2	−.500	0
1.5	.318	−.364	1.682	−1.44	−.161
2	.468	−.064	1.532	−.021	−.202
3	.587	.174	1.413	.041	−.191
4	.606	.212	1.394	.038	−.151
5	.575	.150	1.425	.021	−.122
6	.509	.018	1.491	.002	−.111
7	.416	−.168	1.584	−.015	−.118
8	.298	−.404	1.702	−.030	−.140
9	.160	−.680	1.840	−.041	−.176
10	0	−1	2	−.050	−.222

values of r are taken, as shown in the first column, and the corresponding stresses are to be found in the last column.

With first approximations of σ_1 and σ_2 known, the stress ratio $R = \sigma_1/\sigma_2$ is entered in Table II, and using eq. (19) for $\phi(r)$ function, the values of $r^{-1}\phi(r)$ are calculated. Then the last column of this table is obtained by the summation of the areas under the curve of the function in the preceding column.

Using the same values of R as above in eq. (24), function $\psi(r)$ is calculated in Table III. With values of $r^{-1}\phi(r)dr$ and $\psi(r)$ known and using eq. (26), the function $\Phi(r)$, as well as its summation $\int_d^b \Phi(r)dr$, is computed in Table IV.

Then from eq. (27), now that $\int_d^b \Phi(r)dr$ is known, is

$$\left(\frac{w_d^*}{B}\right)^{1/n} = \frac{0.283 \times 314^2 \times 333}{7.824 \times 386} = 3{,}080$$

and

$$\frac{\gamma}{g}\omega^2 = \frac{0.283 \times 314^2}{386} = 72.4.$$

Table V is made using eq. (28) for σ_1 and eq. (25) for σ_2. These stresses in the disk are the second approximation of the stresses. As will be seen, these stresses are reasonably close to the final ones indicated by this method, but to obtain a closer solution another cycle was made.

TABLE III.

Solution for First Approximation of $\psi(r)$.

r	R	R^2	$R^2 - R + 1$	$(R^2 - R + 1)^{2.5}$	$2 - R$	$\psi(r)$
1	0	0	1.000	1.000	2	1.000
1.5	.318	.101	.783	.543	1.682	.457
2	.468	.219	.751	.489	1.532	.375
3	.587	.344	.757	.498	1.413	.352
4	.606	.366	.760	.503	1.394	.351
5	.575	.330	.755	.495	1.425	.353
6	.509	.258	.749	.486	1.491	.362
7	.415	.173	.757	.498	1.584	.395
8	.298	.089	.791	.557	1.702	.474
9	.160	.026	.866	.697	1.840	.641
10	0	0	1.000	1.000	2	1.000

TABLE IV.

Solution for First Approximation of $\Phi(r)$ and $\int_1^r \Phi(r)dr$.

r	$e^{-\int_1^r r^{-1}\phi dr}$	$\frac{e^{\int r^{-1}\phi dr}}{r\psi(r)}$	$\Phi(r)$	$\int_1^r \Phi(r)dr$
1	1.000	1.000	1.000	0
1.5	1.175	1.240	1.036	.509
2	1.224	1.088	1.014	1.022
3	1.210	.782	.960	2.009
4	1.163	.612	.921	2.949
5	1.130	.502	.891	3.855
6	1.118	.412	.862	4.732
7	1.125	.321	.827	5.577
8	1.150	.229	.782	6.381
9	1.193	.145	.724	7.134
10	1.250	.080	.655	7.824

TABLE V.

Second Approximation of σ_1 and σ_2.

r	$\left(\frac{w_a^2}{B}\right)^{1/n} \int_1^r \Phi dr$	I_r	$\frac{\gamma\omega^2}{g} I_r$	$r\sigma_1$	σ_1	σ_2
1	0	0	0	0	0	3,080
1.5	1,570	.79	57	1,510	1,000	3,190
2	3,150	2.33	169	2,980	1,490	3,120
3	6,190	8.66	628	5,560	1,850	2,960
4	9,090	21.0	1,520	7,570	1,890	2,840
5	11,880	41.3	2,990	8,890	1,780	2,750
6	14,580	71.6	5,190	9,390	1,560	2,660
7	17,200	114	8,250	8,950	1,280	2,550
8	19,640	170	12,300	7,340	920	2,410
9	22,000	242	17,500	4,500	500	2,230
10	24,100	333	24,100	0	0	2,020

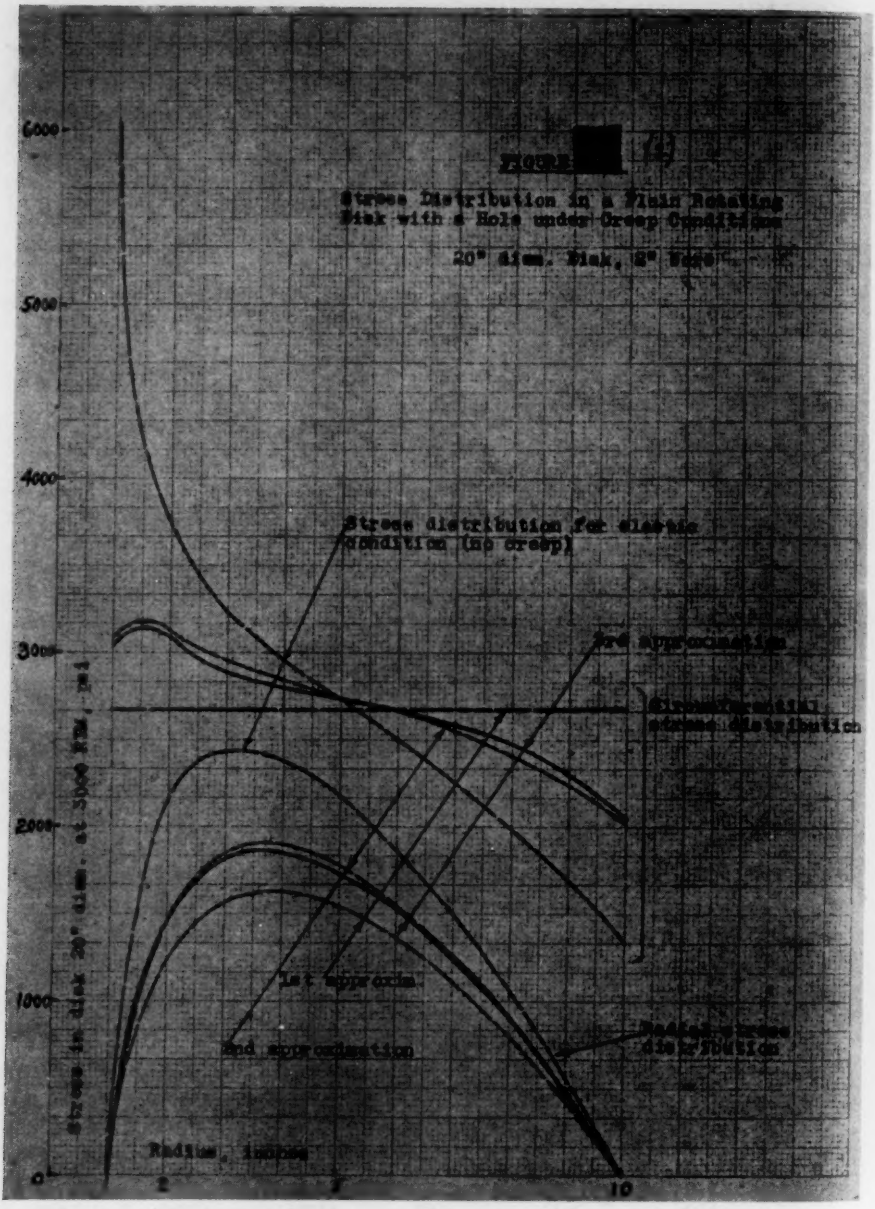

FIG. 2.

The stresses from Table V were used to form new ratios R and a complete cycle of calculations was repeated. Calculations are similar to those of Tables II, III, IV and V. The final values thus obtained are the third approximation of the stresses.

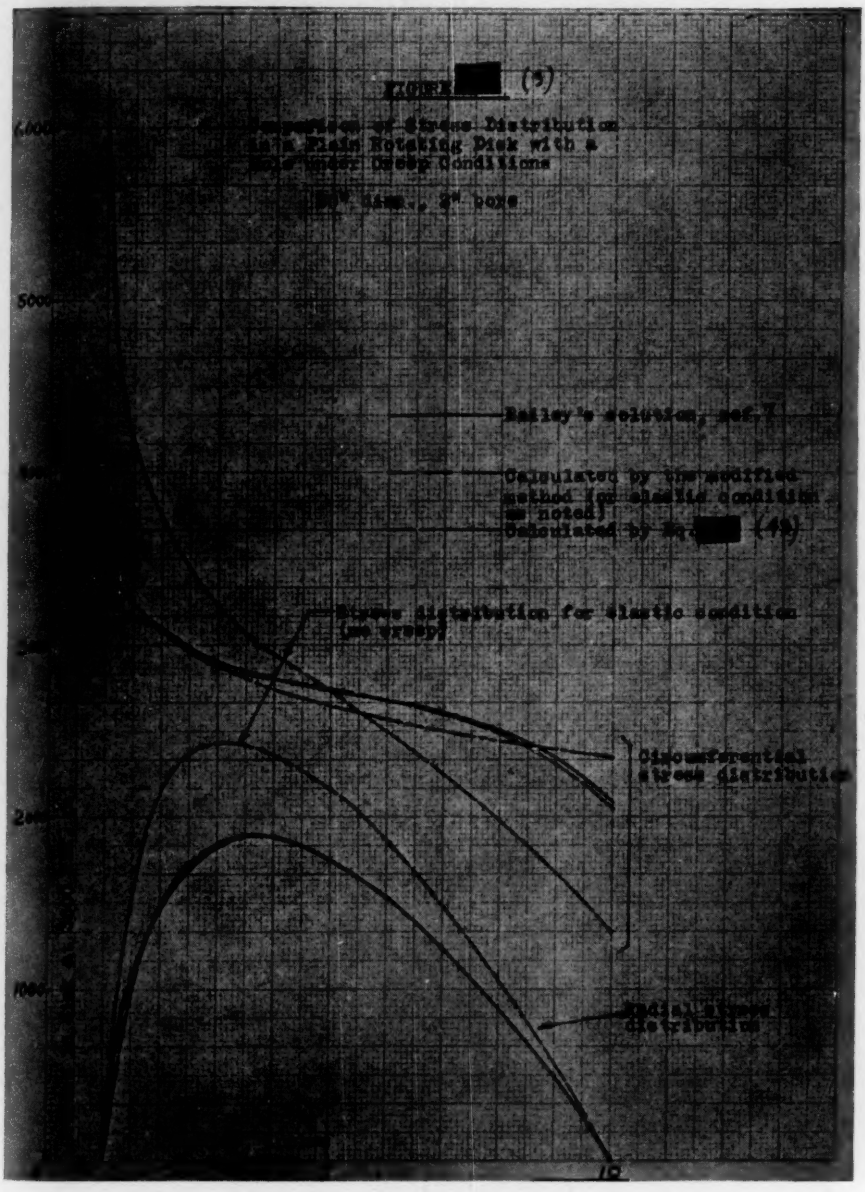
Bailey's solution, ref. 7
Calculated by the modified method (for shrink condition as noted)
Stress distribution for elastic condition (no creep)
Circumferential stress distribution
Radial stress distribution

FIG. 3.

For the purposes of comparison with the elastic stress distribution [16] in an identical disk and to show the convergence of the approximations,

[16] The elastic stress distribution for the disk was computed assuming the Poisson's ratio of 0.3 and using the well known equations. See Timoshenko, S., "Strength of Materials," Part II, Van Nostrand, New York, Second Edition, 1941, p. 247.

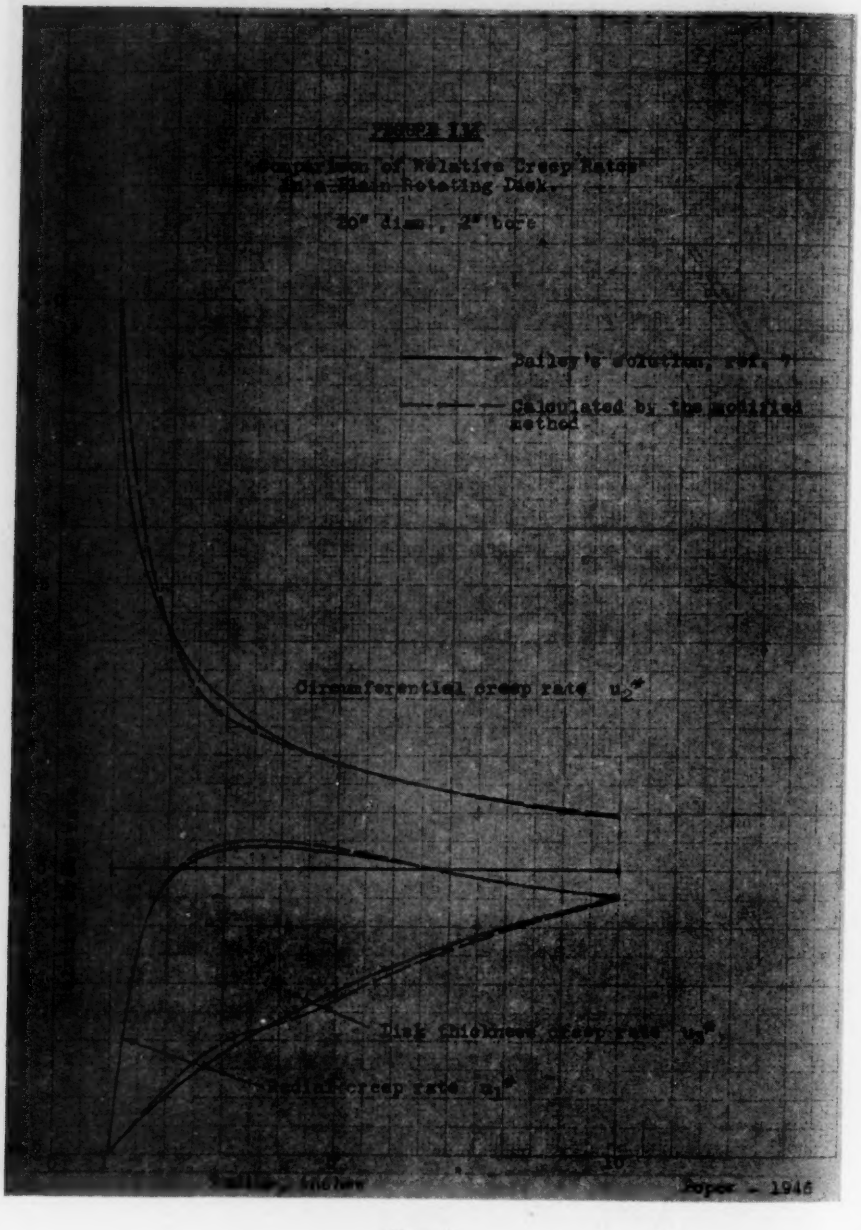
Bailey's solution, ref. 7
Calculated by the modified method
Circumferential creep rate u_2^*
Disk thickness creep rate u_3^*
Radial creep rate u_1^*
Popov - 1946

FIG. 4.

see Fig. 2. It will be observed that the successive approximations rapidly approach the desired solution and the steady stress distribution under creep conditions is very much different from that occurring in purely elastic disks. The maximum circumferential stress is approxi-

mately 50 per cent. of the elastic, and the maximum radial approximately 75 per cent. for the case considered.

As was stated earlier, this particular problem is the same one that Bailey[7] worked out by his theory so that the results may be directly compared. In Fig. 3, Bailey's, as well as the solution by the modified method, presented here, is shown. The agreement between the two is remarkable, and although the modified theory uses one less material constant, apparently the results are not affected.

With stress distribution known, the creep rates may be calculated from eqs. (12), (13) and (29). For our purposes, we will calculate only the relative creep rates. The circumferential creep rate at the bore will be considered unity. This differs from the true creep rates only by a constant, which could be easily determined in an actual problem. The results of these calculations are shown in Fig. 4. Bailey's available solution of the disk for the relative creep rates is also shown. The two methods give results that are in a very satisfactory agreement.

MODIFIED THEORY FOR THE STEADY STATE OF STRESS IN A ROTATING DISK WITHOUT A BORE.

Sometimes in practice there occur important applications of disks without bores when they are made integral with a shaft. The method of successive approximations developed previously is suitable for calculations in such cases with an additional modification. In this case, at the axis, and close to it, $\sigma_1 = \sigma_2$, which is sufficiently true for practical purposes. For the first approximation of stresses, a small hole of say $d = 0.1b$ radius is assumed, and calculations by eqs. (16) and (18) are made as before with $\sigma_{1d} = 0$.

For small values of r and at the center of the disk, the stress ratio $R = 1$; $\phi(r) = 1$ from eq. (19) and $\psi(r) = \frac{1}{2}$ from eq. (24). Introducing these values into eq. (25), and remembering that the two principal stresses are assumed to be equal, we have

$$\sigma_1 = \sigma_2 = \left(\frac{w_d^*}{B}\right)^{1/n}\left[\frac{2e\int_d^r r^{-1}dx}{x}\right]^{1/n} = \left(\frac{w_d^*}{B}\right)^{1/n}\left(\frac{2}{d}\right)^{1/n} \qquad (30)$$

which holds for small values of radius r. The value of the stress from eq. (30) may now be considered as a "boundary radial force" acting on the surface of the assumed bore. Treating it in this manner, substitute eq. (30) into eq. (27), which gives

$$\left(\frac{w_d^*}{B}\right)^{1/n} = \frac{\sigma_{1b}z_b b + \frac{\gamma}{g}\omega^2 I}{z_d d\left(\frac{2}{d}\right)^{1/n} + \int_d^b z\Phi(r)dr}$$

$$= \frac{\sigma_{1b}z_b b + \frac{\gamma}{g}\omega^2 I}{2^{1/n}z_d d^{(n-1)/n} + \int_d^b z\Phi(r)dr}. \qquad (31)$$

The above value is to be used in eq. (25a) for solution of the closer approximation of σ_2. In a similar fashion introducing the "boundary force" into eq. (28), we obtain

$$\sigma_1 = \frac{1}{zr}\left\{\left(\frac{w_d^*}{B}\right)^{1/n}\left[\, 2^{1/n} z_d d^{(n-1)/n} + \int_d^r z\Phi(r)dr \,\right] - \frac{\gamma}{g}\omega^2 I_r \right\} \quad (32)$$

or substituting in it eq. (31), we obtain

$$\sigma_1 = \frac{1}{zr}\left[\left(\sigma_{1b} z_b b + \frac{\gamma}{g}\omega^2 I\right)\frac{2^{1/n} z_d d^{(n-1)/n} + \int_d^r z\Phi(r)dr}{2^{1/n} z_d d^{(n-1)/n} + \int_d^b z\Phi(r)dr} - \frac{\gamma}{g}\omega^2 I_r\right] \quad (33)$$

which gives solution for the closer approximation of the radial force.

Just as for the disk with a bore, several approximations should be made to determine the stresses. Convergence in this case to the desired values is not quite as rapid as in the former case. Creep rates at any point after the stresses have been determined may again be computed from eqs. (12), (13) and (29).

To illustrate the procedure, a numerical example follows.

NUMERICAL EXAMPLE—ROTATING DISK WITHOUT A HOLE.

We will again consider a 20-inch diameter disk at 3,000 R.P.M. of unit thickness, but without a bore. The value of stress exponent $n = 6$. No load at the periphery is assumed. The stresses and relative creep

TABLE VI.

Second Approximation.

r	$\Phi(r)$	$\int_1^r \Phi(r)dr$	$2^{1/n} + \int_1^r \Phi(r)dr$	*	I_r	**	σ_1	σ_2
0		0					3,020	3,020
1	1.000	0	1.122	41.9	.333	41.6	3,010	2,690
1.5	1.036	.509	1.631	60.8	1.12	59.7	2,880	2,780
2	1.014	1.022	2.144	80.0	2.67	77.3	2,800	2,730
3	.960	2.009	3.131	116.7	9.00	107.7	2,590	2,580
4	.921	2.949	4.071	152	21.3	130.7	2,370	2,480
5	.891	3.855	4.977	186	41.7	144.3	2,090	2,400
6	.862	4.732	5.854	218	72.0	146.0	1,760	2,320
7	.827	5.577	6.699	250	114	136	1,410	2,220
8	.782	6.381	7.503	280	171	109	987	2,100
9	.724	7.134	8.256	308	243	65	522	1,940
10	.655	7.824	8.946	333	333	0	0	1,760

$$* = \frac{2^{1/n} + \int_1^r \Phi(r)dr}{2^{1/n} + \int_1^{10} \Phi(r)dr} I_r. \qquad ** = \frac{2^{1/n} + \int_1^r \Phi(r)dr}{2^{1/n} + \int_1^{10} \Phi(r)dr} I_r - I.$$

rates will be determined and, since this problem is also solved by Bailey,[7] the results will be compared.

We will "assume" a bore of 1-inch radius. Thus the first approximation σ_1 and σ_2 is already known as computed for the previous example, Table I, as well as $\Phi(r)$ and $\int_1^r \Phi(r)dr$ (Table IV). Then to obtain the

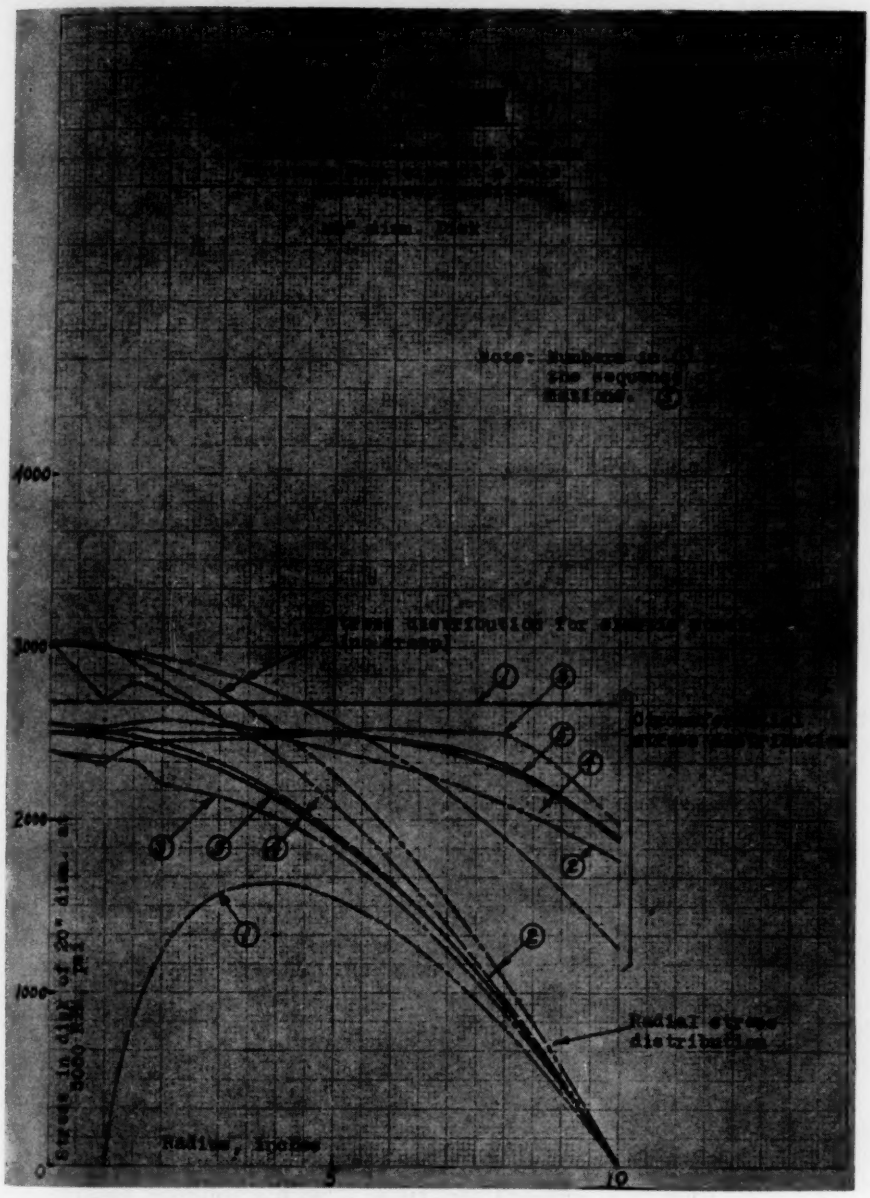

FIG. 5.

second approximation for the stresses, we first use eq. (31) to determine

$$\left(\frac{w_d^*}{B}\right)^{1/n} = \frac{0.283 \times 314^2 \times 333}{386(2^{0.167} + 7.824)} = 2{,}690,$$

which value used in eq. (30) gives the stresses at and near the axis.

The new values of radial stress are calculated in Table VI using eq. (33), which in this particular case reduces to

$$\sigma_1 = \frac{1}{r}\frac{\gamma}{g}\omega^2\left[\frac{2^{1/n} + \int_1^r \Phi(r)dr}{2^{1/n} + \int_1^{10} \Phi(r)dr} I - I_r\right].$$

The corresponding values of the circumferential stress are obtained using eq. (25a) with $(w_d^*/B)^{1/n} = 2{,}690$.

Then three more cycles were repeated. The assumed bore remained 2 inches in diameter in all calculations, so except for the use of eqs. (31) and (33), the procedure is similar to the case where there is an actual bore.

The convergence of solution in this case to the desired stresses is much slower, as may be seen from Fig. 5. An additional two cycles were required to obtain comparable results to the solutions of disks with bores.

The solution obtained is compared with Bailey's for an identical disk, Fig. 6. The agreement again is excellent. However, it is of interest to note that in a disk without a hole, the stress distribution does not deviate as much from the stresses for the elastic condition.

Relative creep rates were also calculated as before, using eqs. (12), (13) and (29). The results obtained, together with Bailey's solution, are shown in Fig. 7. The agreement between the two theories is good.

STRESS DISTRIBUTION DURING THE TRANSIENT PERIOD OF CREEP.

While it is perhaps of greater importance to know the nature of the stress distribution that is ultimately reached and remains for a long time, it is of interest to see how rapidly such stresses stabilize. All of the former discussion was directed at obtaining the steady stress state. But at zero time, the stresses are elastic, as the material, as yet, had no time to creep under the stress. At the instant the disk starts rotating, the stress is properly defined by solving the problem by the theory of elasticity. It takes a definite time for the stresses to become stabilized.

Equations (7) and (9), i.e., of both theories discussed, are specifically derived for the steady stresses and steady creep rates. However, eq. (3) is much more general and a solution has been obtained [8] that permits the determination of stresses at any time. Such a solution has the advantage of generality, but involves much more work for the estimate of the stresses ultimately reached. Computations must be done by carrying calculations from zero time by increments. Moreover, due to mathematical complexity in establishing some relations, approximations are made. However, regardless of some of these difficulties, such a method deserves attention as the trend of stress distribution with time

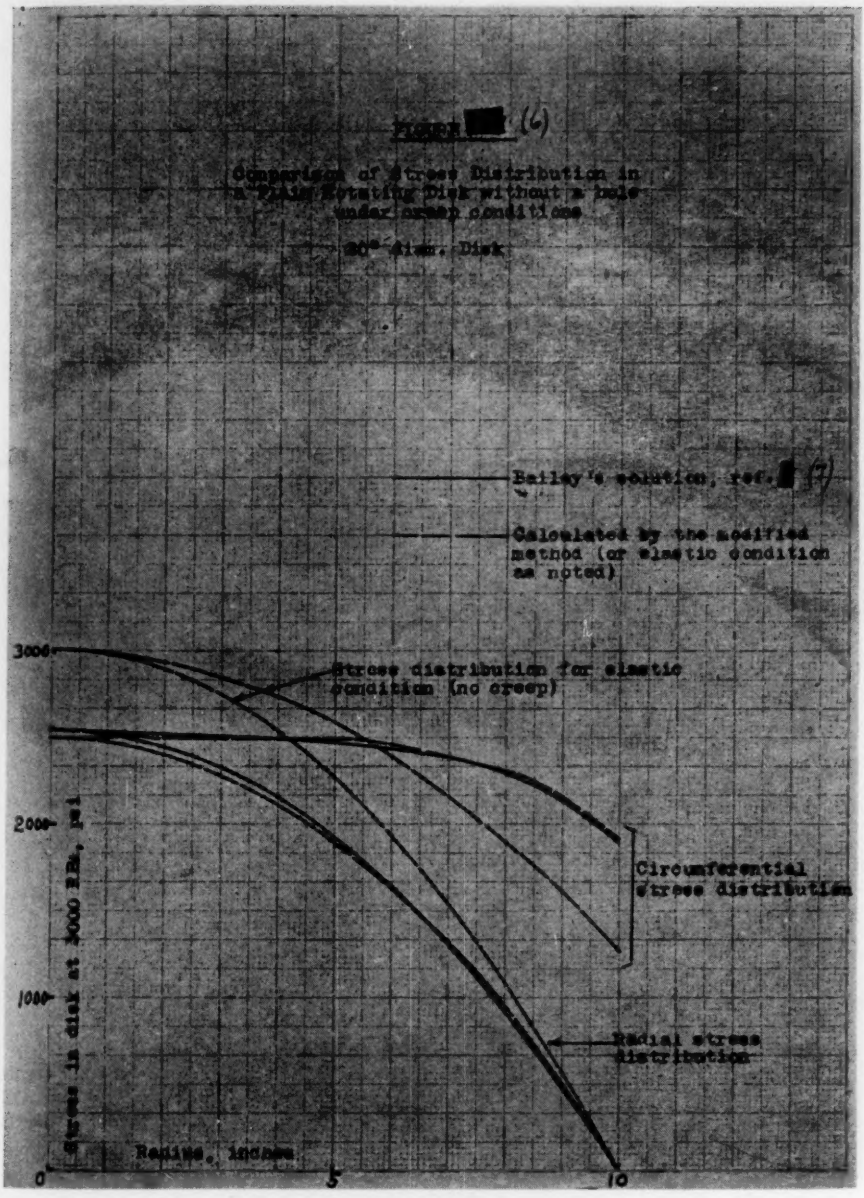
Figure [redacted] (6)
Comparison of Stress Distribution in a Solid Rotating Disk without a Hole under Creep Conditions
20" diam. Disk
Bailey's solution, ref. [redacted] (7)
Calculated by the modified method (or elastic condition as noted)
Stress distribution for elastic condition (no creep)
Circumferential stress distribution
Radial stress distribution
Stress in disk at 3000 R.P., psi
Radius, inches
3000
2000
1000
0
5
10

FIG. 6.

as shown by it is undoubtedly correct. This method, developed by Soderberg, will not be given here, but the results from an example solved by it are reproduced in Fig. 8.

It will be noted that during the first few hours, stresses undergo a

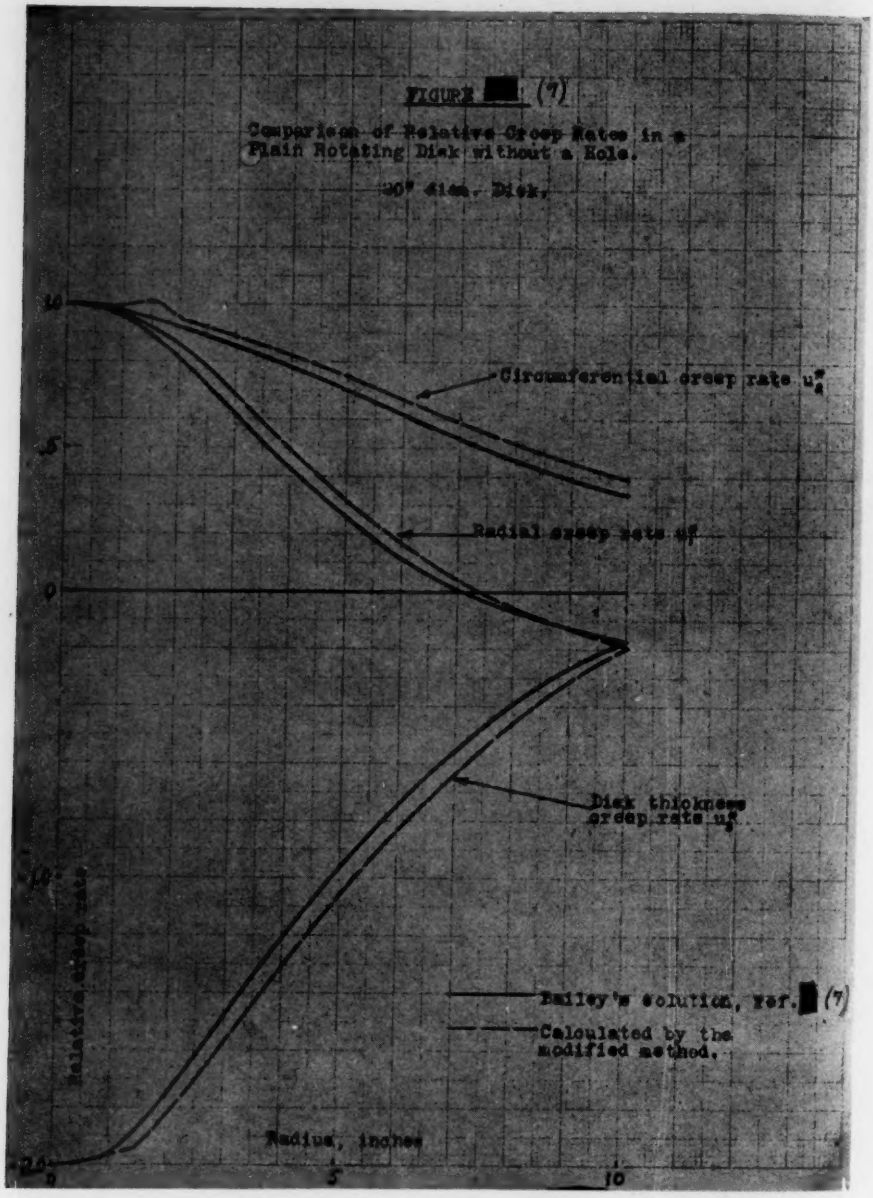

FIG. 7.

rapid change, then even after as little as 200 hours they become nearly stabilized.

This method, while cumbersome for numerical work as noted above, establishes ultimately a very simple criterion for the creep characterizing

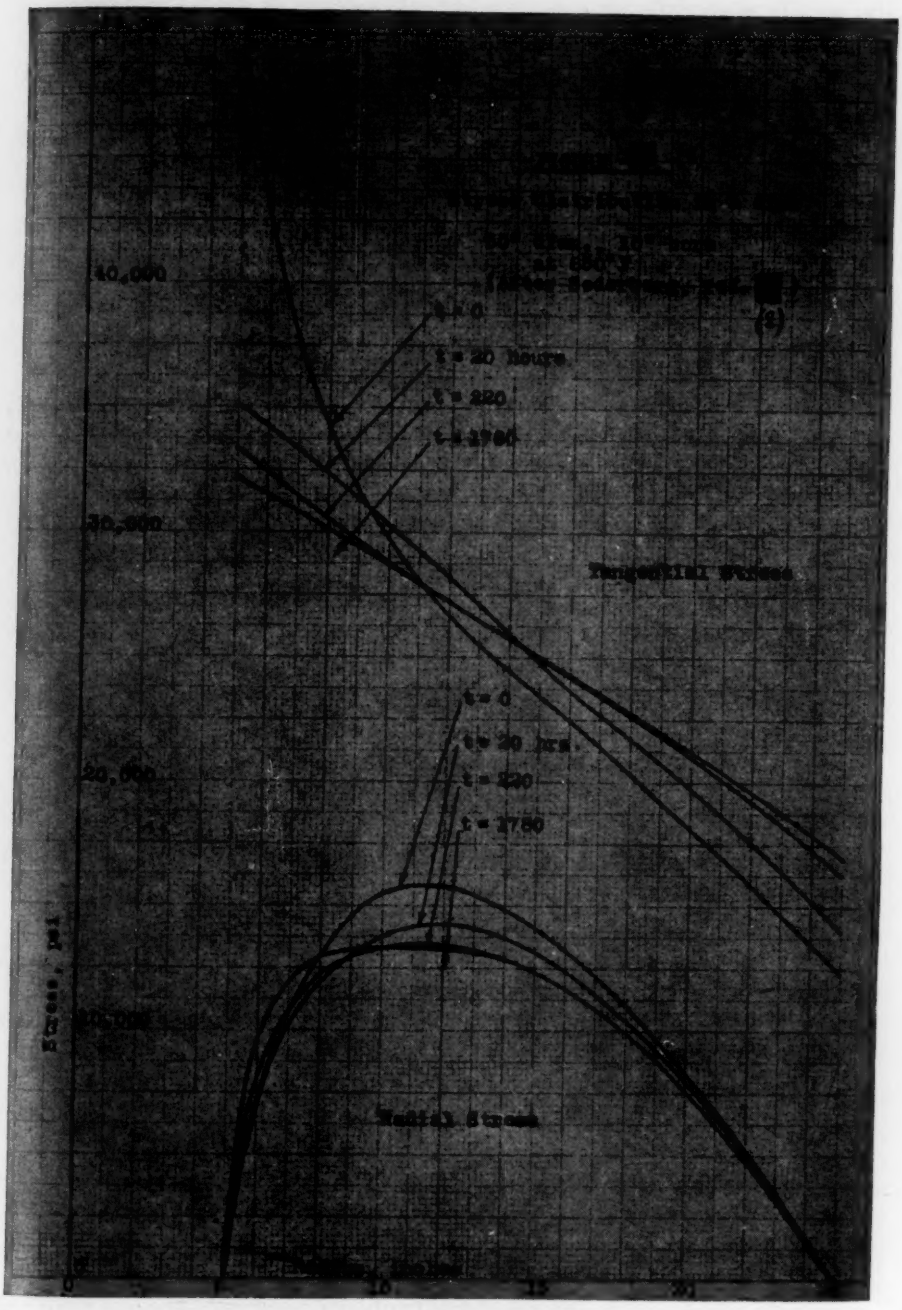
40,000
30,000
20,000
t = 0
t = 20 hours
t = 220
t = 1760
t = 0
t = 20 hrs.
t = 220
t = 1760
Stress, psi

FIG. 8.

the steady state [8,17]

$$u_2^* + Mu_1^* = \frac{C}{r} \tag{34}$$

where u_1^* and u_2^* as before are the radial and circumferential creep strain rates, M is Poisson's ratio, and C a constant adjusted to satisfy the equilibrium forces. Thus the sum $u_2^* + Mu_1^*$ is inversely proportional to the radius r. This expression may be utilized for developing an approximate formula for the tangential stress distribution in which we are normally more interested.

DERIVATION OF AN APPROXIMATE FORMULA FOR THE TANGENTIAL STRESS DISTRIBUTION FOR DISKS WITH LARGE BORES.

Equation (34) may be further simplified if we assume the state of steady creep following an exponential creep law and we substitute into it eq. (6) in which the partial differentiation has been performed, then

$$Bs^{n-1}(\sigma_2 - \tfrac{1}{2}\sigma_1 + M\sigma_1 - \tfrac{1}{2}M\sigma_2) = \frac{C}{r} \tag{35}$$

since $\sigma_3 = 0$ in our case. During creep, the volume remains essentially constant, hence $M = \frac{1}{2}$; then eq. (35) becomes

$$\tfrac{3}{4}B\sigma_2 s^{n-1} = \frac{C}{r} \tag{36}$$

but for a two-dimensional case the octahedral stress from eq. (1) is

$$s = \sqrt{\sigma_1^2 + \sigma_2^2 - \sigma_1\sigma_2}; \tag{37}$$

hence, if we substitute this into eq. (36) and let x be equal to the ratio of the two stresses σ_1/σ_2, we obtain

$$\sigma_2^n(1 + x^2 - x)^{(n-1)/2} = \frac{4C}{3B} \cdot \frac{1}{r} = \frac{K}{r} \tag{38}$$

where K is a constant in a particular case. Rewriting the equation in another form gives

$$\sigma_2(1 + x^2 - x)^{1/2-1/2n} = \left(\frac{K}{r}\right)^{1/n}. \tag{39}$$

So far, except for the assumptions of an exponential creep law, and a theory of compound stress creep, no approximations were introduced. Here, however, we may note that the function $(1 + x^2 - x)^{1/2}$ has nearly a constant value for all values of x from zero to one, which is a complete range of x in any practical problem. Moreover, any reduction

[17] C. R. Soderberg, "Plasticity and Creep in Machine Design," Stephen Timoshenko Anniversary Volume, Contributions to the Mechanics of Solids, Macmillan, New York, 1938.

in the exponent tends to even further stabilize it. We may, then, as a reasonable approximation, write the expression for the tangential stress at any radius r as

$$\sigma_2 = f\left(\frac{K}{r}\right)^{1/n} \tag{40}$$

where f is some factor, which gives an average value of $(1 + x^2 - x)^{1/2-1/2n}$ in a particular case.

The total force existing in a disk across a radial section following the above stress distribution must be the summation of stress multiplied by the area, or

$$\int_d^b \sigma_2 da = \int_d^b fK^{1/n}\frac{1}{r^{1/n}}zdr = fzK^{1/n}\frac{n}{n-1}(b^{(n-1)/n} - d^{(n-1)/n}) \tag{41}$$

where z, the thickness of the disk, is assumed constant, and b and d are the outer and inner radii, respectively. But in a free rotating ring, the conditions of dynamic equilibrium prescribe * that the above total force must be equal to

$$\frac{\gamma\omega^2}{3g}z(b^3 - d^3) \tag{42}$$

where ω as before is the angular velocity, and γ is the density of the material.

Equating (41) and (42), solving for $fK^{1/n}$, and substituting it into eq. (40), we obtain a very convenient approximate expression for the circumferential stress at any point in a rotating disk of uniform † thickness,

$$\sigma_2 = \frac{\gamma\omega^2}{3g}(b^3 - d^3)\cdot\frac{n-1}{n}\cdot\frac{1}{(b^{(n-1)/n} - d^{(n-1)/n})}\cdot\left(\frac{1}{r}\right)^{1/n}. \tag{43}$$

In a particular case once the material constant n, the dimensions of a disk and the angular velocity are known, the equation may be immediately solved. The calculations are very simple, thus for a 20-inch disk with a 2-inch bore at 3,000 R.P.M. and $n = 6$ from eq. (43) the circumferential stress is

$$\sigma_2 = \frac{0.283 \times 314 \times 999 \times 5}{3 \times 386 \times 6}\frac{1}{10^{5/6} - 1}\left(\frac{1}{r}\right)^{1/6} = 3{,}460\left(\frac{1}{r}\right)^{1/6} \text{ psi.}$$

The results are plotted in Fig. 3 and a reasonable solution is obtained

* This expression may be verified, for example, by integrating the tangential stresses along the radial section for an elastic condition.

† For disks of variable thickness, mathematical formulation may become a little more complicated but, by graphical or tabular methods, solutions may be easily made.

as compared with the previous analyses. For disks without holes, this formula fails completely. It also is not satisfactory for solutions of disks with small holes because the criterion for creep characterized by eq. (34) does not hold.

DISCUSSION OF RESULTS.

By comparison, it has been established that the agreement obtained for the steady state stress distribution for disks exhibiting creep by the modified and the Bailey methods is very good. Here it may be of interest to note that when the exponent m in the Bailey theory is equal to $(n - 1)/2$ the two theories give identical expressions for the steady state creep rates. This was not the case in the examples considered ($m = 1$, $n = 6$). The modified solution has the advantage of simplicity as it requires only two experimental constants B and n.[18] This greatly expands the use of much of the available test data.[13] The approximate formula also appears to give reasonable results. It may be useful at least for the preliminary estimate of stresses in a proposed design, but it must not be applied to disks with no or small bores. If refinements in calculations are desired, it minimizes the number of cycles necessary for a solution. The elastic theory for disks operating for extended periods of time at high temperature is completely inadequate and creep of metal must be considered.[19] It is rather notable that considerable reduction of the higher stresses at the bore occurs during the steady state. It is also noteworthy that the shear distortion energy theory, which is found to be applicable in many cases for failure and fatigue of metals, apparently is a satisfactory criterion for creep.

An estimate of the growth of the disk due to creep may also be determined as was shown, although its absolute value appears to be less reliable than the solution for the stresses. While final stresses depend only on the state of creep ultimately reached, the growth depends on the entire cycle of life. During the initial intervals of time, the creep rate is greater than what it eventually attains. The question of an accurate solution for the growth of turbine disks remains a very important problem. The rate of steady creep may be computed by the modified theory, as was done before for the relative case, except that a proper constant B must be used in eqs. (12) and (13). For a disk with a bore, since the radial stresses vanish at the bore and the outside diameter, the points of greatest interest in design, the stress is unidirectional and equations for creep rate reduce to the familiar $u^* = B\sigma^n$. It may be possible that in some cases if the periods of steady stresses

[18] Bailey's theory is still receiving a considerable amount of attention. W. Prager, "Strain Hardening under Combined Stresses," *J. Applied Physics*, Vol. 16, No. 12, Dec. 1945, pp. 837–40.

[19] For a rather complete analysis for disks without creep considerations see A. S. Thompson, "Stresses in Rotating Disks at High Temperatures," *Jl. App. Mech.*, Vol. 13, No. 1, March 1946.

are very long, a reasonable estimate may be made by ignoring the initial stage.

Much work remains to be done before the subject of rotating disks at high temperatures is completely solved, but it is hoped that the approximate equation for the tangential stress and the modified Bailey's theory for the steady state, developed in this paper, will be of benefit for the work that is to follow.

ACKNOWLEDGMENT.

The writer wishes to express his gratitude to Professor Timoshenko under whose guidance this study was made for his generous help.

Remote Instrumentation Best For Jet Planes.—Instruments for jetplanes of the future will be of the electrical remote-reading type for reasons of safety and ease of installation, in the opinion of C. A. Edman, of General Electric's Meter and Instrument Division.

Speaking at a recent ASME meeting on the subject of "Instrumentation for Jet-Propelled Airplanes," Mr. Edman explained that the low vibration inherent in jet engines permits the use of more delicate primary detectors than does the reciprocating engine. He said that d-c selsyn systems using movable contacts have already proved successful in a number of jet plane installations.

"Because of their size, however, these d-c selsyn systems will doubtless be superseded by the inherently smaller a-c types as soon as the proper ranges are developed in the latter systems," Edman said.

Remote-reading instruments are virtually a "must" for jet planes, according to Mr. Edman, because of the need for quick disassembly of the engine from the airframe and the desirability of keeping high-pressure fuel lines outside the cockpit.

The jet plane's gas-turbine engine needs only five basic indicating instruments, as compared with seven required by the conventional reciprocating engine, Edman said. These are the tachometer, tailpipe-temperature indicator, bearing-temperature gage, oil-pressure gage, and fuel pressure gage. However, he pointed out, these instruments will need considerable improvement to meet the special conditions of jet engine indication. The most urgent needs are in tailpipipe-temperature and bearing-temperature indication. Instruments for these purposes will require improved resistance bulbs to withstand high temperatures and corrosive atmosphere.

R. H. O.

Powerful Electro-Magnet Aids Research. (*Power Plant Engineering*, Vol. 50, No. 12.)—An electro-magnet so powerful that the operator must stay at the controls four yards away when it is at peak operation in order to avoid having his pockets picked has been developed by Dr. J. E. Goldman of the Westinghouse Research Laboratories. It is an oil-cooled, $1\frac{1}{2}$ t., iron-core, electro-magnet wound with 6000 turns of square copper, wired and tipped with a special magnetic alloy.

The magnet, 5 ft. long and $2\frac{1}{2}$ ft. high, has adjustable poles so that specimens from $1\frac{1}{2}$ to 12 in. may be attracted and is capable of exerting a concentrated 4000 lb. pull—a force strong enough to make possible new studies in magnetism.

One secret of the high magnetism produced is the special alloy tips. This alloy was developed by the Westinghouse Research Laboratories to give more magnetic energy than ordinary iron.

The variation in the gap between poles is accomplished by the use of adjustable tapered pole-pieces. This feature adds immensely to the versatility of the magnet.

R. H. OPPERMANN.

THE COMPOUND CYLINDER AND THE STRENGTH PROBLEM.[1]

BY

C. W. MacGREGOR[2] AND L. F. COFFIN, JR.[3]

ABSTRACT.

A general discussion is given of the effects of various strength theories on the design of compound cylinders composed of as many as four tubes. Departing from the usual practice in problems of this type, the more modern theories of strength are included.

The problem considered is limited to simultaneous yielding in all component tubes of the cylinder under the action of bore pressure. In addition, new short design procedures employing graphical means are discussed which will considerably reduce the time ordinarily required in such calculations. The methods used are flexible since component tubes of different materials following different strength theories can be treated as easily as cylinders composed of tubes of one material.

INTRODUCTION.

In cases where extremely high pressures are encountered, such as in power plant applications, chemical processes, and gun problems, recourse is often had to the compound cylinder in design. A compound cylinder is defined as a combination of concentric tubes which are nested together either loosely or with shrinkages to effectively resist the action of internal pressure. The component tubes may be of the same material and of similar heat treatment, or, as is often the case, the interior tubes may be of higher strength than the exterior ones.

Design conditions are usually quite rigid in problems of this type because of weight, expense and safety precautions. Commonly the most efficient arrangement by weight is desired for a previously selected factor of safety and set of physical properties. Of paramount importance in this connection is the theory of strength, i.e., the criterion for yielding under states of combined stress. Other conditions being equal, the use of different strength theories will result in compound cylinders having either different overall sizes or different factors of safety.

The authors know of no comprehensive discussion of this problem in the literature, especially as it refers to some of the more modern strength theories.

---

[1] This paper is the result of a portion of a research program carried out at the Massachusetts Institute of Technology from 1942 to the present time under contract with the Bureau of Ordnance, Navy Department. Approval for the release of this information has been received from the Chief of the Bureau of Ordnance. Statements expressed are those of the authors and should in no way be construed as the opinion of the United States Navy.

[2] Professor of Applied Mechanics, Department of Mechanical Engineering, Massachusetts Institute of Technology, Cambridge, Massachusetts.

[3] Assistant Professor of Mechanical Engineering, Department of Mechanical Engineering, Massachusetts Institute of Technology, Cambridge, Massachusetts.

This paper considers the effect of various theories of strength on the design of open-ended thick-walled compound cylinders subjected to a statically applied uniformly distributed internal pressure. The cylinders are assumed to be of infinite length, such that end effects can be neglected. In addition, axial stresses that might be produced through shrinkage in assembly are neglected. Henceforward the component cylinders will be referred to as the first tube, second tube, etc., designating the innermost tube as the first, etc. Calculations have been made as general as possible in order to consider a wide range of materials. However, in the determination of shrinkages and deformations, a Poisson's ratio of 0.3 for steel was used in order to simplify the graphical presentation.

The compound cylinders treated in this paper consider only the most efficient design, namely, simultaneous yielding in all component tubes under the action of bore pressure and according to the theory or theories of strength applied. In some instances such a situation may not be desired because of certain difficulties encountered in the state of rest, i.e., when the bore pressure is removed. A treatment of these latter cases will be discussed in a forthcoming publication.

NOMENCLATURE.

The following nomenclature has been used in this paper:

R_0—the bore or internal radius.
R_n—the external radius of the nth tube or the internal radius of the $(n + 1)$th tube.
r—the radius at an arbitrary point in the compound cylinder.
p_0, P_0—the bore or internal pressure.
p_n—the pressure produced at R_n by shrinkage of a tube or nest of tubes having an internal radius of R_n onto a tube or nest of tubes having an external radius of R_n (plus the shrinkage), referred to as the shrink-fit pressure.
P_n—the pressure in the state of action at radius R_n.
E—the modulus of elasticity of any tube.
ν—Poisson's ratio.
S_r—the radial stress in the cylinder at any arbitrary radius.
S_t—the tangential stress in the cylinder at any arbitrary radius.
Note: A second subscript is used to designate the position of the stress. For example S_{r_1} is the radial stress at radius R_1, S_{t_n} is the tangential stress at radius R_n.
S_0—the yield stress of all tubes in simple tension.
S_0'—the effective stress caused by the state of combined radial and tangential stress at any point in the cylinder.
$(S_0')_n$—the effective stress at radius R_n.
u—the radial deformation of the cylinder at an arbitrary radius.

u_n—the radial deformation at radius R_n.

U—the radial shrinkage existing between tubes or groups of tubes for corresponding radii prior to assembly.

U_n—the radial shrinkage existing at radius R_n between the nth and $(n + 1)$th tube.

THEORIES OF STRENGTH.

Numerous theories of strength have been proposed to predict yielding or failure under states of combined stress for various types of materials. Although considerable attention has been given in recent years to the widely accepted distortion-energy criterion for yielding of ductile metals, design procedures are still followed wherein other theories of strength are used, through reasons of simplicity or available experimental evidence. Brittle and quasi-brittle metals exhibit strength characteristics under combined stress which do not follow the distortion-energy criterion. In order to make this treatment as general as possible six theories of strength are considered and compared in the design of compound cylinders. It is left to the designer to select the appropriate theory for his material. Indeed, certain instances may arise where two or more strength theories may be dealt with in a single compound cylinder, i.e., brittle cast iron liners (first tubes) backed by ductile steel jackets (second tubes). The theories of strength considered are:

(*a*) *Maximum Stress Theory.*—As proposed by Rankine for brittle materials, the tendency to failure is measured by the greatest tensile or compressive stress, which is equal to the corresponding value in simple tension. Expressed analytically, under a state of combined principal stresses S_1, S_2 and S_3 where $|S_1| > |S_2| > |S_3|$, failure occurs when

$$|S_1| = S_0 \tag{1}$$

where S_0 is the stress for failure in simple tension.

(*b*) *Maximum Strain Theory.*—The Maximum Strain Theory, as suggested by Saint Venant, assumes that the greatest absolute elastic strain is the criterion for yielding. This value is considered to be constant at yielding regardless of the stress ratio. This condition may thus be expressed as

$$|S_1 - \nu(S_2 + S_3)| = S_0 \tag{2}$$

where $\left|\frac{S_1}{E} - \frac{\nu}{E}(S_2 + S_3)\right|$ is the greatest principal strain in absolute value.

(*c*) *Total Strain Energy Theory.*—This theory as proposed by Haigh and Beltrami assumes that the total strain energy under any state of combined stress is constant for beginning yielding. This statement

may be resolved mathematically into

$$S_1^2 + S_2^2 + S_3^2 - 2\nu(S_1S_2 + S_2S_3 + S_3S_1) = S_0^2. \quad (3)$$

(*d*) *Distortion-Energy Theory.*—The widely accepted distortion-energy criterion for the yielding of ductile metals suggested independently by von Mises, Huber, and Hencky, assumes that the strain energy associated with the distortion of the material be constant under all states of combined stress for initial yielding. This energy is readily found by subtracting the strain energy due to volume change from the total strain energy, and mathematically is expressed as

$$(S_1 - S_2)^2 + (S_2 - S_3)^2 + (S_3 - S_1)^2 = 2S_0^2. \quad (4)$$

(*e*) *Maximum Shear Theory.*—This theory, attributed to both Coulomb and Guest, defines the maximum shearing stress as the criterion for yielding. Thus if $S_1 > S_2 > S_3$, then

$$S_1 - S_3 = S_0 \quad (5)$$

for initial yielding.

(*f*) *Shear-with-Friction Theory.*—As proposed by Duguet, yielding is governed by a critical shearing stress on one of three planes in a three-dimensional state of stress. However the effect of the normal stress through the action of internal friction is considered, and this acts to rotate the plane of maximum shearing stress from that of the maximum shear theory. For any plane inclined to two principal stress directions and containing the third

$$\tau_0 = \tau_n + fS_n \quad (6)$$

where τ_0 is the critical shearing stress, τ_n and S_n the resolved shearing and normal stresses, respectively, and f a coefficient of internal friction. Duguet claims to have found by many experiments that for yielding by shear under simple tension, the planes of failure make angles of 40° with the normal, while for simple compression this angle is 50°. By maximizing equation (6) under these conditions, he determined f to be 0.176. When $S_1 > S_2 > S_3$, equation (6) may then be expressed as

$$\tau_0 = 0.60S_1 - 0.42S_3. \quad (7)$$

For simple tension equation (7) reduces to $\tau_0 = 0.60S_0$. Thus the shear-with-friction criterion for yielding in terms of the yield stress in simple tension becomes

$$S_0 = S_1 - 0.7S_3. \quad (8)$$

This criterion of yielding gives different yield strengths in simple tension and compression. If S_{0c} is this value for simple compression, it is seen from (8) that $S_0 = -0.7S_{0c}$.

The various strength theories described above may be represented graphically for all possible plane stress combinations as shown in Fig. 1

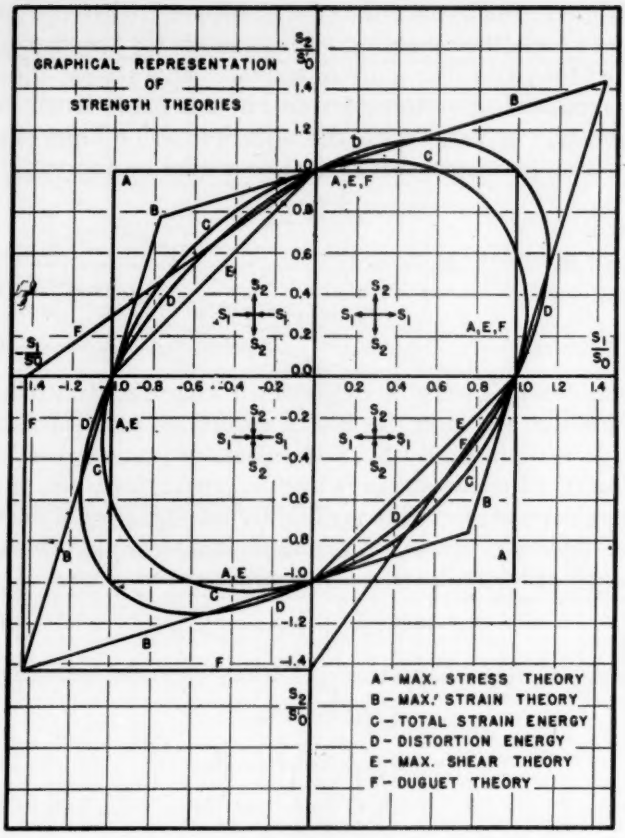
GRAPHICAL REPRESENTATION OF STRENGTH THEORIES
A - MAX. STRESS THEORY
B - MAX. STRAIN THEORY
C - TOTAL STRAIN ENERGY
D - DISTORTION ENERGY
E - MAX. SHEAR THEORY
F - DUGUET THEORY

FIGURE 1

when $\nu = 0.3$. This figure clearly shows that for any one case of combined stress, the various strength criteria considered predict widely different stresses for beginning yielding.

The notation indicating the various theories of strength used in this figure is continued throughout the paper. This notation is as follows:

A. Maximum Stress Theory.
B. Maximum Strain Theory.
C. Total Strain Energy Theory.
D. Distortion Energy Theory.
E. Maximum Shear Theory.
F. Shear-with-Friction Theory.

DETERMINATION OF EFFECTIVE STRESS.

For any state of combined stress where the stresses are known, it is particularly desirable to calculate one value of stress from the strength

theory considered which then may be compared with the yield stress to determine (*a*) whether yielding will occur or (*b*) the factor of safety that exists for this particular state of stress. This stress value has been given various names in the literature and in this paper it will be referred to as the "effective stress," with the notation S_0'. Thus the criterion for yielding with a particular strength theory may be expressed simply as

$$S_0' = S_0 \tag{9}$$

and the factor of safety as

$$\text{Factor of Safety} = \frac{S_0}{S_0'}. \tag{10}$$

The effective stress may be determined analytically if the principal stresses are known, through the use of equations (1), (2), (3), (4), (5), or (8) where S_0 is replaced by S_0'. For cases of plane stress, a graphical determination of effective stress is useful, particularly for the more involved strength theories. This is done by constructing a curve of state of stress vs. effective stress. Consider, for example, the distortion-energy strength criterion in two dimensions

$$S_1^2 - S_1S_2 + S_2^2 = (S_0')^2. \tag{11}$$

Assuming $|S_1| > |S_2|$. Equation (11) may then be rearranged as

$$\frac{S_1}{S_0'} = \sqrt{\frac{1}{\left(\frac{S_2}{S_1}\right)^2 - \frac{S_2}{S_1} + 1}} \tag{12}$$

and S_1/S_0', plotted as ordinate for values of the stress ratio $-1 \leqslant \frac{S_2}{S_1} \leqslant 1$. Thus with the principal stresses known, the stress ratio may be calculated, the term S_1/S_0' found from the plot of equation (12) and the effective stress evaluated.

The various strength theories considered in this paper have been represented in this manner in Fig. 2. Radial and tangential stresses S_r and S_t replace S_1 and S_2 because of the axial symmetry of the problem. When $-1 \leqslant \frac{S_r}{S_t} \leqslant 1$, the coordinates are S_t/S_0', and S_r/S_t, whereas if $-1 \leqslant \frac{S_t}{S_r} \leqslant 1$, the coordinates of this figure are S_t/S_0' and S_r/S_t. The shear-with-friction theory presents certain difficulties when represented in this fashion because of its non-symmetry in two dimensions (see Fig. 1). For this reason, when the stress ratio is positive, two curves exist, namely, when $S_t \leqslant 0$ and $S_t \geqslant 0$. When the stress ratio is negative, two other curves are found, namely, when $|S_r| > |S_t|$ and when $|S_r| < |S_t|$, assuming that S_r is negative for all possible cases.

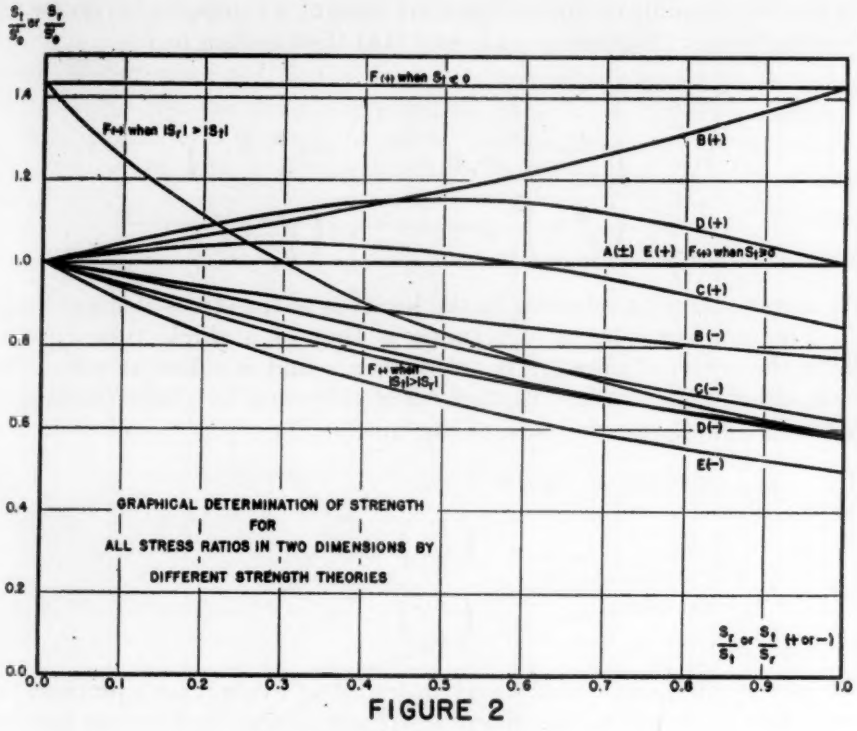

FIGURE 2

ANALYSIS FOR STRENGTH.

For a thick-walled open-ended cylinder of internal radius R_{n-1} and external radius R_n, subjected to an internal pressure P_{n-1} and external pressure P_n both considered to be positive, the radial and tangential stresses at any intermediate radius r are readily found to be [4]

$$S_r = \frac{P_{n-1} - P_n\left(\frac{R_n}{R_{n-1}}\right)^2}{\left(\frac{R_n}{R_{n-1}}\right)^2 - 1} - \frac{(P_{n-1} - P_n)\left(\frac{R_n}{r}\right)^2}{\left(\frac{R_n}{R_{n-1}}\right)^2 - 1}, \qquad (13)$$

$$S_t = \frac{P_{n-1} - P_n\left(\frac{R_n}{R_{n-1}}\right)^2}{\left(\frac{R_n}{R_{n-1}}\right)^2 - 1} + \frac{(P_{n-1} - P_n)\left(\frac{R_n}{r}\right)^2}{\left(\frac{R_n}{R_{n-1}}\right)^2 - 1}. \qquad (14)$$

It should be noted that these stress expressions are independent of any elastic constants. In general the greatest effective stress will occur at the inner radius, so that in future calculations only stresses and strengths

[4] This solution is attributed to Lamé, "Leçons sur la theorie . . . de l'elasticité." Paris, 1852.

at the inner radius of any component tube of a compound cylinder will be considered. Equations (13) and (14) then reduce to

$$S_{r_{n-1}} = -P_{n-1}, \tag{15}$$

$$S_{t_{n-1}} = \frac{\left(\frac{R_n}{R_{n-1}}\right)^2 + 1}{\left(\frac{R_n}{R_{n-1}}\right)^2 - 1} \cdot P_{n-1} - \frac{2\left(\frac{R_n}{R_{n-1}}\right)^2}{\left(\frac{R_n}{R_{n-1}}\right)^2 - 1} \cdot P_n, \tag{16}$$

the stress subscript referring to the location of the stress in the cylinder.

The simplest case to determine is that of a single tube ($n = 1$). Here the external pressure is atmospheric, and is taken as zero. The bore stresses then reduce further when subjected to a bore pressure p_0. Here R_0 and R_1 are the radii of the tube. Thus

$$S_{r_0} = -p_0, \tag{17}$$

$$S_{t_0} = \frac{\left(\frac{R_1}{R_0}\right)^2 + 1}{\left(\frac{R_1}{R_0}\right)^2 - 1} \cdot p_0. \tag{18}$$

The strength of single tubes may be found by evaluating equations (17) and (18), from which the effective stress is determined by the previous section. More generally, if (17) and (18) are rewritten as

$$\frac{S_{r_0}}{p_0} = -1, \tag{19}$$

$$\frac{S_{t_0}}{p_0} = \frac{\left(\frac{R_1}{R_0}\right)^2 + 1}{\left(\frac{R_1}{R_0}\right)^2 - 1}, \tag{20}$$

the stress ratio then becomes

$$\frac{S_{r_0}}{S_{t_0}} = -\frac{\left(\frac{R_1}{R_0}\right)^2 - 1}{\left(\frac{R_1}{R_0}\right)^2 + 1},$$

from which $S_{t_0}/(S_0')_0$ is found from Fig. 2 for a particular wall ratio. By performing the division $\frac{S_{t_0}}{(S_0')_0} \div \frac{S_{t_0}}{p_0}$, the term $p_0/(S_0')_0$ is found. This expression is a dimensionless measure of the strength of the cylinder for a particular wall ratio and strength theory. Fig. 3 expresses this

strength term graphically as a function of wall ratio for each of the six yielding criteria considered. For a known wall ratio and strength theory, the strength $p_0/(S_0')_0$ is found. This term may be interpreted in two ways. By using a predetermined yield stress in simple tension, the bore pressure necessary to cause yielding may be found, since $(S_0')_0 = S_0$ at yielding. Correspondingly, with the bore pressure given,

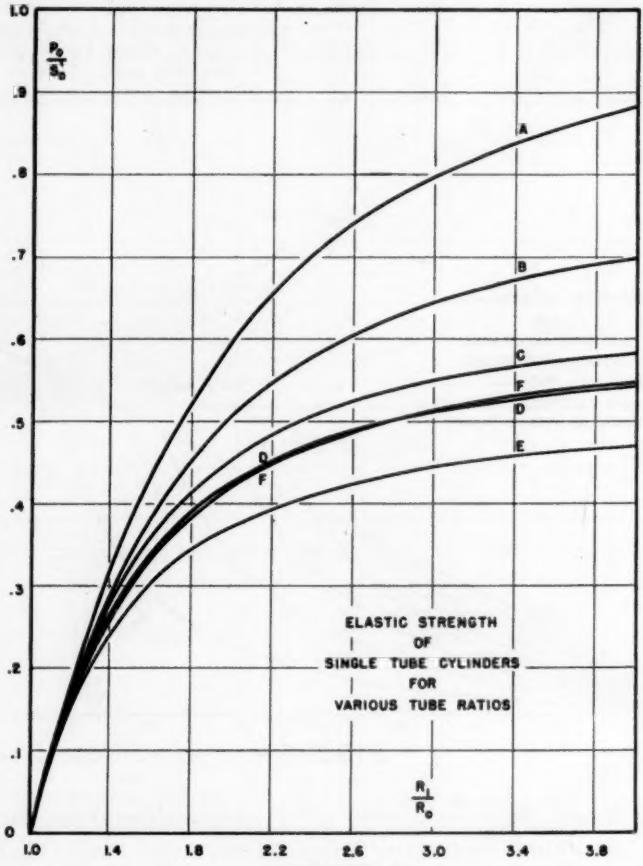

FIGURE 3

the effective stress $(S_0')_0$ is evaluated and compared with the yield stress of the material to determine the factor of safety.

For compound cylinders, the strength may be found readily by a simple graphical procedure, developed by the authors for the Bureau of Ordnance, U. S. Navy, and intended for applications where each component tube will yield simultaneously under the action of a certain bore pressure. This yields the maximum bore pressure obtainable elastically for any combination of tubes. By rewriting equations (15)

and (16),

$$\frac{S_{r_{n-1}}}{P_{n-1}} = -1, \tag{21}$$

$$\frac{S_{t_{n-1}}}{P_{n-1}} = \frac{1 + \left(\frac{R_n}{R_{n-1}}\right)^2 - 2\left(\frac{R_n}{R_{n-1}}\right)^2 \cdot \frac{P_n}{P_{n-1}}}{\left(\frac{R_n}{R_{n-1}}\right)^2 - 1}. \tag{22}$$

The stresses divided by the pressure P_{n-1} may then be evaluated for

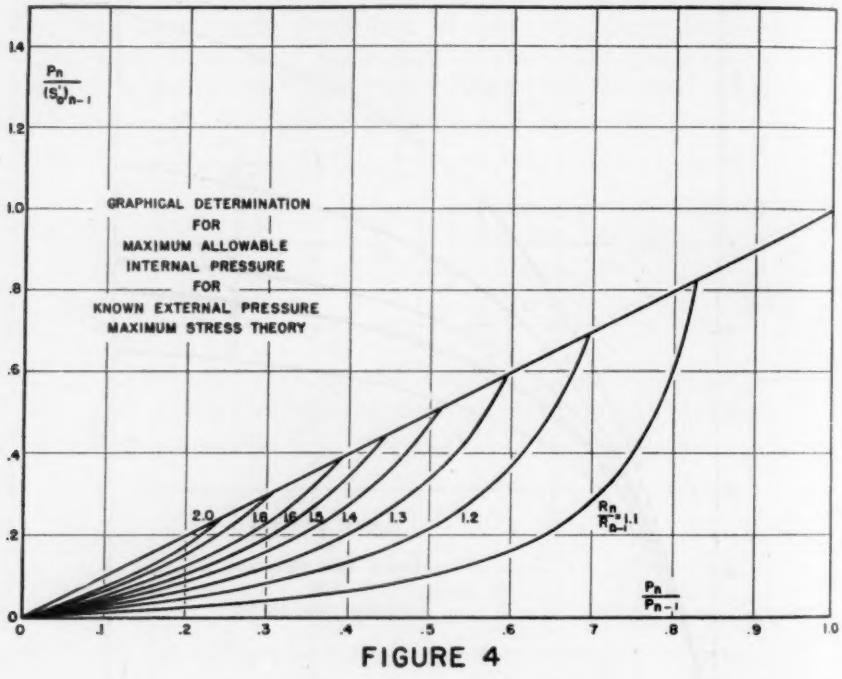

FIGURE 4

suitable wall and pressure ratios. For each wall and pressure ratio, a stress ratio is found, from which $S_{r_{n-1}}/(S_0')_{n-1}$ or $S_{t_{n-1}}/(S_0')_{n-1}$ is determined from Fig. 2 for a particular strength criterion, and $P_{n-1}/(S_0')_{n-1}$ evaluated as before. It will be found convenient to determine for the case considered the term $P_n/(S_0')_{n-1}$, and this is readily done since

$$\frac{P_n}{(S_0')_{n-1}} = \frac{P_{n-1}}{(S_0')_{n-1}} \times \frac{P_n}{P_{n-1}}. \tag{23}$$

Then $P_n/(S_0')_{n-1}$ is plotted vs. P_n/P_{n-1}. This procedure has been carried out for a range of wall ratios and for pressure ratios of $0 \leqslant \frac{P_n}{P_{n-1}} \leqslant 1$ and represented graphically for the six strength theories in Figs. 4 to 9.

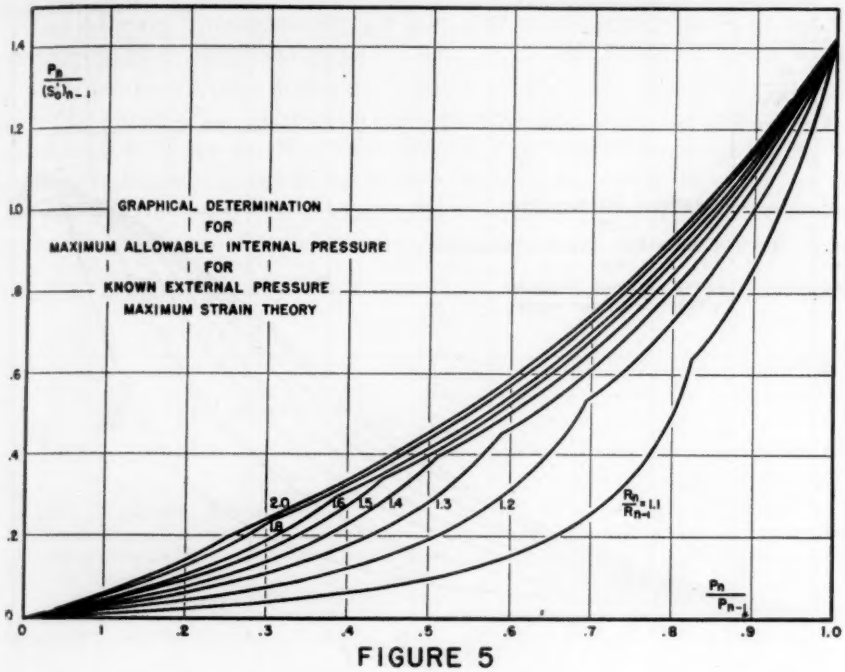

FIGURE 5

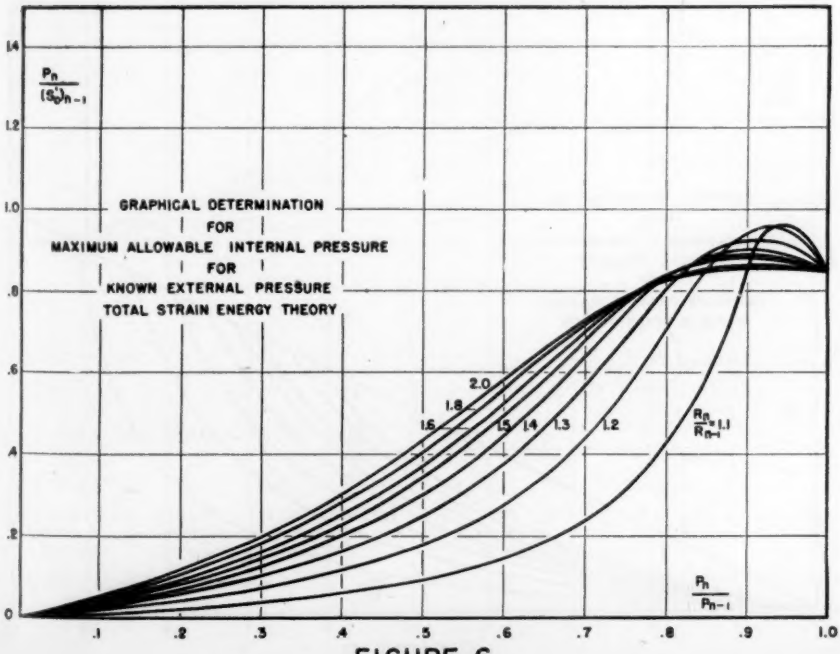

FIGURE 6

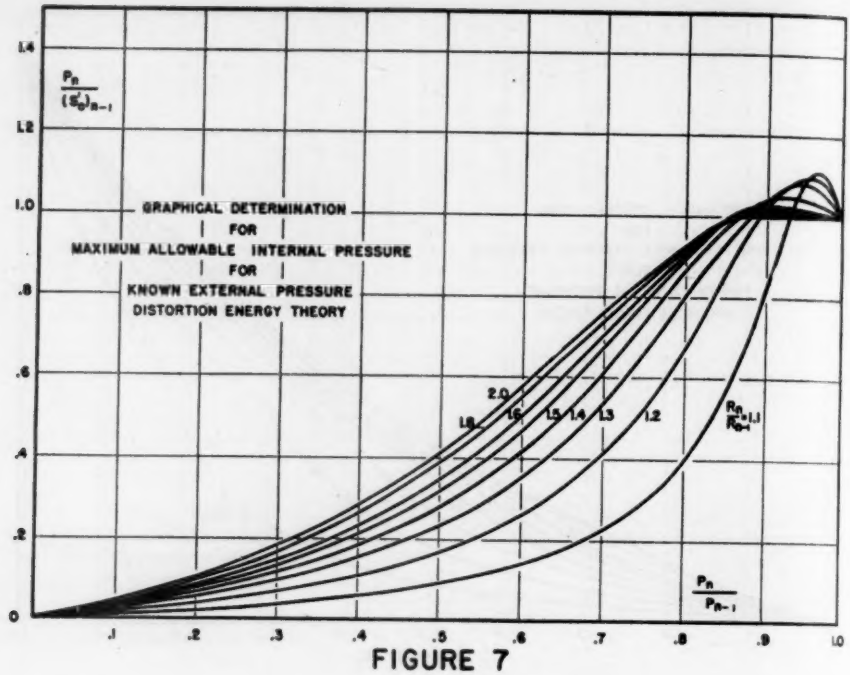

FIGURE 7

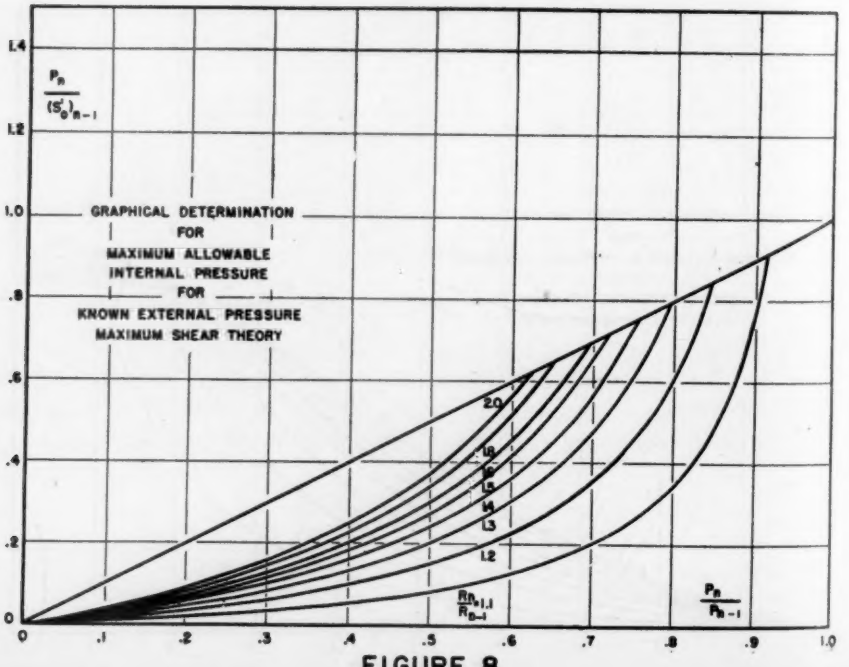

FIGURE 8

Considering a compound cylinder, the outermost tube is given the notation $n + 1$, with the radii R_n and R_{n+1} and internal pressure P_n. Its adjacent inner tube is the nth tube with radii R_{n-1} and R_n and pressures P_{n-1} and P_n. A similar notation is given to the other tubes. The strength of the outside tube $P_n/(S_0')_n$ is first found, following the analytical procedure outlined above for single tube cylinders, or by applying Fig. 3, using the strength criterion desired and the proper wall ratio. If $(S_0)_{n-1}$ is the yield strength of the adjacent inner tube, then $P_n/(S_0')_{n-1}$ is found since $\frac{P_n}{(S_0')_{n-1}} = \frac{P_n}{(S_0')_n} \cdot \frac{(S_0)_n}{(S_0)_{n-1}}$.* With the strength

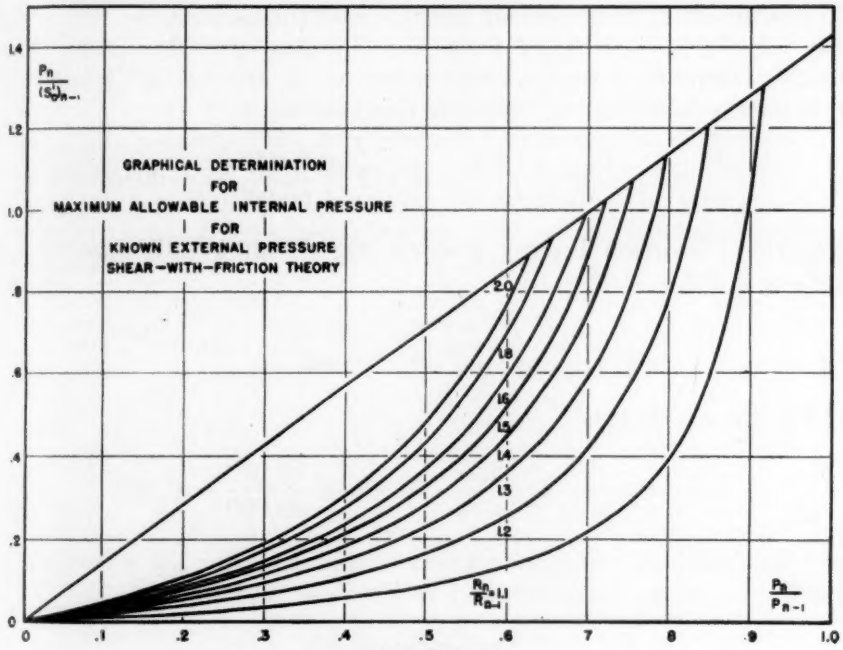

FIGURE 9

criterion selected for this tube, recourse is had to the appropriate one of Figs. 4 to 9. Using $P_n/(S_0')_{n-1}$ as ordinate, the abscissa P_n/P_{n-1} is found for the known wall ratio. Thus $\frac{P_{n-1}}{(S_0')_{n-1}} = \frac{P_n}{(S_0')_{n-1}} \div \frac{P_n}{P_{n-1}}$ is found for the inner tube. The procedure is continued for all the component cylinders, applying the particular wall ratio, yield strength and yielding criterion applicable to each component cylinder. Finally the term $P_0/(S_0')_0$ is found for the innermost tube from which the bore pressure $p_0 = P_0$ is determined for a particular yield stress or effective stress.

* This adjustment is necessary to maintain a constant factor of safety in all tubes.

As an example, consider the extreme case of a compound cylinder with component wall ratios $R_1/R_0 = 1.2$, $R_2/R_1 = 1.4$, $R_3/R_2 = 1.3$ and $R_4/R_3 = 1.2$. Assume that the yield strength of the first tube is 70,000 psi and subject to the Maximum Stress Theory, that the second tube obeys the Maximum Strain Theory with a yield strength of 80,000 psi, that the Distortion Energy Theory is to be used for the third tube with a yield stress of 60,000 psi, and finally the fourth tube has a yield value of 40,000 psi according to the Maximum Shear Theory. The bore pressure necessary for each component cylinder to yield simultaneously by its proper theory may then be found as easily for this example as for the case of equal yield stresses and identical strength criterion in all the component tubes. For the outer tube, with wall ratio 1.2, $P_3/(S_0')_3 = 0.152$ from Fig. 3, using the Maximum Shear Theory. Here P_3 is the pressure acting at R_3 and $(S_0')_3$ the effective stress for the fourth tube. For the third tube

$$\frac{P_3}{(S_0')_2} = \frac{P_3}{(S_0')_3} \times \frac{(S_0)_3}{(S_0)_2} = 0.152 \times \frac{40{,}000}{60{,}000} = 0.0946.$$

Using the Distortion Energy Theory, Fig. 7, for a wall ratio of 1.3, $P_3/P_2 = 0.290$ so that

$$\frac{P_2}{(S_0')_2} = \frac{P_3}{(S_0')_2} \div \frac{P_3}{P_2} = \frac{.0946}{.290} = .326$$

and for the second tube

$$\frac{P_2}{(S_0')_1} = \frac{P_2}{(S_0')_2} \times \frac{(S_0)_2}{(S_0)_1} = 0.326 \times \frac{60{,}000}{80{,}000} = 0.245.$$

Since the Maximum Strain criterion is applicable for the second tube, from Fig. 5, with a wall ratio of 1.4, $P_2/P_1 = .413$, and

$$\frac{P_1}{(S_0')_1} = \frac{P_2}{(S_0')_1} \div \frac{P_2}{P_1} = \frac{.245}{.413} = 0.592.$$

Finally for the first tube

$$\frac{P_1}{(S_0')_0} = \frac{P_1}{(S_0')_1} \times \frac{(S_0)_1}{(S_0)_0} = 0.592 \times \frac{80{,}000}{70{,}000} = 0.677.$$

Since the Maximum Stress Theory applies to the liner, and the wall ratio is 1.2, $P_1/P_0 = .691$ from Fig. 4. Then

$$\frac{p_0}{(S_0')_0} = \frac{P_0}{(S_0')_0} = \frac{P_1}{(S_0')_0} \div \frac{P_1}{P_0} = \frac{.677}{.691} = .979.$$

Letting $(S_0')_0 = (S_0)_0$ then $p_0 = .979 \times 70{,}000 = 68{,}600$ psi for simul-

taneous yielding in all tubes. If $(S_0')_0 \times \text{F.S.} = (S_0)_0$, then

$$p_0 = \frac{.979 \times 70{,}000}{\text{F.S.}}$$

and each tube will have this same factor of safety.

Not all combinations of wall ratios and strength theories will lead to simultaneous yielding of the component tubes of compound cylinders. The method outlined above for computing the bore pressure and the intermediate pressures will readily determine whether such a combination is possible. When no value of pressure ratio P_n/P_{n-1} exists for any one of Figs. 4 to 9 with a known value of $P_n/(S_0')_{n-1}$ and wall ratio R_n/R_{n-1}, that particular tube cannot yield simultaneously with previously considered outer tubes.

Having determined the bore pressure p_0 and the intermediate pressures P_1, P_2, etc., it is necessary to examine the effective stresses in the state of rest, i.e., when the bore pressure has been reduced to zero. For practical cases in the state of rest the effective stress at the inner radius of any component tube is generally the largest. The stresses at this point are those of equations (15) and (16) when reduced by relief of the bore pressure or

$$S_{r_{n-1}} = -P_{n-1} + \frac{\left(\frac{R_4}{r}\right)^2 - 1}{\left(\frac{R_4}{R_0}\right)^2 - 1} \cdot p_0 \tag{24}$$

$$S_{t_{n-1}} = \frac{\left(\frac{R_n}{R_{n-1}}\right)^2 + 1}{\left(\frac{R_n}{R_{n-1}}\right)^2 - 1} \cdot P_{n-1} - \frac{2\left(\frac{R_n}{R_{n-1}}\right)^2}{\left(\frac{R_n}{R_{n-1}}\right)^2 - 1} \cdot P_n - \frac{\left(\frac{R_4}{r}\right)^2 + 1}{\left(\frac{R_4}{R_0}\right)^2 - 1} \cdot p_0 \tag{25}$$

where p_0 is the bore pressure, R_0 the bore radius and R_4 the outer radius of the compound cylinder. Since P_0, P_{n-1} and P_n have been determined by the above analysis, equations (24) and (25) are readily evaluated. The effective stress for each tube in rest is found by determining the stress ratio and making use of Fig. 2 for the proper strength criterion as previously described. Should the effective stress exceed the yield strength of the tube material, then yielding will occur in the state of rest for the compound cylinder in question, and, hence, this cylinder is not suitably designed. It will be found convenient to determine for the component tube the dimensionless ratio $P_{n-1}/(S_0')_{n-1}$ as previously

found for the state of action, to serve as an indication of strength. Thus the rest strength at the bore of the cylinder becomes p_0/S_0'. Yielding will then occur in rest for a particular tube when

$$\frac{P_{n-1}}{(S_0')_{n-1}} < \frac{P_{n-1}}{(S_0)_{n-1}}. \tag{26}$$

ALTERNATIVE METHOD OF STRENGTH ANALYSIS.

An alternative method may be used for the determination of bore and component tube pressures for any multi-tube cylinder subjected to simultaneous yielding conditions. In this method the graphical representation of the strength theories given in Fig. 1 is used when S_0 is replaced by S_0' together with equations (15) and (16).*

* Equation (16) is first rewritten as

$$\frac{S_{t_{n-1}}}{(S_0')_{n-1}} = \frac{\left(\frac{R_n}{R_{n-1}}\right)^2 + 1}{\left(\frac{R_n}{R_{n-1}}\right)^2 - 1} \cdot \frac{P_{n-1}}{(S_0')_{n-1}} - \frac{2\left(\frac{R_n}{R_{n-1}}\right)^2}{\left(\frac{R_n}{R_{n-1}}\right)^2 - 1} \cdot \frac{P_n}{(S_0')_{n-1}}. \tag{26a}$$

It is seen that (26a) is the equation of a straight line when represented on the coordinates of Fig. 1, since by equation (15) $P_{n-1} = -S_{r_{n-1}}$. Here $P_n/(S_0')_{n-1}$ merely acts as a parameter, and is assumed to be known for the wall ratio and strength theory in question. The intersection of (26a) with the proper strength theory curve then determines the radial and tangential stresses necessary to produce the required yield stress for the component tube.

As an illustration of the method, consider again the above example. The outer tube is first analyzed, having a wall ratio of 1.2 and a yield stress of 40,000 psi subjected to the Maximum Shear Theory. Here $n = 4$ and equation (26a) becomes

$$\frac{S_{t_3}}{(S_0')_3} = -5.546 \frac{S_{r_3}}{(S_0')_3}.$$

This equation is represented on Fig. 10 which is identical with Fig. 1. Intersection with curve E gives $S_{r_3}/(S_0')_3 = -.152$, $S_{t_3}/(S_0')_3 = .845$. For the third tube, subjected to the Distortion Energy Theory, having a wall ratio of 1.3 and a yield stress of 60,000 psi, equation (26a) becomes

$$\frac{S_{t_2}}{(S_0')_2} = 3.899 \frac{P_2}{(S_0')_2} - 4.899 \frac{P_2}{(S_0')_2}$$

$$= -3.899 \frac{S_{r_2}}{(S_0')_2} + 4.899 \times \frac{40{,}000}{60{,}000} \times \frac{S_{r_3}}{(S_0')_3}$$

by making the necessary substitutions. Since $S_{r_3}/(S_0')_3$ is known from above, this expression is represented in Fig. 10 from which for the Distortion Energy Theory (curve D) $S_{r_2}/(S_0')_2 = -.326$ and $S_{t_2}/(S_0')_2 = .795$. The process is continued for the second tube having a wall ratio of 1.4, a yield stress of 80,000 psi, according to the Maximum Strain Theory. Equation (26a) then simplifies to

$$\frac{S_{t_1}}{(S_0')_1} = -3.083 \frac{S_{r_1}}{(S_0')_1} + 4.083 \frac{S_{r_2}}{(S_0')_2} \times \frac{60{,}000}{80{,}000}.$$

Plotting this equation on Fig. 10, for the Maximum Strain Theory (curve B) $S_{r_1}/(S_0')_1 = -.592$ and $S_{t_1}/(S_0')_1 = .821$. Finally for the first tube with ratio 1.2 where the Maximum Stress Theory has been adopted for a yield stress of 70,000 psi, equation (26a) may be expressed as

$$\frac{S_{t_0}}{(S_0')_0} = -5.546 \frac{S_{r_0}}{(S_0')_0} + 6.546 \frac{S_{r_1}}{(S_0')_1} \times \frac{80{,}000}{70{,}000}.$$

The intersection of this equation with curve A of Fig. 10 gives $S_{r_0}/(S_0')_0 = -.979$ and $S_{t_0}/(S_0')_0 = 1.000$. Since $p_0 = -S_{r_0}$, the maximum allowable bore pressure for this combination of tubes under simultaneous yielding conditions is $p_0 = .979 \times 70{,}000 = 68{,}600$ psi as above.

DETERMINATION OF SHRINKAGES.

To complete the design of a compound cylinder for simultaneous yielding there remains the determination of the proper shrinkages which will produce the necessary pressures between the component tubes in the state of rest. In this paper shrinkage is defined as the difference between corresponding radii of the partially assembled compound cylinder and the next component tube prior to its assembly. It should be pointed out that the method of assembly, i.e., the sequence in which tubes are added in assembling the compound cylinder, influences the values of these shrinkages. To eliminate the many variables that could occur in building up a multi-tube cylinder, the method of assembly most frequently used will be adopted, namely, the addition of the adjacent outside tubes starting from the second tube, followed by assembly of the whole onto the liner or first tube. Thus for a four-tube cylinder, the second tube is followed by the third, followed by the fourth, and finally the first is added. This method of assembly is called two-three-four-one.

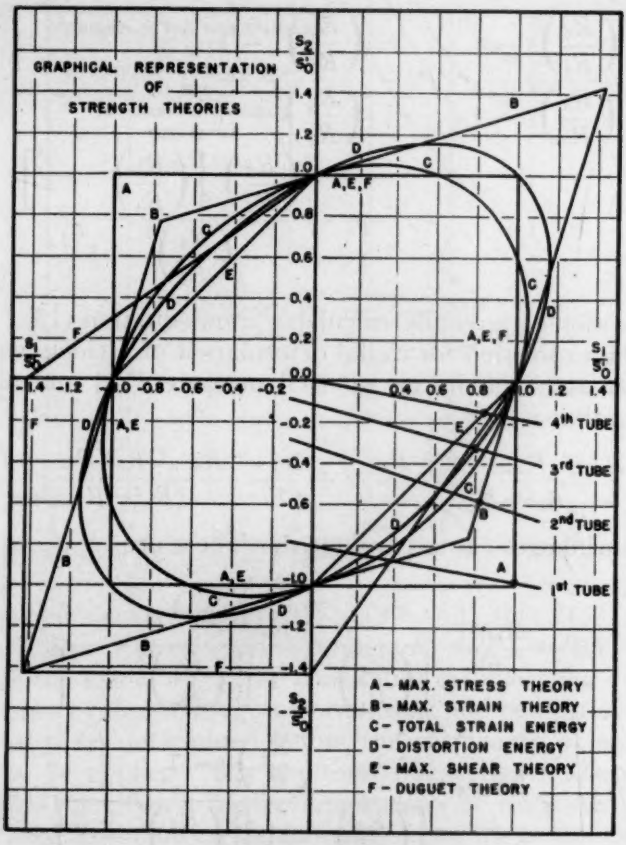

FIGURE 10

It will be found convenient to determine the shrink-fit pressure, i.e., the pressure which is developed between the partially assembled cylinder and the newly added component tube. The shrinkages may then be readily found from this pressure. These shrink-fit pressures can be determined from the pressures existing between the cylinders in action, namely, P_1, P_2, P_3, etc. Letting p_1, p_2, p_3, etc., be the shrink-fit pressures, for a four-tube compound cylinder assembled as above, then

$$p_1 = P_1 - \frac{\left(\frac{R_4}{R_1}\right)^2 - 1}{\left(\frac{R_4}{R_0}\right)^2 - 1} \cdot P_0, \tag{27}$$

$$p_3 = P_3 - \frac{\left(\frac{R_4}{R_3}\right)^2 - 1}{\left(\frac{R_4}{R_0}\right)^2 - 1} \cdot P_0 - \frac{\left(\frac{R_4}{R_3}\right)^2 - 1}{\left(\frac{R_4}{R_1}\right)^2 - 1} \cdot p_1, \tag{28}$$

$$p_2 = P_2 - \frac{\left(\frac{R_4}{R_2}\right)^2 - 1}{\left(\frac{R_4}{R_0}\right)^2 - 1} \cdot P_0 - \frac{\left(\frac{R_4}{R_2}\right)^2 - 1}{\left(\frac{R_4}{R_1}\right)^2 - 1} \cdot p_1 - \frac{\left(\frac{R_3}{R_2}\right)^2\left[\left(\frac{R_2}{R_1}\right)^2 - 1\right]}{\left(\frac{R_3}{R_1}\right)^2 - 1} \cdot p_3. \tag{29}$$

These expressions are readily calculable from equation (13).

From the expression for radial deformation of a thick-walled open-end cylinder acted on by an internal pressure P_{n-1} and an external pressure P_n, that is,

$$u = \frac{1-\nu}{E} \cdot \frac{R_{n-1}^2 \cdot P_{n-1} - R_n^2 \cdot P_n}{R_n^2 - R_{n-1}^2} \cdot r + \frac{1+\nu}{E} \cdot \frac{R_{n-1}^2 \cdot R_n^2 (P_{n-1} - P_n)}{(R_n^2 - R_{n-1}^2) \cdot r}, \tag{30}$$

the radial shrinkages can be evaluated. These are

$$U_1 = \frac{2R_1 p_1}{E} \cdot \frac{\left(\frac{R_4}{R_0}\right)^2 - 1}{\left[\left(\frac{R_4}{R_1}\right)^2 - 1\right]\left[\left(\frac{R_1}{R_0}\right)^2 - 1\right]}, \tag{31}$$

$$U_2 = \frac{2R_2 p_2}{E} \cdot \frac{\left(\frac{R_3}{R_1}\right)^2 - 1}{\left[\left(\frac{R_3}{R_2}\right)^2 - 1\right]\left[\left(\frac{R_2}{R_1}\right)^2 - 1\right]}, \tag{32}$$

$$U_3 = \frac{2R_3p_3}{E} \cdot \frac{\left(\frac{R_4}{R_1}\right)^2 - 1}{\left[\left(\frac{R_3}{R_1}\right)^2 - 1\right]\left[\left(\frac{R_4}{R_3}\right)^2 - 1\right]}, \tag{33}$$

where U_1 is the radial shrinkage at R_1, etc., as described above. For

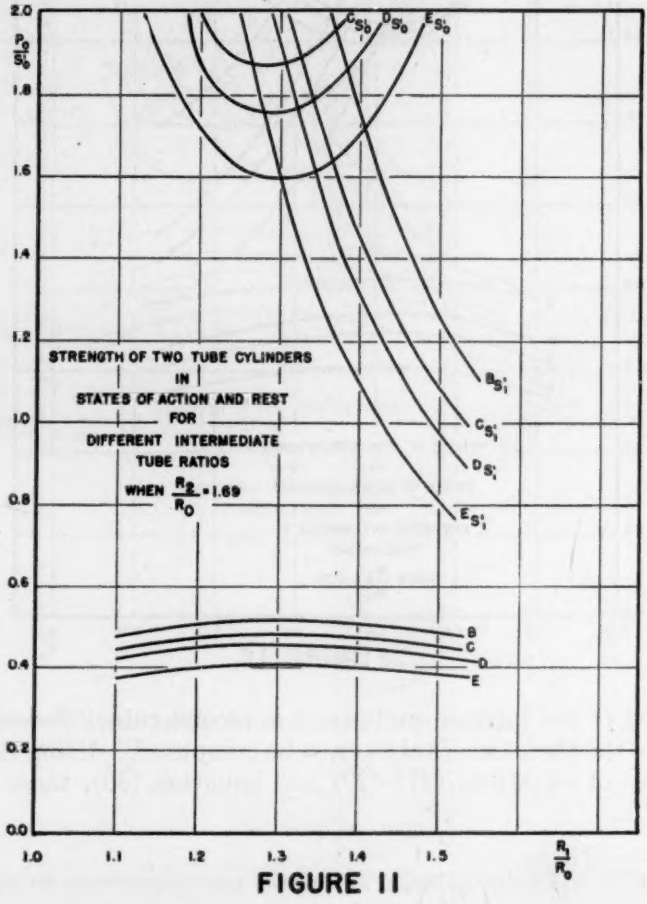

FIGURE 11

three-tube cylinders equations (27) to (29) and (31) to (33) may be used where $R_4 = R_3$. For two-tube cylinders $R_4 = R_3 = R_2$.

During the assembly of the compound cylinder, the dimensions of the component tubes undergo deformations and certain of these deformations must be determined before the shrinkages of equations (31) to (33) can be applied. For the four-tube cylinder assembled in the manner two-three-four-one the deformation of the external radius of the third tube R_3, following its shrinkage upon the second tube, and the

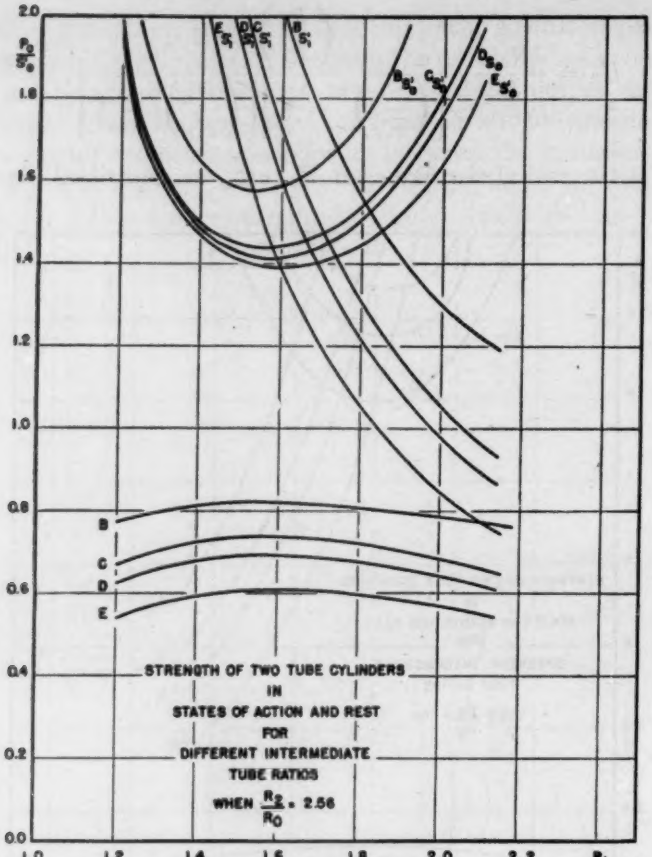

FIGURE 12

deformation of the internal radius of the second tube following the assemblage of the three outer tubes must be computed. Using the shrink-fit pressures of equations (27)–(29) and equation (30), these deformations are

$$u_3 = \frac{2R_3p_2}{E} \cdot \frac{1}{\left(\frac{R_3}{R_2}\right)^2 - 1} \tag{34}$$

$$u_1 = -\frac{2R_1p_2}{E} \cdot \frac{\left(\frac{R_2}{R_1}\right)^2}{\left(\frac{R_2}{R_1}\right)^2 - 1} - \frac{2R_1p_3}{E} \cdot \frac{\left(\frac{R_3}{R_1}\right)^2}{\left(\frac{R_3}{R_1}\right)^2 - 1}. \tag{35}$$

From equations (31)–(33) together with equations (34) and (35), the shrinkages of the unassembled tubes can be found. Denoting the un-

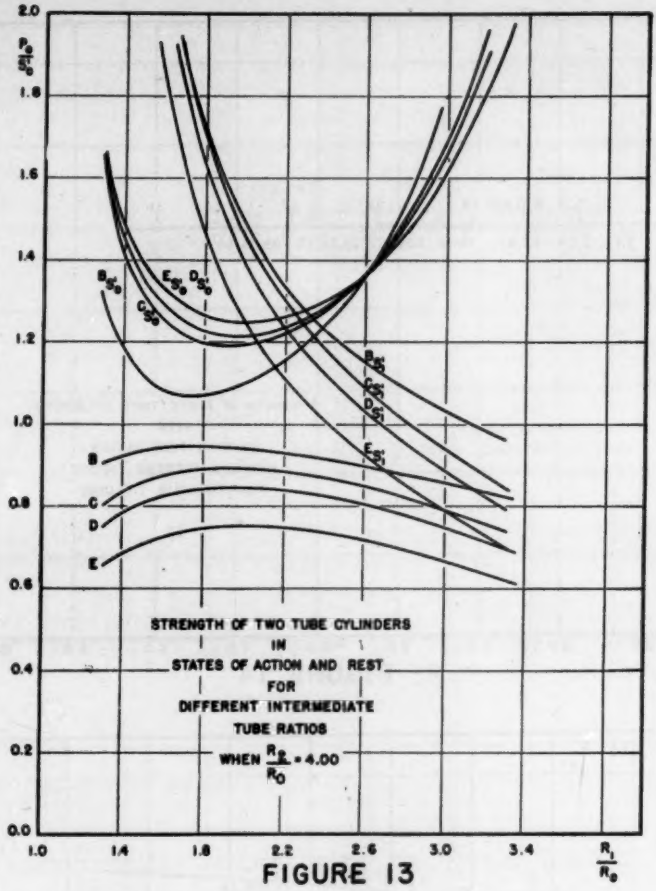

FIGURE 13

assembled shrinkages with a prime mark, these are

$$U_1' = U_1 - u_1,$$
$$U_2' = U_2$$
$$U_3' = U_3 - u_3.$$

SELECTION OF COMPONENT WALL RATIOS FOR MAXIMUM STRENGTH OF CYLINDER.

It has been pointed out that for any combination of component tubes in a compound cylinder, maximum strength occurs when all tubes yield simultaneously. The question now arises as to whether, for a given overall wall ratio of a compound cylinder, certain combinations of component wall ratios will predict greater strength under simultaneous yielding conditions than others. Formal analysis for this optimum condition is quite tedious in multi-tube cylinders, except perhaps for the simpler strength criteria. Certain examples have been worked out from which one may generalize with few exceptions that for a given

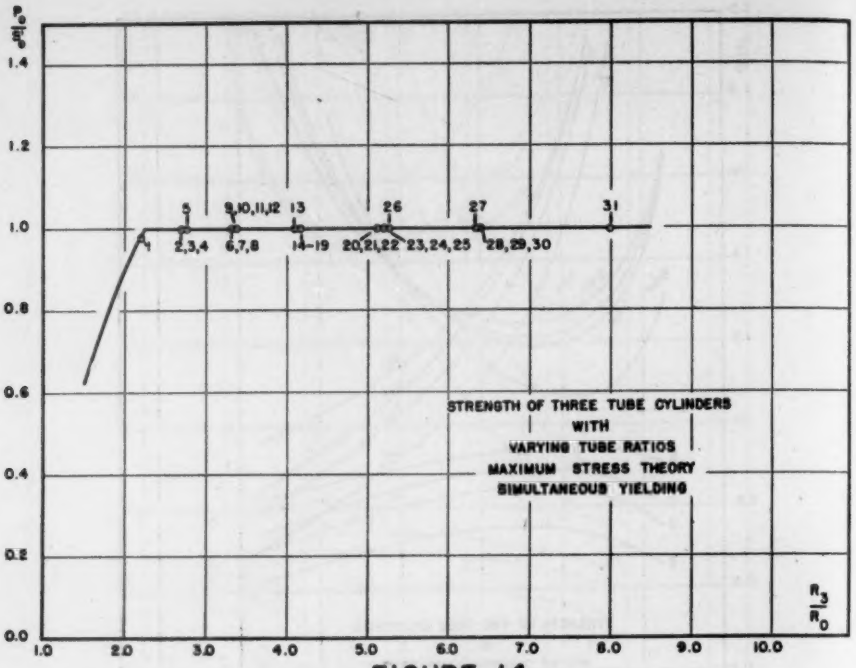

FIGURE 14

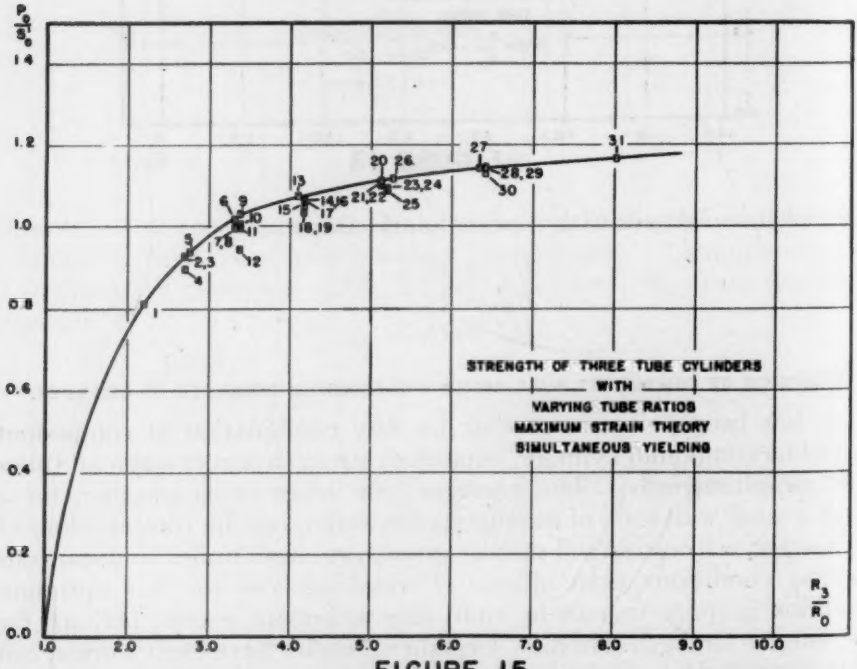

FIGURE 15

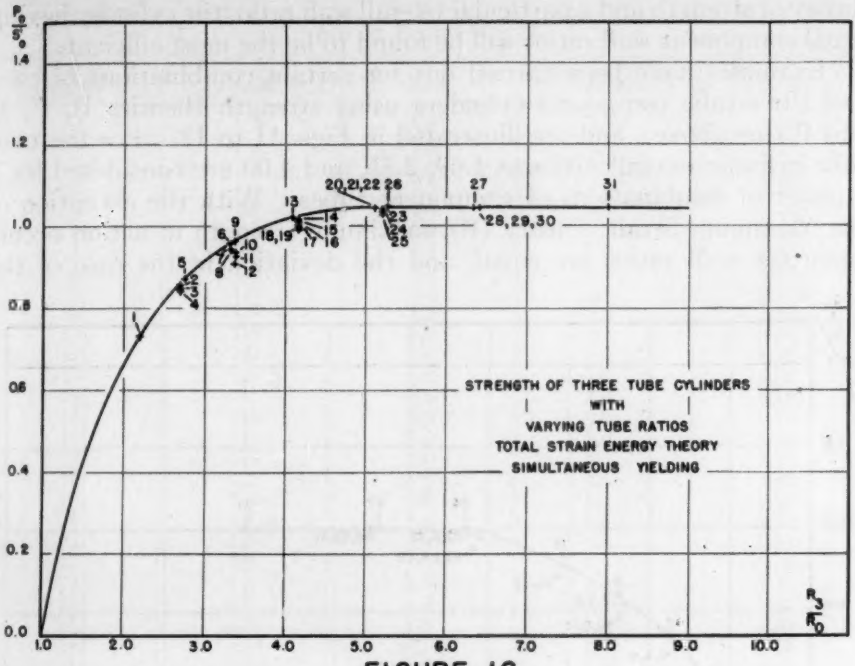

FIGURE 16

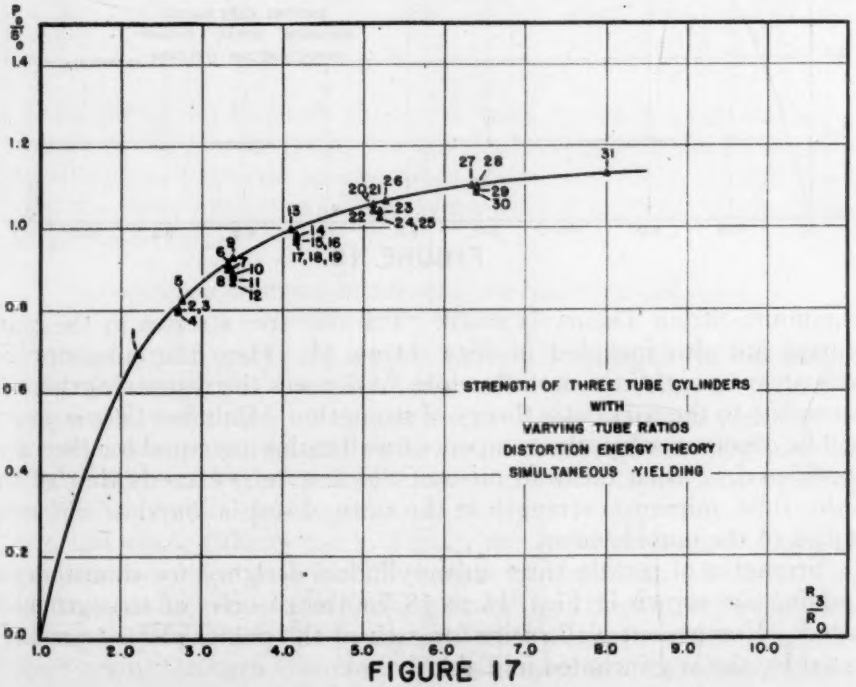

FIGURE 17

theory of strength and a particular overall wall ratio, the cylinder having equal component wall ratios will be found to be the most efficient.

Examples have been carried out for certain combinations of two- and three-tube compound cylinders using strength theories B, C, D and E (see above), and are illustrated in Figs. 11 to 18. For the two-tube cylinder overall ratios of 1.69, 2.56, and 4.00 are considered for a number of combinations of component tubes. With the exception of the Maximum Strain Theory (B), maximum strength in action occurs when the wall ratios are equal, and the deviation in the case of the

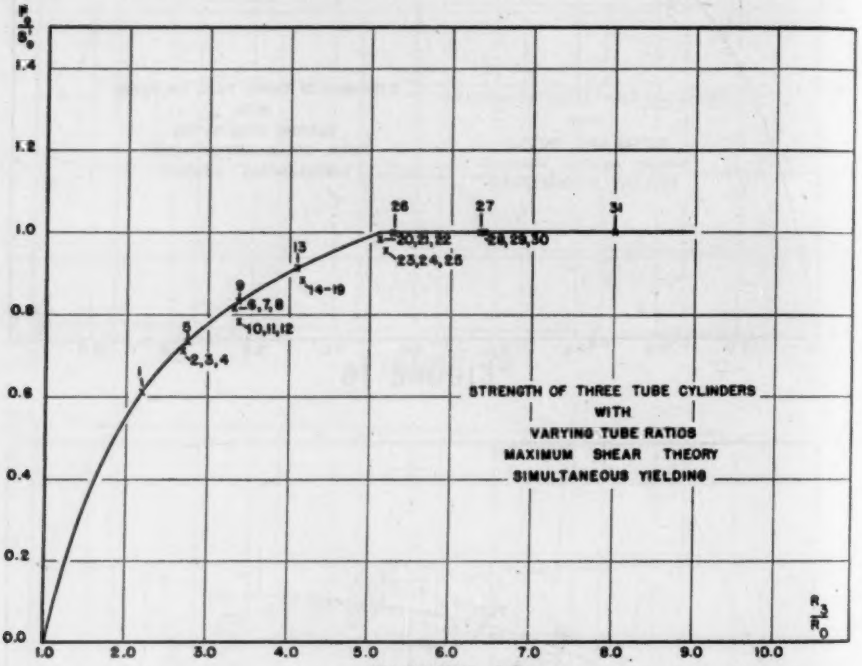

FIGURE 18

Maximum Strain Theory is small. The effective stresses in the state of rest are also included in Figs. 11 to 13. Here the subscript S_0' indicates strength in rest at R_0 while S_1' denotes the rest strength at R_1 according to the particular theory of strength. Minimum bore strength will be observed when the component wall ratios are equal for the cases considered. When the wall ratio of the first tube exceeds that of the outer tube, minimum strength in the state of rest is found at the inner radius of the outside tube.

Strengths of certain three tube cylinders designed for simultaneous yielding are shown in Figs. 14 to 18 for the theories of strength indicated. Component wall ratios for each of the points plotted are indicated by the key included in Table I.

TABLE I.
Key for Figures 14 to 18.

Number	R_1/R_0	R_2/R_1	R_3/R_2	R_3/R_0
1	1.3	1.3	1.3	2.195
2	1.3	1.3	1.6	2.70
3	1.3	1.6	1.3	2.70
4	1.6	1.3	1.3	2.70
5	1.4	1.4	1.4	2.745
6	1.3	1.6	1.6	3.32
7	1.6	1.3	1.6	3.32
8	1.6	1.6	1.3	3.32
9	1.5	1.5	1.5	3.375
10	1.3	1.3	2.0	3.38
11	1.3	2.0	1.3	3.38
12	2.0	1.3	1.3	3.38
13	1.6	1.6	1.6	4.09
14	1.3	1.6	2.0	4.16
15	1.3	2.0	1.6	4.16
16	1.6	1.3	2.0	4.16
17	1.6	2.0	1.3	4.16
18	2.0	1.3	1.6	4.16
19	2.0	1.6	1.3	4.16
20	1.6	1.6	2.0	5.12
21	1.6	2.0	1.6	5.12
22	2.0	1.6	1.6	5.12
23	1.3	2.0	2.0	5.20
24	2.0	1.3	2.0	5.20
25	2.0	2.0	1.3	5.20
26	1.74	1.74	1.74	5.27
27	1.85	1.85	1.85	6.33
28	1.6	2.0	2.0	6.40
29	2.0	1.6	2.0	6.40
30	2.0	2.0	1.6	6.40
31	2.0	2.0	2.0	8.0

For a particular strength theory, a curve drawn through the upper boundary of the plotted points contains only those combinations where the wall ratios of the component tubes are equal. Unequal wall ratios having the same overall ratio give lower strengths under simultaneous yielding conditions.

COMPARISON OF STRENGTH THEORIES FOR COMPOUND CYLINDERS OF MAXIMUM EFFICIENCY.

Figure 3 and Figs. 19–21 include curves of strength for compound cylinders of one, two, three and four component tubes respectively having equal wall ratios under conditions of simultaneous yielding for both the states of action and rest. From these figures there may be readily observed the comparative strengths of the various yielding criteria considered in this paper.

For the single tube cylinder, Fig. 3, the strength defined above as p_0/S_0' increases rapidly for small changes of wall ratio when the wall ratio is low, and approaches a limiting strength as the wall ratio becomes quite large. Wide variation in the predicted strength will be observed for the various strength theories. For example, the most conservative

Maximum Shear Theory predicts strengths about one-half of the least conservative Maximum Stress Theory when the wall ratio is large. The other theories fall within these bounds. Of particular interest is the close agreement between the widely-accepted Distortion Energy Theory and the Shear-with-Friction Theory. This is not surprising in view of the close agreement of these two theories over a portion of the fourth quadrant of Fig. 1.

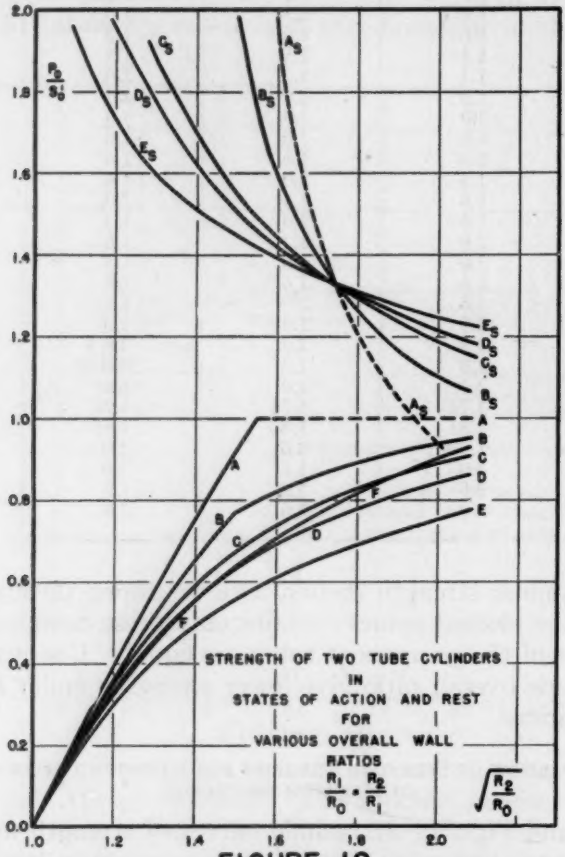

FIGURE 19

The strength of the two-tube cylinder is depicted in Fig. 19. For low wall ratios the spread of the curves is not as marked as in the single tube case, and a convergence is indicated as the wall ratio is increased. The Maximum Stress Theory (A) rapidly reaches its limiting strength of $p_0/S_0' = 1.000$, and the Maximum Strain Theory (B) shows a discontinuity in slope, reflecting the discontinuity in slope found in the fourth quadrant of Fig. 1 for this theory. Agreement between the Distortion Energy Theory (D) and the Shear-with-Friction Theory (F)

becomes poorer for large wall ratios. Strengths at the bore in the state of rest are included and indicated by the subscripts. For low wall ratios those theories which are conservative in action are also conservative in rest, but as the wall ratio increases, this condition reverses itself. Strengths in rest for the Shear-with-Friction Theory are too large to be included on this figure and serve to indicate that this theory is far too optimistic in predicting strengths in compression.

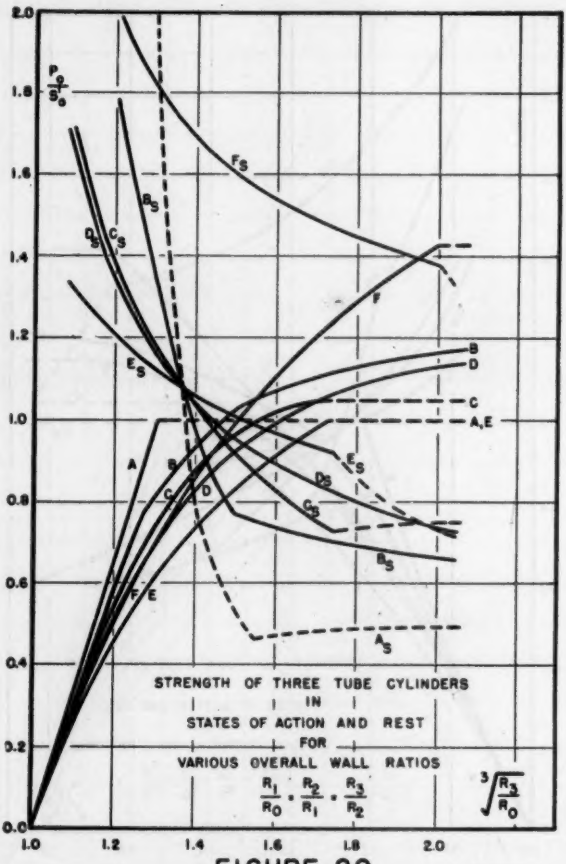

FIGURE 20

In the three-tube compound cylinder, Fig. 20, strengths in action for low wall ratios behave similarly to the single and two-tube cylinder. For larger tube ratios certain strength theories such as (A), (C) and (E) reach limiting values while certain of the more conservative theories now exceed them in strength. The Shear-with-Friction theory becomes exceedingly optimistic in its predicted strength. For a given component tube ratio, strengths in action are greater than for the two-tube cylinder,

while strengths in the state of rest are lower. As before the Shear-with-Friction theory is excessive in the state of rest.

The four-tube cylinder shows the same trends as the three-tube case. Most of the theories have approached their limiting strength in action, while strengths for any given component tube ratio are somewhat higher. Rest stresses are correspondingly lower than for the three tube case.

For any particular theory the design limitation would be that com-

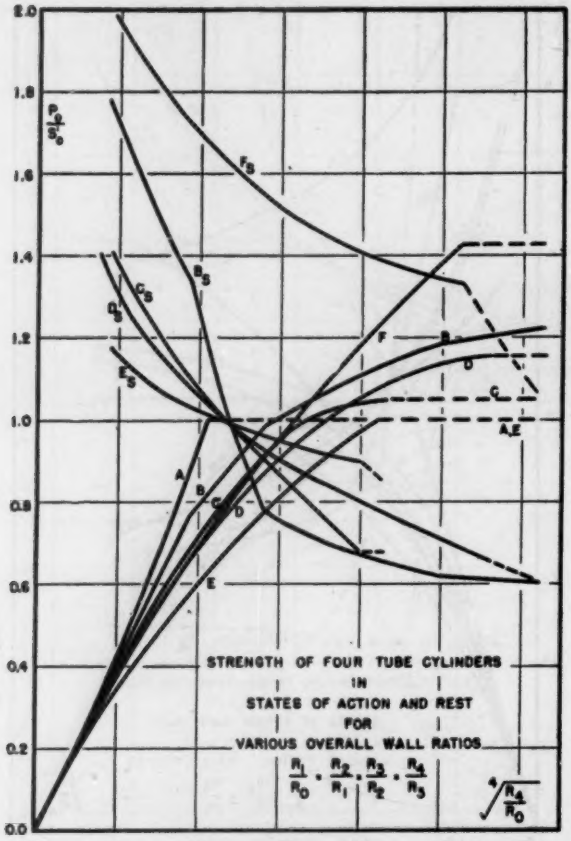

FIGURE 21

ponent wall ratio when the strength in action and rest are equal. This component wall ratio decreases as the number of component tubes increases. Thus for the Distortion Energy Theory (D), the limiting wall ratio is infinite for a single tube cylinder, 3.65 (by extrapolation) for the two-tube case, 1.520 for three tubes, and 1.297 for four tubes. This corresponds to an overall ratio of 13.3 for two tubes, 3.505 for three tubes and 2.835 for four component tubes. The strengths correspond-

ing to these ratios drop from 0.998 for two tubes to 0.940 for three tubes and to 0.901 for four tubes. It is evident, then, that the efficiency of the section increases considerably as the number of component tubes increases, while the maximum available strength for equal yielding conditions in action and rest decreases.

CURVES OF SHRINKAGE.

The curves of shrinkage as a function of the component wall ratio for compound cylinders yielding simultaneously with equal wall ratios

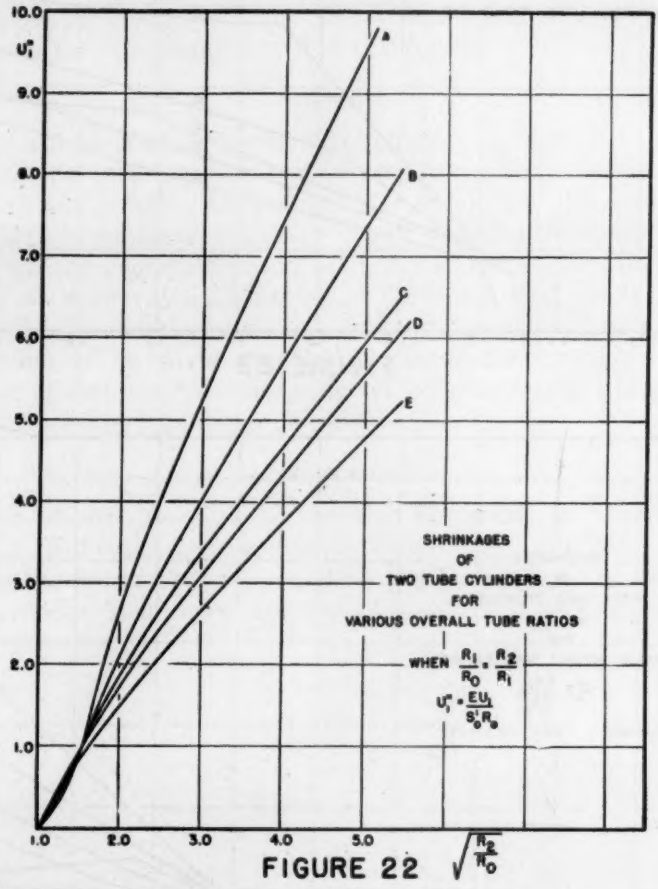

FIGURE 22

are included in Figs. 22, 23 and 24 for two- and three-tube cylinders. In Fig. 22, for two-tube cylinders the dimensionless term $U_1'' = EU_1/S_0'R_0$ is used to represent the radial shrinkage between the two cylinders and the data in this figure may be calculated from equation (31) when $R_4 = R_2$, using the shrink-fit pressures associated with the different strength theories. No great difference in shrinkages for the various

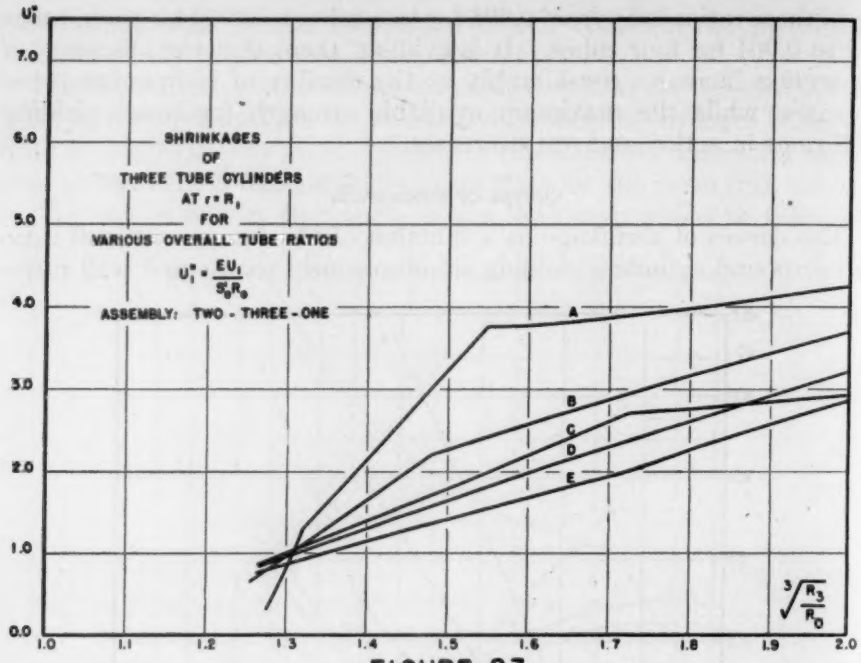

FIGURE 23

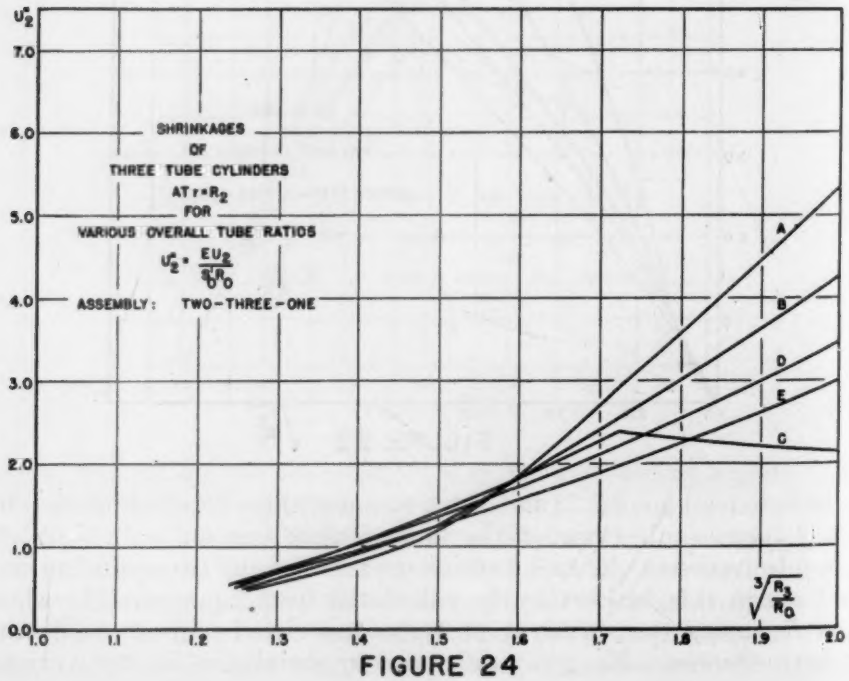

FIGURE 24

strength theories is noted when the wall ratio is small, but the divergence and spread is quite marked above a wall ratio of 1.5.

For three-tube cylinders when the method of assembly is two-three-one, the shrinkages at R_1 and R_2 are included in Figs. 23 and 24. The spread is quite noticeable over the range of wall ratios considered for the radial shrinkage U_1, and three of the theories show discontinuities in slope, corresponding to the discontinuities in slope in the strength curves, Fig. 20. The shrinkages at R_2 for the various strength theories are not markedly different until the larger cylinders are approached when divergence begins. Only the Total Strain Energy Theory (C) shows a noticeable discontinuity in this figure.

SUMMARY.

A general discussion is given of the effects of various strength theories on the design of compound cylinders. Six different yielding criteria have been examined. These include some of the oldest and also the latest theories of strength. New short design procedures of general application are suggested which will serve to reduce the time ordinarily required in such calculations. The methods used are flexible since compound cylinders composed of tubes of different materials and following different strength theories can be handled as easily as a cylinder composed of tubes of only one material. Considerable design information of immediate application is included.

ACKNOWLEDGMENT.

The problem discussed herein was suggested to the authors by Captain F. F. Foster, Commander B. D. Mills, Jr., and Mr. C. B. Green all of the Bureau of Ordnance, United States Navy. The authors wish to acknowledge their encouragement, support, and suggestions throughout the investigation.

Refining Vegetable Oils by Petroleum Methods. (*Chemical Engineering*, Vol. 53, No. 12.)—By the application of various engineering principles and techniques developed in their work in the petroleum refining industry, and in addition, by the utilization of chemical engineering methods, the M. W. Kellogg Co. has developed a new process for the refining of vegetable oils, fish oils, animal fats, waxes and fatty substances in general. While it has only recently been announced it has been quietly winning acceptance in industry since the end of the war, notably in paints and varnishes, soaps and related products, vitamins, and various edible oils. At present seven commercial plants are under construction in the United States and abroad.

The Solexol refining process is a solvent (propane) extraction and fractionation method. It is a countercurrent process which works automatically in a completely closed system. The solvent follows a circulating course around the system and is used over and over again. It costs less than five cents a gallon and the loss, as it circulates repeatedly through the columns, is so small as to be an insignificant factor of operating cost. The process deodorizes, decolorizes, extracts, and concentrates the basic factors of the oils and fats.

On the economic side, the process is said to assure increased earning power to oil processors through two advantages: (*a*) low cost of operation; and (*b*) recovery of various products having high market value from oils which in their present state sell at low prices.

While it is applicable to all types of vegetable oils, the process work to date has been concentrated on soybean oil and cottonseed oil. Refining of soybean oil by this method has brought forth a diversity of oil products, both edible and industrial, which have already established their marketability. For example, 100 lb. of soybean oil, when processed, yields various fractional oils—decolorized, deodorized, and refined. The yield includes: 68.5 lb. of salad oil, 30 lb. of quick drying paint oil, and 1.5 lb. of lecithin and other products.

R. H. OPPERMANN.

Old Process Solves Gas Turbine Problem. (*Power Plant Engineering*, Vol. 50, No. 12.)—Mass production of precision-cast blades for aviation gas turbines is now possible by using a 16th century wax model process originated by the Florentine sculptor, Benvenuto Cellini. A precision-casting laboratory set up by the Westinghouse Electric Corp. is producing metal turbine blades by this process.

Turbine blades were previously stamped out of red-hot metal by a heavy forge. Development of a more durable metal alloy made the blades so hard that the drop forge dies suffered excessive wear and frequently broke. Using the wax model process, blades are now turned out as precisely as if each had been machined on a lathe. The only machining now required is in making a master pattern of the turbine blade desired. A metal die is made from the master pattern and molten wax injected into it to produce a wax model. Twelve of these models are mounted on a wax base and covered with a metal flask into which is poured a mixture of clay and silica. When the cement hardens, the flasks are put into an oven where the wax melts and burns away, leaving cavities in the cement into which molten metal will be poured to form the finished turbine blades.

R. H. OPPERMANN

NOTES FROM THE NATIONAL BUREAU OF STANDARDS.*

STANDARDS FOR ANALYTICAL FILTER PAPERS.

Standards of quality for analytical filter papers, previously nonexistent for this important item in chemical research and analysis, are being developed by the Bureau's Paper Laboratory through a critical evaluation of all currently available brands. Based on improved testing methods perfected at the Bureau, together with established procedure for certain basic determinations, it is believed the standards finally recommended will provide a ready means of determining the suitability of a particular paper for its intended use. Requirements will be included for the three classes of general analytical work involving coarse, medium, and fine precipitates.

Analytical filter papers, like many other laboratory materials, have an importance to science and industry far in excess of their dollar value. Many industrial processes require quick, accurate analyses for their control and these depend, in many cases, on the speed, retentiveness, and purity of the filter paper used in making the analyses.

Filter papers have been used and bought by brand names, practically as a tradition among laboratory workers, and preference has usually been given to imported papers, most of which have come from England, Germany, and Sweden. When the war made supplies from these sources uncertain, American manufacturers began production of grades of analytical papers that had not previously been made in this country. In order to provide data that would be useful as a guide to manufacturers and users in comparing the quality of different papers, as well as to eliminate dependence on brand names, the Bureau undertook an investigation of the physical and chemical properties of the papers.

Improved methods were developed for determination of rate of flow of water through the papers, retention of fine precipitates, and ash content, as well as a method for measuring the bursting strength of wet paper. Density, purity of cellulose, and acidity, for which definite testing procedures were already available, are also important determinations.

The method for rate of flow of water is of special interest. Unique in that it does not require the use of special, complicated apparatus, it posesses the advantage of simulating the manner in which filtrations are made. The filter paper is folded in a cone in the usual way, taking care to expel air pockets. Instead of placing in a funnel, however, the cone is suspended freely in a wire loop, thus eliminating the variables

* Communicated by the Director.

such as design, angle, and stem dimensions of the funnel. It was found necessary to prefilter the water used in the test, but when this was done, highly reproducible results were obtained.

The investigation was also extended to include a study of "shelf life" of filter papers. It was found that some papers not only became brittle with age, but that decomposition products were formed that might contaminate the solutions being filtered. An accelerated aging test previously developed for paper generally enabled a satisfactory prediction of stability to be made.

This work has shown significant differences among filter papers which, if studied critically, may point the way to future improvements. For example, some papers of equal retentiveness differ in speed, and hence may yield a clue as to how still faster papers may be made.

Measurements of the quality of three foreign and two domestic brands of analytical filter paper have shown that the American-made papers are fully equal to the imported papers. It is anticipated that the application of quality standards based on quantitative measurements will eliminate traditional buying practices and permit free competition among all suppliers.

NEW DIAMOND DIE DRILLING METHOD REVOLUTIONIZES INDUSTRY.

A new, electrical method, for drilling small diamond dies, used in drawing and shaping extremely hard and fine wire, has been developed at the National Bureau of Standards, eliminating almost 100 man-hours from older processes. This discovery has completely revolutionized the fine-wire diamond die industry, introducing it into the United States for the first time in history.

Although dies of tungsten, molybdenum, or boron carbide have, in recent years, competed with diamond dies, the diamond is still the only tool used in shaping the harder and tougher materials, such as chrome nickel, brass and phosphor bronze, and high-carbon steel wires. Moreover, wires finer than 15 thousandths of an inch in diameter can be drawn only by diamond dies. In addition, the diamond is indispensable whenever precision of size and perfect roundness are essential considerations. Important uses for diamond-drawn wire are in radar and radio equipment, in high-frequency coil windings, as filaments for small tungsten lamps, and in delicate and precise electrical instruments. Wires of this type have become increasingly important with the expansion of the electronic and allied industries.

Prior to 1940, the indispensable small diamond dies were imported from Europe because labor costs made their manufacture unprofitable in this country. During the war, with all supplies from Europe cut off, the National Bureau of Standards undertook an investigation to speed

up the manufacturing process and improve the quality of dies to meet the emergency requirements for many vital war products.

A diamond die consists of five surface areas: the primary cone, the secondary cone, the reduction cone, the bearing, and the exit cone. In appearance such a die is similar to a wine glass. The portion of the die where the wire enters, the primary cone, corresponds to the goblet part of a wine glass. The narrowing stem from the bottom of the goblet to the base of the glass corresponds to the secondary cone, the reduction cone, and the bearing. Actual wire shaping takes place at the bearing. Finally, the base of the wine glass represents the exit cone.

The new process, developed by C. G. Peters, Chief of the Interferometry Section, and his associates, W. B. Emerson, K. F. Nefflen, F. K. Harris, and I. L. Cooter, replaces the older mechanical die cutting with high-voltage drilling followed by electrolytic drilling.

The primary cone is drilled by means of high-voltage sparks formed at the point of a needle electrode in contact with the face of the diamond. These sparks release the energy stored in a condenser which has been charged to a high voltage by a transformer. The condenser is charged through a "quenched" gap consisting of a number of very small gaps in series.

When rising voltage is applied to the circuit, sparking occurs first at the quenched gap. This is followed, as the voltage is increased, by a discharge across the face of the diamond between the needle electrode and the brass block on which the diamond is mounted. Without the quenched gaps in the circuit, the discharge would be a more or less continuous arc, overheating the diamond and producing a dark deposit on its surface. The rate of drilling increases with the power input into the circuit until a limit is reached where the temperature of the diamond is too high and its surface takes on a frosty appearance. The drilling needle, which is 0.02 inch in diameter, becomes red hot at its tip before this "frosting" point is reached and the reddening point of the electrode is used as a criterion in adjusting the power input to the circuit.

The secondary cone is formed by the action of a low-voltage spark in an electrolytic solution. The diamond is mounted on an insulating post in a shallow glass dish and enough of the electrolyte is used to fill the dish and just cover the diamond. The "Drilling" electrode is a platinum-iridium needle that is lowered into contact with the bottom of the primary cone and rests with very light pressure (around one fifth of a gram) on the diamond. A second electrode dips into the solution at some distance from the diamond.

When a low voltage (around 90 volts) is applied between the electrodes, sparking occurs at the tip of the drilling needle and a smooth-walled conical hole is formed in the diamond directly under the needle. The shape of the hole and the angle of its walls are controlled by the type of electrolyte used, while the hole size is controlled by the pressure

of the needle against the diamond. The power input into the circuit is controlled by the depth of the solution covering the diamond and by the voltage applied.

The National Bureau of Standards method of making small diamond dies consists essentially of ten steps, which combine electrical with some mechanical drilling. The die blank which is used in these operations has two plane-parallel faces between which the die will be formed, and a side window for viewing the progress of the drilling. These are cut on the diamond, using a rotating cast-iron lap with diamond powder as an abrasive. The cutting action of the lap is accelerated by the application of a high-voltage electric arc across the face of the diamond being cut.

In the first operation, ten minutes of high-voltage drilling of the blank, called spotting, produces a cone 0.014 to 0.020 inches deep that serves as a pilot hole for the next operation. This is followed by 30 to 40 minutes of mechanical drilling to come out the hole, using diamond powder in a gelatin solution as the abrasive. Operation three is repetition of the first high-voltage drilling and is followed by step four, mechanical coning. The final fore-drilling, operation five, should bring the bottom of the cone to between 0.006 and 0.008 inches from the back surface of the diamond. For exceptionally thick blanks, additional drilling and coning may be required. Step six, the final primary coning, demands greater care than the other similar operations to assure a symmetrical shape, free from drilling rings, and with either a polished or fine matt surface. The diameter of the cone immediately above its apex should be between 0.002 and 0.003 inch for good blending of the primary and secondary cones.

Operation seven begins the series of three electrolytic drilling operations, using two different solutions—sodium chloride and potassium nitrate. The first drilling of the secondary cone utilizes a 5 per cent. aqueous solution of sodium chloride.

Although an electrolyte of potassium nitrate produces a relatively long, narrow cone of correct size and shape for the secondary cone, the hole drilled using this solution tends to be out of alignment with the primary cone if drilling is attempted directly in a primary cone with a broad, unpointed, or irregular bottom. Excellent alignment and better blending of the primary and secondary cone is obtained using sodium chloride, although an additional thirty minutes for this step are needed.

Drilling the main body of the secondary cone with potassium nitrate is similar to operation seven except that the electrolyte solution is stronger and the tip diameter of the drilling electrode is smaller, ranging from 0.0010 to 0.0015 inch. After 40 to 45 minutes drilling time the drill will have pierced the back face of the die, giving a smooth-bore cone with a length of about 0.006 inch and a diameter at the bottom of 0.0005 to 0.0005 inch. If the initial distance between the bottom of

the primary cone and the back of the die was greater than 0.005 inch, the drilling may not pierce the back of the diamond and an additional 40 minutes drilling with potassium nitrate, using a resharpened electrode, is necessary.

The sharp edge formed at the intersection of the secondary cone and the back surface is given a slight countersink in operation nine to prevent damage when wire is drawn through the die. This countersink is made by inverting the die beneath the drilling electrode and drilling electrolytically from the back for four or five minutes, using the solution of sodium chloride.

The final step is finishing and polishing, a mechanical operation that improves the blend between the primary and secondary cones, improves the roundness of the die, and improves the shape and polish of its working parts.

Electric drilling, producing superior dies, takes 7 to 15 hours, depending on the type of die, with 10 hours as an average for this new process. Actual man-hours are considerably less than this, averaging about 2 man-hours per die, because almost every stage in the process is easily adaptable to multiple production.

Dies produced by the National Bureau of Standards method have better wearing characteristics in service than those produced by purely mechanical methods. In mechanically drilled dies, holes are started in the top and bottom of the diamond by "bruting" or gouging the face of the diamond with a small diamond chip. The hole is drilled through the body of the diamond by "packing" it with a spinning steel needle charged with diamond powder, a sort of "star-drilling" process. These operations result in severe strains and minute fractures in the walls of the die cones, and although the magnitude of the strain resulting from mechanical drilling decreases with reduced load on the drilling needle and with the size of the diamond powder used, it is still present in most mechanically drilled secondary cones. Frequent failure by chipping at the intersection of the secondary and exit cones of dies so drilled is ascribed to weakening of the material by the mechanical treatment. Likewise, rapid wear of some dies at their initial size may be attributed to disruption of material, underlying the working surfaces of the dies, that has not been removed by sufficient polishing.

In contrast to the condition found in mechanically drilled dies, cones produced by either the high-voltage or the electrolytic drilling process show no strain in the surrounding material when examined under polarized light. The freedom from strain and fractures results in less wear as the die is used to draw wires. The electrical methods of die formation are therefore particularly adapted for small dies used in drawing wires, 0.0015 inch in diameter, or smaller.

The electric method requires no special skills or long training on the

part of operators. Equipment is inexpensive and the drilling technique is simple, making the work less tedious and more practical for small as well as large scale enterprise. A satisfying development of the National Bureau of Standards investigation is that domestic die makers now find it advantageous to produce these small dies that formerly were obtained only through importation.

NEW PYROMETER FOR GAS TURBINES AND JET ENGINES.

With the recent development of gas turbines and jet engines as practical power plants has come a need for accurate and responsive temperature-sensing instruments. Such instruments would serve not only for evaluating engine efficiency, but also for protecting experimental and service equipment from damage by excessive temperature of various parts. An improved pyrometer for measuring the temperatures of these high-temperature high-velocity gas streams has been developed by Andrew I. Dahl in the Bureau's Temperature Measurements Laboratory in cooperation with the Bureau of Ships, Navy Department.

The new pyrometer consists essentially of an ordinary thermocouple junction around which is pressed a small, light, silver shield. The junction, made by conventional methods, is inserted one-half inch into a silver tube three-fourths inch long that is slightly flattened. A thin mica strip is inserted within the silver tube on each side of the junction and the assembly is pressed to form a rigid unit with good thermal contact between shield and junction. The main problem in measuring the temperature of the hot gases is preventing the transfer of heat to or from the thermocouple junction by radiation. The shields formerly used for this purpose are not only bulky and slow to respond to changes in temperature, but also offer considerable obstruction to the stream of gas. The use of a silver shield overcomes these limitations since silver, being a good reflector and a poor emitter for radiant heat energy, keeps the temperature of the shielded junction nearly the same as that of the gas.

The new device was found accurate to within five degrees Fahrenheit in experiments utilizing a stream of gas at 1,500 degrees flowing with a velocity at 250 feet per second through a pipe with walls at 1,200 degrees. In addition to high accuracy, laboratory tests indicate that this pyrometer responds quickly to changes in temperature, is simple to construct and easy to install, and that the new junction creates a minimun of disturbance to gas flow.

The maximum dimension of the shielded junction need not exceed the diameter of the porcelain tube used to insulate the thermocouple wires from each other. Various types of steel protecting tubes can be used to protect the unit without loss of accuracy or sensitivity. Several of the new instruments have been constructed and sent to commercial turbine manufacturers for service tests in full-scale operating turbines.

OFFICIAL ANNOUNCEMENT FROM THE NATIONAL BUREAU OF STANDARDS REGARDING CHANGES IN ELECTRICAL AND PHOTOMETRIC UNITS.

By E. U. CONDON, Director.

I General Announcement.

In pursuance of decisions of the International Committee on Weights and Measures, the National Bureau of Standards will introduce as of January 1, 1948, revised values of the units of electricity and of light. While the definitions of the units and the methods of fixing their magnitudes will be quite different from those of the present practical systems, the changes in magnitude will be so small as to affect appreciably only measurements of high precision. In certificates for standards and instruments issued by the Bureau during 1947 values will be given in both the old and the new units.

The electrical units of the "international" system will be superseded by those of the "absolute" system derived from the fundamental mechanical units of length, mass, and time by use of accepted principles of electromagnetism, with the value of the permeability of space taken as unity in the centimeter-gram-second system or as 10^{-7} in the corresponding meter-kilogram-second system. Actually all of the common electrical units fall into the mks system. This revision constitutes a return to the basic principle, always recognized as desirable, of having the electrical units consistent with the fundamental mechanical units.

The international ohm and volt now in use are slightly larger than the corresponding absolute units; consequently numerical values of resistance and voltage are slightly larger when expressed in absolute units than when expressed in international units. In the United States the factors recommended for conversion to the absolute basis are 1.000495 for resistances and 1.00033 for voltages. For power or energy therefore the factor is 1.000165, but for most purposes the round value 1.0002 is amply precise.

The new system of photometric units takes as the primary standard a black-body radiator operated at the temperature of freezing platinum. The "candle," unit of intensity, is defined as one-sixtieth of the intensity of one square centimeter of such a radiator. Other units are derived from the candle, with the provision that when differences of color are involved the evaluation shall be made by means of standard spectral luminosity factors which have been adopted by the International Commission on Illumination and the International Committee on Weights and Measures. For the types of lamps now in common use the ratings under this new system will be practically the same as those now in effect.

THE FRANKLIN INSTITUTE.

MEDAL DAY MEETING.

WEDNESDAY, APRIL 16, 1947.

The annual Medal Day exercises at The Franklin Institute began at 6:30 P.M. on the evening of Wednesday, April 16. There were approximately 410 members and friends of the Institute who attended the dinner and the presentation of the awards.

A reception in honor of the Medallists and their friends was held prior to the dinner. Mr. Guy Marriner, Associate Director of our Music Department, played the National Anthem which opened the evening's programme.

At 9 o'clock, Mr. Richard T. Nalle, President of The Franklin Institute, opened the exercises with a few words of greeting to the guests.

Mr. Nalle then announced that Medal Day was also a Stated Monthly Meeting of The Franklin Institute and that minutes of the February meeting were printed in full in the March issue of the JOURNAL. Since there were no corrections or additions, the minutes were approved as printed.

The programme and list of Medallists follow. A detailed statement of these exercises will be printed in full in a subsequent issue of the JOURNAL.

PROGRAMME

Reception to Medallists ..... THE HOSTESS COMMITTEE

NATIONAL ANTHEM ..... GUY MARRINER

Dinner ..... MEDALLISTS, OFFICIALS AND GUESTS

Toast to Benjamin Franklin ..... RICHARD T. NALLE
President, The Franklin Institute

Greetings ..... RICHARD T. NALLE
President, The Franklin Institute

Introduction of Medallists of Other Years ..... THE PRESIDENT

The Institute in 1947 ..... HENRY BUTLER ALLEN
Executive Vice-President and Secretary, The Franklin Institute

Presentation of Awards ..... THE PRESIDENT

Penicillin Chemistry ..... SIR ROBERT ROBINSON

The Future of Nuclear Physics ..... PROFESSOR ENRICO FERMI

MEDALLISTS.

Presentation of Certificates of Merit (1882)

JOSEPH RAZEK
Consulting Physicist
Havertown, Pa.

PETER J. MULDER
Training Director
Letterkenny Ordnance Depot
Chambersburg, Pa.

Presentation of Longstreth Medals (1890)

SAMUEL BERMAN
Associate Director
Waugh Laboratories
New York

HAROLD JOHN WARREN FAY
President
Submarine Signal Company
Boston, Massachusetts

Presentation of Potts Medals (1906)

ROBERT HARRINGTON KENT
Associate Director
Ballistics Research Laboratory,
Aberdeen Proving Ground
Aberdeen, Maryland

VLADIMIR KOSMA ZWORYKIN
Director of Electronic Research, RCA
Princeton, New Jersey

Presentation of Levy Medals (1923)

EVERETT MCMULLIN BARBER
Supervisor
Engineering Research Department
Beacon Research Laboratory
Texas Co.
Beacon, New York

JAY BRENT MALIN
Mechanical Engineer
Engineering Research Department
Beacon Research Laboratory
Texas Co.
Beacon, New York

JOSEPH JOHN MIKITA
Formerly Associate Director of Research
Refining Dept.
Texas Co.
Beacon, New York

Presentation of Henderson Medals (1924)

LARS OLAI GRONDAHL
Director, Research and Engineering
Union Switch & Signal Company
Swissvale, Pennsylvania

SEDGWICK NORTH WIGHT
Engineer, Train Operation
General Railway Signal Company
Rochester, New York

Presentation of Wetherill Medal (1925)

KENNETH SEYMOUR MOORHEAD DAVIDSON
Professor
Stevens Institute of Technology
Hoboken, New Jersey

Presentation of Clark Medal (1926)

EDWARD GEORGE BOYER
Manager of Gas Dept.
Philadelphia Electric Co.
Philadelphia, Pennsylvania

Presentation of Brown Medal (1938)

KARL P. BILLNER
President
Vacuum Concrete, Inc.
Philadelphia, Pennsylvania

Presentation of Clamer Medal (1943)

EDGAR H. DIX, JR.
Assistant Director of Research
Aluminum Company of America
New Kensington, Pennsylvania

Presentation of Newcomen Medal (1943)

EVERETT G. ACKART
Consulting Engineer
Wilmington, Delaware

Presentation of Ballantine Medal (1946)

GEORGE CLARK SOUTHWORTH
Waveguide Research Engineer
Bell Telephone Laboratories
New York

Presentation of the Franklin Medal (1914) and Certificate of Honorary Membership

ENRICO FERMI
Professor,
Institute of Nuclear Studies
The University of Chicago
Chicago, Illinois

Presentation of the Franklin Medal (1914) and Certificate of Honorary Membership

SIR ROBERT ROBINSON
Professor of Chemistry
Oxford University
Oxford, England

LIBRARY NOTES.

The Committee on Library desires to add to the collections any technical works that members would wish to contribute. Contributions will be gratefully acknowledged and placed in the library. Duplicates received will be transferred to other libraries as gifts of the donor.

Photostat Service. Photostat prints of any material in the collections can be supplied on request. Orders received in the morning are filled the same day. The average cost for a print 9 × 14 inches is thirty-five cents.

The library and reading room are open on Mondays, Tuesdays, Fridays and Saturdays from 9 A.M. until 5 P.M., Wednesdays and Thursdays from 2 P.M. until 10 P.M. AFTER June 1, Mondays, Tuesdays, Wednesdays and Fridays from 9 A.M. to 5 P.M., Thursdays from 2 P.M. to 10 P.M., Saturdays from 9 A.M. to 12 noon.

RECENT ADDITIONS.

ARCHITECTURE AND BUILDING.

ALLEN, J. R., J. H. WALKER, AND J. W. JAMES. Heating and Air Conditioning. 1946.

BIOGRAPHIES.

BARLOW, NORA, ed. Charles Darwin and the Voyage of the Beagle. 1946.

CHEMISTRY.

BOND, HORATIO, ed. Fire and the Air War. 1946.

DISCERENS, LOUIS. Die Neuesten Fortschritte in der Anwendung der Farbstoffe Volume 1, 1946.

ENGELDER, CARL. Fundamentals of Semi-Micro Qualitative Analysis. 1947.

HAWK, P. B., B. L. OSER, AND W. SUMMERSON. Practical Physiological Chemistry. Twelfth edition. 1947.

HIRSCH, IRVING. Manufacturing of Whiskey, Brandy and Cordials. 1937.

PIGMAN, W. W., AND M. L. WOLFROM. Advances in Carbohydrate Chemistry. Volume 2. 1946.

SADTLER, SAMUEL S. Chemistry of Familiar Things. Eighth edition. 1946.

TEXTILE CHEMICAL SPECIALTY GUIDE. 1946-47.

YOE, JOHN H., AND A. BURGER. German for Chemists. 1946.

DICTIONARIES.

BENNETT, HARRY, ed. Concise Dictionary and Technical Dictionary. 1947.

ULRICH, CAROLYN F., ed. Periodical Dictionary Fifth edition. 1947.

ELECTRICAL ENGINEERING.

BATCHER, R. R., AND WILLIAM MAULIC. The Electronic Engineering Handbook. 1946.

BATCHER, R. R., AND WILLIAM MAULIC. The Electronic Control Handbook. 1946.

GAFFERT, GUSTAF A. Steam Power Stations. 1946.

ENGINEERING.

ELLIS, DOUGLAS STEWART. Elements of Hydraulic Engineering. 1947.

MATHEMATICS.

KNOPP, KONRAD. Theory of Functions Volumes 1 and 2. 1945.

TAYLOR, JAMES HENRY. Vector Analysis with an Introduction to Tensor Analysis. 1946.

MECHANICAL ENGINEERING.

BEGEMAN, MYRON LOUIS. Manufacturing Process. 1947.

JUDGE, ARTHUR W. Maintenance of High Speed Diesel Engines. Third edition. 1946.

SCHWAMB, P., AND OTHERS. Elements of Mechanism. Sixth edition. 1947.

METALLURGY.

DAESEN, JOHN R. Galvanizing Handbook. 1946.

MILITARY ENGINEERING.

HICKS, JAMES E. Nathan Starr. (The First Official Sword Maker.) 1940.

OPTICS.

POHL, ROBERT WICHARD. Einfuhring in die Optik. 1943.

PHARMACY AND PUBLIC HEALTH.

POWERS, J. L., AND G. E. CROSSEN. Scouilles, the Art of Compounding. 1946.

PHYSICS.

CORK, JAMES M. Radioactivity and Nuclear Physics. 1946.
SWIETOSLAWSKI, W. Microcalorimetry. 1946.

SANITARY ENGINEERING.

COX, CHARLES R. Laboratory of Water Purification. 1946.

SCIENCE

STOKLEY, JAMES. Science Remakes Our World. 1946.

SUGAR.

HANN, R., AND N. K. RICHTMEYER, ed. Collected Papers of C. S. Hudson. 1946.

TEXTILES.

ROSE, H. WICKLIFFE. The Rayon and Synthetic Fiber Industry of Japan. 1946.
WATSON, WILLIAM. Textile Design and Colourist. Fifth edition. 1946.

NOTES FROM THE BIOCHEMICAL RESEARCH FOUNDATION.

The Blood Picture of Normal Laboratory Animals.[1] A Review of the Literature, 1936–1946.—MARY VIRGINIA GARDNER.

THE HAMSTER.

Few hematological studies have been reported on the hamster. This may be attributable in part to the difficulty experienced in obtaining blood from the tiny ears or short stumpy tail in quantities sufficient for routine examination.

Method of Obtaining Blood.—Tail blood, obtained under ether anesthesia, was used by Stein and Carrier (1). Blood from the saphenous vein or from the jugular vein of etherized animals was studied by Hu and Pai (2). After several unsuccessful attempts to obtain sufficient quantities of tail blood, Stewart, Florio and Mugrage (3) used blood obtained by cardiac puncture from hamsters under anesthesia induced by ethyl chloride and maintained by ether.

Erythrocytes.—The red blood cell of the hamster was described by Stewart, Florio and Mugrage (3) as a biconcave disc which took an acid

TABLE I.

Erythrocytes.

Age of Hamsters	No. and Sex of Hamsters	Erythrocytes × 10^6/cmm.		Reported by
		Average	Range	
20 days	2 M	5.06	5.03–5.08	Stein (1)
21 days	M	5.4		Stein (4)
33–34 days	5 M	5.96	5.36–6.69	Stein (1)
1–2 months	12 M	7.0		Stewart (3)
1–2 months	11 F	7.01		Stewart (3)
40–43 days	3 M	6.98	6.40–7.55	Stein (1)
47–50 days	3 M	7.94	7.84–8.01	Stein (1)
57–62 days	6 M	8.60	8.16–9.29	Stein (1)
85–100 days	5 M	9.14	9.06–9.22	Stein (1)
2–4 months	25 M	7.50		Stewart (3)
2–4 months	22 F	7.10		Stewart (3)
40–226 days	M	8.8		Stein (4)
9 months or more	24 M+F	7.5		Stewart (3)
adult	10	9.57		Hu (2)

stain. Few basophilic erythrocytes and only occasional nucleated forms were found by them. Variable reticulocyte counts were found by Stein and Jacobson (4).

The average erythrocyte levels reported for different ages are shown in Table I.

[1] Continued from page 258, Vol. 243, No. 3.

The mean diameter of the erythrocytes of male and female hamsters of 1 to more than 9 months of age was shown by Stewart, Florio and Mugrage (3) to range between 6.2 and 7.0 μ. The erythrocytes of young animals were found by Stein and Jacobson (4) to be slightly larger in diameter than those of older animals.

Hemoglobin.—The reported average values for hemoglobin concentration in the blood of hamsters of various ages are shown in Table II.

TABLE II.

Hemoglobin.

Age of Hamsters	No. and Sex of Hamsters	Hemoglobin g./100 cc.		Method	Reported by
		Average	Range		
36–37 days	4 M	17.04		Newcomer	Stein (1)
47–50 days	3 M	18.3		Newcomer	Stein (1)
1–2 months	12 M	16.4		Klett-Sahli	Stewart (3)
1–2 months	11 F	16.9		Klett-Sahli	Stewart (3)
66–70 days	5 M	18.94		Newcomer	Stein (1)
2–4 months	25 M	17.1		Klett-Sahli	Stewart (3)
2–4 months	22 F	16.4		Klett-Sahli	Stewart (3)
108–131 days	5 M	15.65		Newcomer	Stein (1)
9 months or more	24 M+F	17.6		Klett-Sahli	Stewart (3)
adult	M	20.6		—	Stein (4)

TABLE III.

Leukocytes.

Age of Hamsters	No. and Sex of Hamsters	Leukocytes per c.mm.		Cells per 100 Leukocytes					Reported by
		Average	Range	Neut.	Eo.	Lymph.	Mono.	Other	
1–2 months	12 M	7,470		21.4	0.38	75.7	1.1	1.44	Stewart (3)
1–2 months	11 F	8,210		23.4	0.63	75.1	0.85	—	Stewart (3)
2–4 months	25 M	8,150		32.0	0.81	65.8	1.4	—	Stewart (3)
2–4 months	22 F	7,870		34.2	1.0	63.0	1.8	—	Stewart (3)
9 months or more	24 M+F	8,560		29.0	0.68	67.9	2.43	—	Stewart (3)
				supravital staining					
adult	10	10,070		11	3.7	77.0	0	8.3 (blasts)	Hu (2)
				May Grünwald-Giemsa stain					
				16	2.8	81.2	—	—	Hu (2)

White Blood Cells.—Lymphocytes of various ages, ranging from very immature blast forms to the small adult type, were found by Hu and Pai (2) in supravitally stained preparations. The cytoplasm of the lymphocyte was found by them to become increasingly clear, the mitochondria to become finer, and the neutral red bodies more numerous an the cells became older. The lymphocyte of fixed and stained smears was described by Stewart, Florio and Mugrage (3) as small with a dense, deep blue nucleus and a narrow, light blue zone of cytoplasm which contained occasional azurophilic granules. The monocyte was found to be

large, with clear, bright blue cytoplasm and a slightly indented, kidney-shaped nucleus, which contained stringy chromatin. A rosette of neutral red bodies was found by Hu and Pai (2) at the indentation of the nucleus in supravitally stained preparations.

The neutrophil of normal hamsters was shown by Hu and Pai (2) to contain usually a figure 8 or a U-shaped nucleus, less commonly a ring-shaped or lobulated nucleus. Basophils were not reported in any of the investigations reviewed here, but typical eosinophils, containing large, bright red granules, were described by Stewart, Florio and Mugrage (3).

The reported average leukocyte values are shown in Table III.

Hematocrit.—The volume of packed red cells in the blood of the male hamster was found by Stein and Carrier (1) to vary with age, ranging from 47.5 per cent. at 33–34 days to 53.2 per cent. at 108–131 days. The hematocrit of 23 hamsters of both sexes was found to average 47.5 per cent. at 1–2 months of age and that of 24 animals to average 47.4 per cent. at more than 9 months of age by Stewart, Florio and Mugrage (3).

No values for blood volume, sedimentation rate, coagulation time, specific gravity or platelet number were found in the literature.

Blood studies on the hamster were not included in Scarborough's review (5).

(*To be continued*)

REFERENCES.

(1) STEIN, K. F., AND CARRIER, E., *Proc. Soc. Exptl. Biol. Med.*, **60**: 313 (1945).
(2) HU, C. H., AND PAI, H. C., *Chinese Med. J. Suppl.*, p. 131 (1938).
(3) STEWART, M. O., FLORIO, L., AND MUGRAGE, E. R., *J. Exptl. Med.*, **80**: 189 (1944).
(4) STEIN, K. F., AND JACOBSON, B., *Anat. Rec.*, **88**: 459 (1944).
(5) SCARBOROUGH, R. A., *Yale J. Biol. Med.*, **3**: 63, 169 (1930); **3**: 267, 359, 433, 547 (1931); **4**: 69, 199 (1931); **4**: 324 (1932).

BOOK REVIEWS.

PHOTOGRAPHY BY INFRARED, by Walter Clark. Second edition. 272 pages, illustrations, 14 × 22 cms. New York, John Wiley & Sons, Inc., 1946. Price $6.00.

The range of wave lengths which can be recorded by photography in the invisible infrared is about twice as great as the range which the eye can see. It is, however, but a small fraction of the whole range of the infrared, and a still smaller part of the gamut of known radiations. There are a number of factors which interfere with the preparation and handling of photographic materials sensitive to long wave lengths, so that it appears that progress in infrared photography beyond the present limit must be very slow. Infrared photography with the ease of ordinary photography is a relatively new subject and only the fringe of its usefulness has been touched. It has been surrounded with all the glamor and charms which the vivid imagination of the popular press is capable of bestowing. It has emerged from it as a proved useful weapon for the practical photographer and the investigator in the fields of science and technology. Further study cannot fail to find new uses for it.

It is the purpose of this book to survey what has been done up to the time of writing and to consider in detail the practical methods and underlying principles, a knowledge of which should aid in the proper application of the subject to the solution of new problems. Now in its second edition, the material has been revised to include many recent developments and applications. The starting point of the book is a chapter summary of the chief points to be borne in mind in the use of the infrared for general photographic purposes. The detailed treatment follows progressing through photographic dark room practice, characteristics of photographic materials, sensitizing for the infrared, the Herschel Effect, sources of infrared radiation, and examination and differentiation of materials by infrared. Chapters on the application of this type of photography include medicine, botany and palaeontology, photomicrography, camouflage detection, and penetration of radiation through the atmosphere, fog and haze. The last chapter is devoted to optical characteristics of materials in the infrared. There is a name and subject index.

A great number of references is cited in this work. It is an up-to-date exposition of knowledge of the subject presented in a not too technical and useful way. Those interested in this subject would do well to have it within reach.

R. H. OPPERMANN.

ELECTRICAL TRANSMISSION IN STEADY STATE, by Paul J. Selgin. 427 pages, drawings, 14 × 22 cms. New York, McGraw-Hill Book Company, Inc., 1946. Price $5.00.

The author states in the preface of this book that it aims primarily at broadening and strengthening the foundations for a superstructure of technological knowledge which the reader may be about to acquire or may have acquired through the exercise of his profession. As such it presumes a basic knowledge beforehand, that which has become second nature through constant reference, for example the concepts of elementary alternating current theory and the average mathematical preparation. It therefore avoids these and likewise excludes a working knowledge of vector analysis as would be applied in the general solution of dynamic field problems in three dimensions.

The book starts by introducing the four terminal network as a circuit element and gives attention to the study of chain connected networks, the conclusions of which find an immediate and useful application in the study of the transmission line where the problem of establishing the overall performance of a matched line is reduced to the determination of the line dissipation factors and characteristic frequency. Next, distortion in transmission lines is taken up, and reflection at the terminals of networks and lines which derives fundamental equations governing the performance of a network or line when the load impedance has a generic value. This leads

into a consideration of the transmitted power, or the power absorbed by the load. In treating on the behavior of electrically long lines having small dissipation it is shown that the peculiar behavior of mismatched lines can sometimes be used to advantage.

Following sections are devoted to the problem of coupling a generator to its load so as to obtain the highest flow of power, and the matching of a line to its terminations. A brief review of the electromagnetic theory is then given relating to static fields, followed by a treatment of Maxwell's equations and their application to circuit elements devoted chiefly to the application of the laws of electromagnetism to lumped systems. This leads to coverage of exponential lines wherein there is considered the application of field laws to the plane-field structure. The latter portion of the book is devoted to inductive coupling and transformers and capacitive coupling, an application of the four pole theory to the vacuum tube, and the flow of power through high frequency amplifiers. In the back of the book is a bibliography of references covering fields bordering upon the subject matter of the book. A subject index completes the work.

Being of the nature of a review progressing to new viewpoints with many different ideas, this book should have usefulness to practicing engineers.

R. H. OPPERMANN.

PUBLICATIONS RECEIVED.

Directory of Libraries and Information Sources in Philadelphia and Vicinity, edited by Catharine C. Grady for the Special Libraries Council of Philadelphia and Vicinity. 130 pages, 13 × 19 cms. Philadelphia, Special Libraries Council of Philadelphia and Vicinity, 1947. Price $1.75.

The Technology of Adhesives, by John Delmonte. 516 pages, drawings and illustrations, 15 × 23 cms. New York, Reinhold Publishing Corporation, 1947. Price $8.00.

Russian-English Technical and Chemical Dictionary, by Ludmilla Ignatiev Callaham. 749 pages, 14 × 20 cms. New York; John Wiley & Sons, Inc., London: Chapman & Hall, Limited, 1947. Price $10.00.

The Chemistry of Portland Cement, by Robert Herman Bogue. 572 pages, tables, drawings and illustrations, 15 × 24 cms. New York, Reinhold Publishing Corporation, 1947. Price $10.00.

Toward Better Photography, by Vincent McGarrett. 260 pages, illustrations, 14 × 20 cms. Boston, American Photographic Publishing Co., 1947. Price $3.00.

The Rare-Earth Elements and Their Compounds, by Don M. Yost, Horace Russell, Jr., and Clifford S. Garner. 92 pages, drawings and tables. New York; John Wiley & Sons, Inc., London; Chapman & Hall, Limited, 1947. Price $2.50.

Tungsten, by K. C. Li and Chung Yu Wang. Second edition. 430 pages, tables and illustrations, 15 × 24 cms. American Chemical Society Monograph No. 94. New York, Reinhold Publishing Corporation, 1947. Price $8.50.